Politecnico di Milano

Engineering Faculty

Electrical Department

PhD Thesis in Electrical Engineering
XXIV Cycle 2009-2011

**SUPERCACITOR STORAGE SYSTEMS:
MODELING, CONTROL STRATEGIES, APPLICATIONS
AND SIZING CRITERIA**

Candidate:	Eng. Vincenzo Musolino, matriculation number: 738557
Tutor and Supervisor:	Prof. Enrico Tironi
Coordinator:	Prof. Alberto Berizzi

ABSTRACT

A confluence of industry, social and economic drivers, are creating new interest in electric storage systems for grid, transportation and more general for industrial applications. Energy storage has become a key issue for achieving goals connected with increasing the efficiency of both producers and the users; the presence of a storage system makes it possible, over a time period ranging from seconds up to hours, to store the excess of energy and to reuse it when really needed. In this way it is possible, not only to recover or regenerate energy, but also to design the overall system based on the average power requested by the application while the power requests over or below the average power is ensured by the presence of the storage system.

This thesis describes in detail the supercapacitor devices as key storage technology for their excellent properties in terms of specific power, expected lifetime and a wide operative temperature range. In addition their stabilized production process makes them very interesting in many industrial applications where the availability of a technology over the time is very important to technically sustain new designs.

Theory, modeling and simulation are investigated in order to provide insight into mechanisms, predict the device performances and understanding next evolution and improvement of this technology. In particular a simple procedure to identify the parameters of the model, that can be used to characterize a supercapacitor before use, is presented and, an extended experimental activity to prove the model validity over a wide range of supercapacitor devices is reported.

A comprehensive analysis to address supercapacitor system integration is also presented based on different control strategies to ensure the correct energy flows and to optimize the overall system operations according to the application requirements. In addition in order to evaluate the total installed costs, performances and capabilities related to the integration of innovative supercapacitor storage system, the sizing of the storage is evaluated considering not only the technical design but also the economic return of the investment. According to the application the deterministic as the probabilistic method, based on Monte Carlo simulations, are presented, and their results are compared.

Contents

INTRODUCTION

The interdependence between the environmental, social, and economic aspects of today's society is becoming increasingly clearer and more cohesive. The key point is related to the limited availability of the earth's resources. This is a crucial point because the availability of resources such as food, space, and energy must match the requirements as the population growth in order to maintain the current standards of living and protect the ecosystem. At present, human activities require a large amount of energy and, despite the actual global recession that began in 2008 and continues to show evident effects, the total worldwide energy consumption over the last decades has continued to grow. As reported in a 2010 international energy outlook document provided by the U.S. energy information administration office (DOE/EIA-0484-2010), projections for the next three decades show an increase of 14% in OECD (Organisation for Economic Co-operation and Development) countries and a significant 84% in non-OECD countries. Although energy is needed for human activities, its use impacts the availability of energy resources in the global ecosystem. In fact, the pollution effects related to the use of energy are not localized to the place of utilization but affect the entire environment.

According to this, no energy resource presently exists that meets all of the economic, social, and environmental requirements. One possible solution seems to be increasing the use of renewable energy resources, which has attracted major attention for energy saving. Saving energy, in fact, is the first energy resource because it is environmentally friendly, available in all countries, unrelated to the fossil fuel energy resources, and a source of income, not only from an economic point of view, but also from a technical and industrial point of view. Investing in energy saving is investing in innovation, technical skills, and environmental sustainable activities. More generally, it is investing in the next generation because it actually takes into account the limited availability of resources.

In this general context, among the different forms of energy, electrical energy assumes an important role in our society due to the multiple properties this form of energy presents. In the last decades, the gross domestic products (GDPs) of more developed countries have been characterized by trends involving electric energy consumption. It is possible to transport electrical energy over long distances with high efficiency. It is easy to diffuse, produces no emissions in the place of its utilization, and is easy to convert into other forms of energy in a reversible way. Because of the above-mentioned properties,

electric energy is increasingly being diffused, not only for all of the typical grid-connected applications, but also in many others industrial and transportation applications that have not traditionally used electrical energy because they have been characterized by the direct conversion of a primary energy source, typically a fossil fuel source, into mechanical energy. Actually, the multiple benefits arising from a hybridization based on the conversion of the primary energy into electrical energy is enlarging the portfolio of applications where electricity is the winning solution.

In this general framework, independently from the application, the most important goal is the possibility of increasing the total system efficiency in such a way that the same mission can be accomplished with lower resources. However, due to the general considerations, the environmental and economic aspects must also be taken into account.

Nowadays, electrical storage systems play an important role in different solutions. Although the difficulty of storing electrical energy has been an historical limitation of this kind of energy, nowadays the emergence of new needs and new applications is introducing new exigencies for the electrical storage system devices. In many applications, ranging from electrical grid applications to industrial, civil, and transportation ones, in order to improve the efficiency and ensure energy and/or economic savings, it is very important to exploit the presence of a storage system that is capable, over a time period ranging from seconds up to hours, of storing excess energy and reusing it when really needed. In fact, this makes it possible, not only to recover or regenerate energy, but also to design the overall system based on the average power requested by the application because power requests over or below the average power is ensured by the presence of the storage system. In this way, all solutions can be designed and optimized based on the average power with consistent advantages in terms of weight, efficiency, and reliability.

Although there are many storage technologies today, none is able to fulfill all of the different system requirements, especially when all of the performances in terms of specific energy, specific power, lifetime, operative temperature range, safety, availability, and cost are taken into account. In the last few years, consistent technological improvements and cost reductions have characterized the evolution of many storage systems, so that more and more attention has been given to implementing, using, and exploiting their benefits in real applications.

Among the different technologies, this work focuses on supercapacitor storage devices. This choice is related to different considerations. First, despite the fact that supercapacitors are relatively new for industrial applications (about ten years old), they are characterized by a stabilized production process, with no significant changes in the technology over a period of time. From a technical and economic point of view, this is very important because it indicates the possibility of realizing new designs based on a stable and available technology over a period of years. Second, supercapacitors, as storage devices, show excellent properties in terms of specific power, expected lifetime (up to one million charge/discharge cycles), and a wide operative temperature range, making them very interesting in numerous applications. Third, unlike other storage technologies, supercapacitors are made of abundant and recyclable materials available on the earth.

The main limitation is related to their specific energy; in fact, supercapacitors are more closely related to a "power oriented" storage definition that to a traditional "energy oriented" storage device. In other words, supercapacitors are the winning solution from a technical and economic point of view, when the energy required from the storage in a discharge or charge cycle is typically in a maximum time interval of up to one hundred seconds. Their limited specific energy, but significant specific power and cycle lifetime, make supercapacitor technology a suitable solution in all applications where energy recovery at high dynamic rates, as the regenerated energy from moving parts electrically braked, and the peak shaving function of the power delivered by the main source are important key aspects to ensure the efficiency, availability, quality, and effective system cost of the electrical energy supplied. From this, it is clear that supercapacitors are very important to guarantee new innovative system functions, but only if correctly integrated, sized, and operated in the final system. In fact, when considered for single and stand-alone storage systems, the number of direct applications is very limited. The work carried out in this thesis aims to correctly address the above considerations.

After a general overview of storage technology options in chapter one, the second chapter provides a focused description of the supercapacitor technology. In particular, in order to correctly manage and integrate supercapacitor devices, chapter three introduces a new supercapacitor equivalent electrical model. Modeling is very important, especially when the device is used in a wide range of applications that influence the typical device performances. Supercapacitors are not an exception, in fact their behaviors in terms of

dynamic response during cycling, efficiency, and self discharge change significantly according to the dynamic of use. The peculiarity of this model is its ability to correctly represent the complete dynamic of the device when operated with a cycle frequency ranging from DC up to 1 kHz. In addition, it is also very important to use model parameters that have clear physical meanings and can be simply determined in order to ensure the model usability. For this, chapter three presents a new and very simplified parameter identification procedure: the peculiarity is that the model order can be a priori chosen according to the accuracy and dynamic that you want to represent.

In order to verify the introduced model, in chapter four, an extensive experimental analysis of supercapacitor storage devices at the cell and module levels is presented. In particular, the analysis aims not only to verify the model validity, but also to point out real supercapacitor performances according to the dynamic of use, especially evaluating the specific energy as a function of the specific power and device efficiency.

The equivalent model that is realized represents a valid and indispensable tool to address supercapacitor system integration. Due to the limited specific energy, supercapacitors, when integrated at the system level, need to be correctly managed according to the application requirements in order to ensure the correct energy flows and optimize the system operations. Thus, in chapter five, two control strategies for supercapacitor storage devices are presented: the first aims to reduce the voltage fluctuations on a distribution bus where multiple loads and storage systems are connected, while the second aims to reduce the overall system losses. In particular, these control strategies are supported by extensive experimental activity on a real industrial application, and the benefits arising from the system integration of the innovative supercapacitor devices coupled with a traditional storage technology (a lead acid battery) are presented and discussed.

Finally, due to the importance of a correct design for the integrated system, not only from a technical point of view but also under the economic profile, chapter six addresses the sizing of the supercapacitor storage, considering the economic impact of the solution. Considering the current component costs, the return of the investment arising from economic energy saving is evaluated. In particular, two sizing criteria are analyzed. The first one is a deterministic criterion that is useful when the application consists of a well known power profile absorbed by the equivalent load, while the second one addresses the

sizing of a centralized storage system using a probabilistic approach when multiple loads are connected to the same distribution bus. In this case, in fact, the equivalent load power profile and, consequently, the energy storage size needed to fulfill the required load functions, cannot be evaluated by means of a deterministic method. The mathematical approach and some experimental results based on Monte Carlo simulations are presented, and their results are compared with the deterministic method.

1. STORAGE TECHNOLOGY OPTIONS

A confluence of industrial, social, environmental, and economic drivers is creating new interest in electric energy storage systems. The limitation in the availability of energy resources, the continuing increase in fossil fuels cost, and the greater attention being given to the earth's ecosystem, are making storage systems a suitable solution in many applications ranging from grid applications to industrial and transportation ones.

Electrical storage systems have generated great interest because of importance that electrical energy has in our society. In fact, electrical energy is characterized by:

- easy portability according to the transmission and distribution infrastructure;

- disjunction between production sites and user sites;

- no gas emissions at the user sites;

- high efficiency of production, transmission, and conversion;

- easy reversibility in converting this form of energy into mechanical and vice versa.

As shown in Figure 1.1, [1], the growth of the forecasted global net electricity generation is approximately +80% in the reference period 2007-2035.
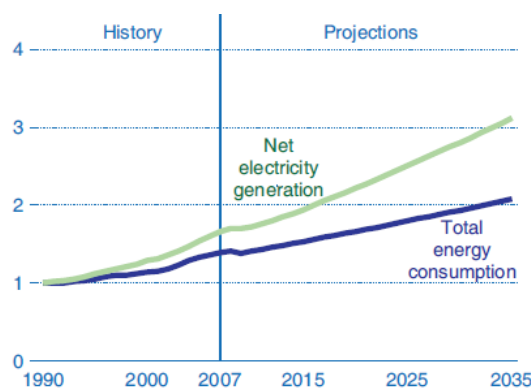
Figure 1.1 **Growth in world electric power generation and total energy consumption, 1990-2035 (index, 1990 = 1) [1].**

These growth projections are also related to the potential impact that electric urban mobility will have in the near future in order to ensure green, low-impact, and sustainable transportation solutions.

1.1. IMPORTANCE OF ENERGY STORAGE SYSTEMS (ESS) IN TODAY'S SOCIETY

In the last decade, due to great changes in the global industrial and economic assets and new energy needs, also related to environmental impacts, our electrical systems have been prepared to meet new requirements; in particular, what is changing is the concept of integration and the vision of the electric system as a whole. The traditional distinctions between the production, transmission, and distribution of electrical energy are changing, and there is a continuing reduction of the boundaries between them. The main changes aim to increase electric mobility and spread generation, of renewable energy sources in particular. Thus, the electrical layouts of our plants are being reconsidered. The new issues are related to:

- the power flow direction, which is not necessarily a top down distribution;
- the presence of active loads at the distribution level;
- the intermittence of renewable energy sources;
- the possible huge presence of electric loads related to the plug and play vehicles market.

All of these changes are reflected in the availability, reliability, power quality, and safety of electrical energy over time. The technological solutions actually under consideration to meet these new requirements see the presence of:

- DC and/or smart distribution grids;
- power electronic converters;
- Information Communication Technologies (ICT) to monitor and control the power systems;
- Energy Storage Systems (ESS).

The introduction of ESS represents one of the most prominent technical solutions to meet the new electrical system requirements. The availability of ESS is an historical need in electric system in order to separate the generation profile from the demand profile over time. Due to the lack of consistent ESS technology, with the exception of pumped hydro-storage system, commonly the generation profile has to follow the demand profile in each instant to guarantee the electric system quality and stability. With actual changes related to renewable energy production, the high capital cost of managing grid peak demands and

large investments in grid infrastructure for reliability [2] from one side, and the actual potential electric vehicles industry market from the other side, new interests in energy storage systems are emerging. In these new applications, in fact, the requirements for the Energy Storage System are widely varying according to the application. As shown in Table 1.1 [3], where a list of potential benefits arising from the adoption of ESS in today's power grid is reported, the technical requirements in terms of energy and installed capacity differ widely according to the application.

Table 1.1.   Summary of potential benefits and technical requirements for ESS in Power Grid [3]

#	Benefit Type	Discharge Duration		Capacity	
		Low	High	Low	High
1	Electric Energy Time-shit	2 hour	8 hour	1 MW	500 MW
2	Electric Supply Capacity	4 hour	6 hour	1 MW	500 MW
3	Load Following	2 hour	4 hour	1 MW	500 MW
4	Area Regulation	15 min	30 min	1 MW	40 MW
5	Electric Supply Reserve Capacity	1 hour	2 hour	1 MW	500 MW
6	Voltage Support	15 min	1 hour	1 MW	10 MW
7	Transmission Support	2 sec	5 sec	10 MW	100 MW
8	Transmission Congestion Relief	3 hour	6 hour	1 MW	100 MW
9	T&D Upgrade Deferral	3 hour	6 hour	250 kW	5 MW
10	Substation On-site Power	8 hour	16 hour	1.5 kW	5 kW
11	Time-of-use Energy Cost Management	4 hour	6 hour	1 kW	1 MW
12	Demand Charge Management	5 hour	11 hour	50 kW	10 MW
13	Electric Service Reliability	5 min	1 hour	0.2 kW	10 MW
14	Electric Service Power Quality	10 sec	1 min	0.2 kW	10 MW
15	Renewable Energy Time-shift	3 hour	5 hour	1 kW	500 MW
16	Renewable Capacity Firming	2 hour	4 hour	1 kW	500 MW
17	Wind Generation Grid Integration	10 sec	6 hour	0.2 kW	500 MW

Similarly, the same is true for the electric vehicle industry, where the ESS requirements vary according to the vehicle mission. The main categories of electric vehicles can be summarized as:

- Pure electric vehicle

- Hybrid electric vehicle

- Plug-in electric vehicle

The distinctions among the three categories are related to the amount of storable electrical energy in the vehicle. In pure electric vehicles, the storage is the unique reserve of energy capable of fulfilling all of the vehicle functionalities. In hybrid vehicles, according to the level of hybridization (Micro, Mild, Strong), an electric storage system, which can fulfill an electric mission up to a maximum of 1 km, is coupled to a traditional fuel storage with its internal combustion engine (ICE). Finally, plug-in vehicles, which can

reach an electric autonomy of up to 70 km, are characterized by an electric storage system that is rechargeable both from the electric grid and from the ICE, in addition to the recovered energy coming from regeneration.

In Table 1.2 a summary of the technical specifications of the electrical ESS for different kinds of electrical vehicles is reported [4].

Table 1.2.   **Electrical ESS Requirements for Pure Electric, Hybrid and Plug-in Vehicles [4, 5]**

	Pure Electric		Hybrid		Plug-in	
Parameter	**Minimum Goals**	**Long Term Goal**	**Minimum Goals**	**Long Term Goal**	**High Power/Energy Ratio Battery**	**High Energy/Power Ratio Battery**
Power - Discharge	80 kW	80 kW	25 kW (10 s)	40 kW (10 s)	45 kW (10 s)	38 kW (10 s)
Power - Regeneration	40 kW	40 kW	20 kW (10 s)	35 kW (10 s)	30 kW (10 s)	25 kW (10 s)
Available energy	40 kWh	40 kWh	0.3 kWh	0.5 kWh	3.4 kWh	11.6 kWh
Calendar Life	10 years	10 years	15 years	15 years	15 years	15 years
Cycle life	1000, 80% DOD	1000, 80% DOD	300k 25Wh cycle	300k 50Wh cycle	-	-
Operating Environment	-40 to +50	-40 to +85	-30 to +52	-30 to +52	-30 to +52	-30 to +52
Production price	< 6000 $ 25k units/year	4000 $ 25k units/year	500 $ 100k units/year	800 $ 100k units/year	1700 $ 100k units/year	3400 $ 100k units/year

More and more attention is being given to the industrial market for storage systems related to the multiple opportunities that storage allows in different huge industrial markets (electric grids and electric vehicles). Thus, in the last decade, much funding has been allocated to the research and development of affordable, reliable, and cost effective Energy Storage Systems. In addition, many activities are related to developing adequate tools for system analysis, optimal sizing, placements, and control strategy algorithms for ESS integrations [6].

In the following, a general summary of energy storage technologies will be presented, giving a look at actual research and development funding programs related to Energy Storage Systems.

1.2. *ENERGY STORAGE TECHNOLOGIES*

In order to have a comprehensive view of storage system technology options, in Figure 1.2 shows a Ragone plot that compares the most current and interesting types of storage systems in terms of energy and power density. It is important to note that this graph does not show the best storage system device, but rather the best to choose based on the application requirements. In addition, the storage system performance also has to be evaluated under the cycle life, expected life, efficiency, operative temperature, system integration, and installed cost.
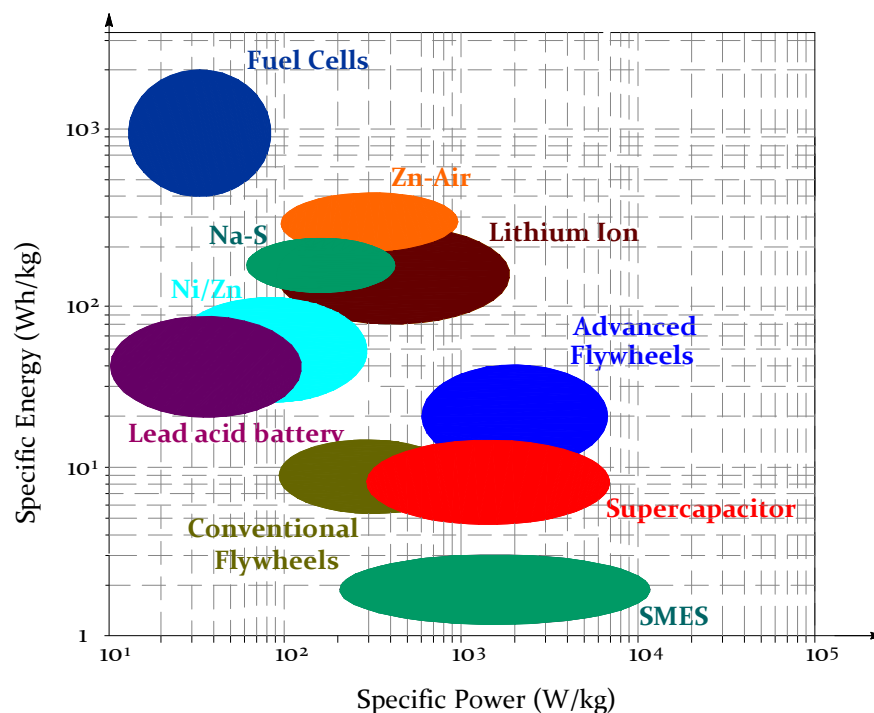
Figure 1.2.   **Ragone plot of different storage technologies.**

1.2.1. *COMPRESSED AIR ENERGY STORAGE (CAES)*

These systems store energy as a compressed gas (normally air) in an enclosed reservoir (typically underground) at a pressure of 70–100 bar. The compression phase, by means of electric compressors, uses low cost electric energy (typically produced during the night) or the excess energy produced by renewable sources. When needed, typically during the peak power hours, the compressed air is heated and expanded in a traditional turbine-generator to produce electricity. In a newer second-generation CAES plant, the compressed air is directly expanded in a turbo-gas generator to avoid the compression

phase. The time-shift between the storage phase and following discharge phase makes it possible to realize a positive revenue. The typical system layout is reported in Figure 1.3.
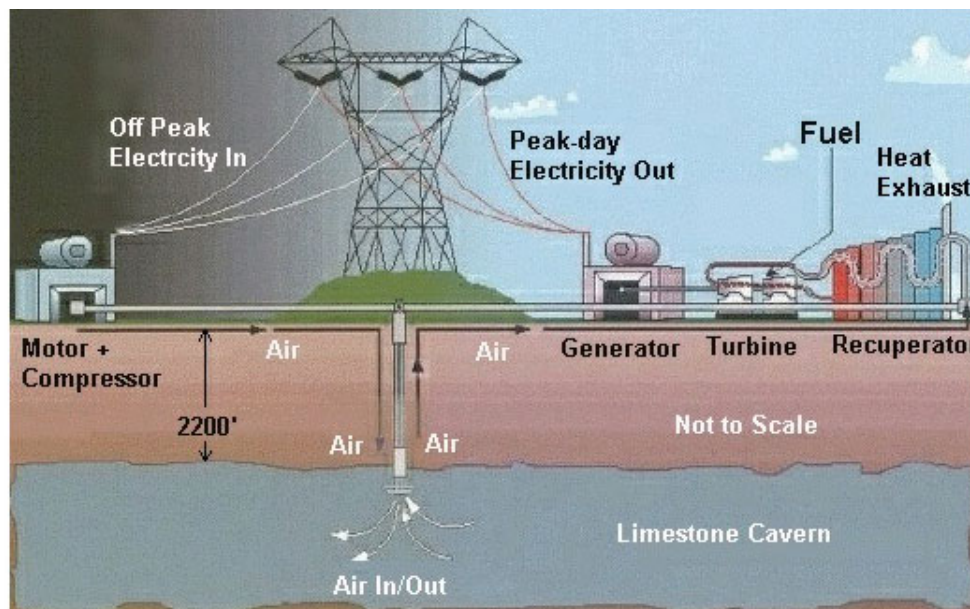
Figure 1.3. **Schematic layout of underground CAES**

The reservoir must be impermeable. In order to reduce the total infrastructure cost, existing geological structures such as limestone mines or salt caves are typically used because they have this feature.

The first CAES storage system was realized in 1978 in Hundorf (Germany). It had a rated power of 290 MW. A second one with a rated power of 110 MW was installed in 1991 in Alabama. This plant was realized in 30 months with a capital cost of $600/kW.

In 2009, DOE funded two projects (for New York State Electric & Gas and PG&E) involving the construction of 150 MW/10 hour and 300 MW/10 hour advanced second generation CAES units, respectively.

Research on this kind of storage is still taking place, with the current development of "Adiabatic CAES" (A-CAES). The idea is to capture the heat generated during the compression phase and reuse it to preheat the compressed air before expansion during the discharge phase. An aboveground demonstration of an A-CAES system could materialize by 2015 [3].

1.2.2. PUMPED HYDRO

This kind of storage, historically the most famous, has a technical functionality very similar to the previous. Storage is performed by transferring a certain amount of water from a lower basin to an upper one. With a total system efficiency in the range of 0.76–0.85, it is possible to exploit the price difference between high and low electrical energy production costs in order to generate revenue. In Figure 1.4 a typical schematic layout is reported.
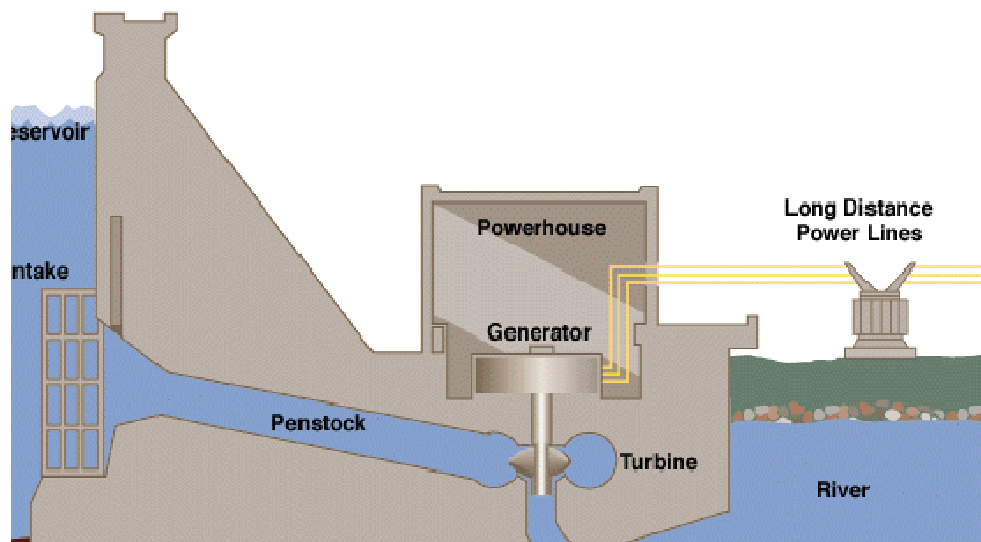
Figure 1.4   Schematic layout of a pumped hydro plant.

In favorable situations, it is technically possible to obtain natural underground reservoirs using natural basins or former mines. The open sea can be used as a downstream reservoir. An example is the pumped 30-MW hydro plant built in 1999 in Yanbaru, Japan. Pumping systems have been manufactured in Italy and Switzerland since 1890. Of these plants, which are essential to the operation, regulation, and management of electricity in the transmission networks, there are currently more than 130-GW of production capability installed all over the world, with over 40 capable of producing more than 1 GW. The installation cost greatly depends on the morphology of the territory and the technical requirements for the designed site. Thus, the costs can vary from 150 €/kW (U.S.) to more than 2000 €/kW (Japan). Despite this, storage systems are necessary and convenient, even when they are very expensive.

1.2.3. FLYWHEEL

Flywheels are electromechanical devices that are capable of storing kinetic energy by means of a spinning rotor. In order to exchange this energy with the electric grid, a motor/generator machine is coupled to the flywheel, with a power converter added to enlarge the working machine's operating range. During the charging phase, electricity is converted into kinetic energy and the rotor speed is increased; while in the discharge phase, the opposite process takes place.

As shown in Figure 1.5 the electric machine and rotor are well integrated and the bearings are often a magnetic type in order to optimize the total system efficiency and reduce the device noise.
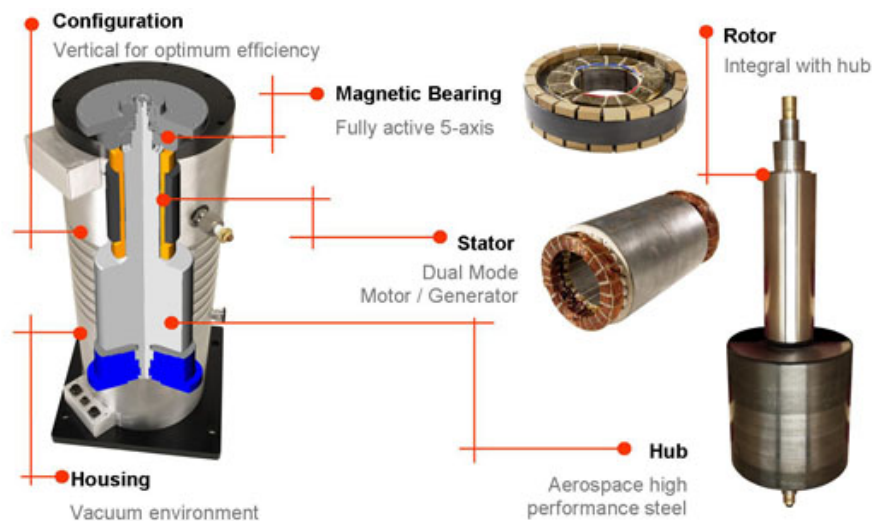
Figure 1.5.   Schematic layout of flywheel storage.

In designing this type of device, two strategies can be adopted in order to increase the specific energy [7]. The first one consists of increasing the rotor inertia by acting on the diameter of the rotor, which is typically steel, with a rotation speed of up to 10,000 rpm. This kind of device is typically used as a UPS, and its main limitation is due to its weight and size. The second design approach uses a smaller diameter rotor and increases the rotation speed up to 100,000 rpm. In this way, it is possible to realize more compact and modular flywheels. Typical applications are in telecommunication, with a size on the order of tenths of a kW for various quantities of minutes.

Due to the fast response of these devices, up to 4 milliseconds, along with a system efficiency of up to 0.93 and an estimated lifetime of up to 20 years, these devices are very suitable for power quality [8-9], regulation services [10-11], and UPS functions such as for

energy recovery functions in transportation systems [12-13]. They can be sized with a rated power between 100 kW and more than 1 MW for up to 1 hour.

Interestingly, the Beacon Power project is developing megawatt-scale flywheel plants with a total rated power of 20 MW to support the frequency regulation market [3].

1.2.4. ELECTROCHEMICAL BATTERY

Today's secondary (rechargeable) electrochemical batteries are the most investigated storage devices. The peculiarity of these devices is that they can reversibly convert electricity into chemical energy without additional machines. Since the first battery was realized in 1799 by Alessandro Volta, many other technologies have been developed and many others are in a research phase.

The attention focused on these devices is related to the wide assortment of applications in which they can be used, from stationary grid applications to the electric vehicle market and practically all industrial applications. The requirements vary considerably with the application. Yet, there have been such huge industrial drivers and interests over the last decades that much public and private funding is converging in the research and development of new electrochemical batteries.

The main motivation of this research is that, with the exception of lead acid batteries, there is no well-established technology that is able to fulfill all of the technical, environmental, and safety requirements, even considering the prominent performances of each technology. As indicated in [14], there are many fundamental gaps in our understanding of the atomic- and molecular-level processes that govern a battery's operation, performance limitations, and failure. Fundamental research is critically needed to uncover the underlying principles that govern these complex and interrelated processes.

The main battery technologies for industrial use are:

- $Pb-H_2SO_4$:   Lead acid battery;
- Ni-Cd: Nickel-Cadmium battery;
- Ni-MH   Nickel-Metal hydride battery;
- Na-S   Sodium-Sulfur batteries;
- $Na-NiCl_2$ Z.E.B.R.A. battery;
- Li-ion   Lithium ion battery;
- VRB :   Vanadium redox battery;
- Zn-Br   Zinc-Bromine battery;

- *Lead acid battery (Pb-H2SO₄)*

This is the most mature, well known electrical storage technology used in all industrial applications, ranging from UPS, automotive, and telecom applications up to naval and submarine applications. Many models [15 – 18] and experimental activities [19 - 22] have been used over the years to investigate and improve this technology. The main disadvantage is related to a lower energy density and cycle life compared to the newer technologies.

Significant, not for its nominal power but for its system life, is the 1 MW/1.5 MWh lead acid storage system located in a remote island of Alaska by GNB Industrial Power and Exide. This storage system, which had been operative for 12 years showing limited visible performance degradation, was finally replaced in 2008.

Because it is a very low cost solution, this kind of technology is onboard all internal combustion engine vehicles in order to guarantee the engine switch on and to realize a stabilization function for the automotive electric plant. Its limited energy density prevents this technology from being considered for hybrid or pure electric vehicles.

In order to improve lead acid battery technical performances, while maintaining their low system cost, researchers have added carbon-enhanced electrodes to create advanced lead acid batteries. The theoretical specific energy of lead-carbon batteries is 166 Wh/kg, but actually only 70–80% of this value is reached [23]. Especially for the automotive market in the U.S., the DOE is supporting Exide Technologies with Axion Power International and East Penn Manufacturing Co. for the production of advanced lead-acid batteries. The idea is to couple the traditional lead acid technology with a carbon supercapacitor in order to fulfill the micro and mild hybrid applications [24, 25].

Regarding the system integration, the East Penn Manufacturing Co., USA, received additional funding ($2.5 million for a total project cost of $5 million) [6] to demonstrate the economic and technical availability of a 3-MW grid-scale, advanced energy storage system using advanced lead-acid batteries.

- *Nickel-Cadmium battery (Ni-Cd)*

Nickel cadmium batteries, both the oldest type and the vented pocket-plate, are very reliable, sturdy, no memory effect, and long-life batteries, which can be operated effectively at relatively high discharge rates and over a wide temperature range. They are

typically produced in a range of 5–1200 Ah and are used in many industrial, military, telecommunications, uninterruptible power supply, and emergency lighting applications [26]. They have very good charge retention properties, and can be stored for long periods of time under any condition without deterioration.

An important key aspect of this type of battery lies in its low cost compared with other innovative technologies, which in any case is greater than traditional lead acid storage. The limitations in using this kind of battery are related to the presence of cadmium and the limited specific energy density compared with the innovative ones.

Due to its particular reliability and rugged performances in terms of electrical and mechanical abuse tests, this kind of battery has been suitable for the automotive market. Deutsche Automobilgesellschaft GmbH (DAUG) developed a new electrode structure, the fiber-structured electrode for electric vehicle applications. This technology is presently applied in all types of nickel-cadmium, as well as nickel-metal hydride, batteries.

A further innovation regards the plastic-bonded or pressed-plate electrode, where the active material, cadmium oxide, is mixed with PTFE and a solvent to produce an isotropic paste. In this way, the production cycle is well standardized and issues related to dust during manufacturing are eliminated.

Fiber plate and plastic-bonded nickel-cadmium batteries find many applications in traction, power stations, substations, aircraft, and other applications.

Typical specific energy values are 25 Wh/kg for pocket plate batteries, 40 Wh/kg for larger fiber plate batteries, and up to 56 Wh/kg for plastic-bonded plate batteries.

- *Nickel-Metal hydride battery (Ni-MH)*

In order to eliminate the presence of cadmium as an active negative material, an evolution of the traditional nickel-cadmium battery is the nickel-metal-hydride battery, where the cadmium is replaced with hydrogen absorbed in a metal alloy.

As shown in [26], industrially available nickel-metal-hydride batteries fit many of the technical requirements required by United States Advanced Battery Consortium's (USABC) performance goals for the EV batteries. It should be noted that commercial Ni-MH batteries are characterized by a specific energy of 70 Wh/kg, specific power of 220 W/kg, and an environmental operating temperature of -30 to 65°C, making them very suitable for the automotive market.

The continuing improvement in this kind of technology and excellent performances in terms of safe operations at high voltage, charge and discharge safety (including tolerance to abusive overcharging and overdischarging), maintenance free, excellent thermal properties, capability to utilize regenerative braking energy, simple and inexpensive charging and electronic control circuits, and environmentally acceptable and recyclable materials are the main drivers of this kind of technology. Active interest in the research and development of Ni-MH batteries is being shown by the US Department of energy [24, 25], which is actually funding Johnson Controls, Inc, with an award of $299.2 million for the production of nickel-cobalt-metal battery cells and packs, as well as the production of battery separators (by partner Entek) for hybrid and electric vehicles

- *Sodium-Sulfur batteries (Na-S)*

Sodium-sulfur batteries belong to the family of sodium batteries. In the mid-1990's, this kind of battery was the best candidate for stationary electric energy storage applications due to its potential low cost system, high cycle life, high specific energy (120–220 Wh/kg), good specific power (up to 170 W/kg), and high energy efficiency (up to 90%). In addition, the use of inexpensive and abundant materials avoid problems related to availability. Due to the presence of a solid electrolyte at ambient temperature, sodium batteries have to operate at a high temperature (300–350°C) in order to maintain the electrolyte as a liquid. This is one of the main issues related to this technology, along with the corrosion of the insulators, which is typical in the harsh chemical environment and gradually causes conductive properties and increases the self-discharge rate.

The main technology developer is a Japanese collaboration between NGK Insulator, Ltd. and Tokyo Electric Power Company (TEPCO), which started in 1984. Actually, more than 316 MW of Na-S batteries are installed around the world, with a discharge capacity of 1896 MWh. The installed capacity is expected to double by 2012 [3].

Figure 1.6. **NewYork Electric Power 1.2MW / 7.2MWh Sodium Sulfur Battery Facility [3].**

- ***Z.E.B.R.A. battery (Na-NiCl₂)***

In order to improve the performances of Na-S batteries and, in particular, the issues related to the corrosion of the insulating material and the dendritic sodium growth, different makers (ABB, SPL, and MES DEA) have reached a relatively advanced state in developing electric-vehicle battery technologies based on a sodium battery (ZEBRA battery).

The ZEBRA battery operates at 245 °C and is characterized by a specific energy range of 100–130 Wh/kg and a specific power range of 170–240 W/kg [26]. The development team efforts have concentrated on realizing an affordable, reliable, and safe sodium battery storage system. Particularly significant is the comprehensive ABB experience, which tested its ZEBRA batteries in a wide variety of car manufacturer's vehicles (BMW E-1 electric car, Chrysler minivan T115, the Daimler Benz 190, two VW vehicles, and a number of Ford Ecostar demonstration vehicles). Despite this, in the mid-1990's ABB and SPL discontinued their programs on this technology. In contrast, after a certain period of lower interest, on February 1, 2010, MES-DEA and FIAMM founded a new company called FZ Sonick SA for the production of ZEBRA batteries for the electric vehicle market and stationary grid applications.

Figure 1.7. **FZ Sonick ZEBRA battery with rated voltage of 557 V and 32 Ah for electric vehicle applications.**

- ***Lithium ion battery (Li-ion)***

This is today's most investigated electrochemical storage technology in terms of material development, and cell and system assembly.

They are characterized by a typical specific energy of 150 Wh/kg (a little more than sodium batteries), a low self discharge rate (typically 2–8% per month), long cycle life (more than 1000 cycle at 80% DOD), and extended temperature range of operation.

The main drivers making this technology more interesting than others are the high specific energy, high cell rated voltage (up to 4.2 V), high rate capability, sealed cell, and no maintenance operation.

Actually, the research is still open in defining the most suitable configuration in terms of anode and cathode materials, cell geometry, system monitoring, and assembly. According to [25], Li-Ion technology issues related to the chemistry and associated materials can be improved and solved by means of adequate cell and system failure identification models, system optimization, and system design. The continuing development of new electrode materials does not establish this process. In order to summarize the different Li-ion batteries topologies, Table 1.3 shows a comparison of different technologies according to the cathode and anode materials.

Until now, major efforts have been devoted to designing a suitable Li-ion battery for the electric and hybrid vehicle market and, as reported in [24] and [25], public funds have consistently been allocated to numerous industrial companies (more than $1 billion from the U.S. DOE in the last 2 years). The growing interest, as reported in [3], is also for several utility grid-support applications such as Distributed Energy Storage Systems (DESS), transportable systems for grid support, commercial end-user energy management frequency regulation, and wind and photovoltaic peak smoothing. Many experts believe that the stationary market for Li-ion batteries could exceed that for transportation.

Table 1.3. **Matrix of actual Li-ion battery technologies**

		ANODE MATERIAL		
		Graphite	Hard Carbon	LTO
CATHODE MATERIAL	LiFePO4	+ safety + life + flat characteristic U vs. SOC - low cell voltage - energy density	+ safety + low temperature performance + life + higher power compared to graphite - low cell voltage - steep characteristic U vs. SOC - cost - energy density	+ safety + no cooling required + life + highest power + low temperature performance - low cell voltage - cost - energy density
	NMC	+ high cell voltage + energy density - safety - low temperature performance	+ low temperature performance + higher power compared to graphite - steep characteristic U vs. SOC - safety - cost - energy density	+ low temperature performance + life + very high performance - low cell voltage - cost - energy density
	Mixed Oxide	+ highest cell voltage + energy density - low temperature performance	+ low temperature performance + higher power compared to graphite - steep characteristic U vs. SOC - cost	+ safety + low temperature performance + life + very high power -low cell voltage - cost - energy density
	Stoichmetric spinel type LiMn$_2$O$_4$	+ cost + high cell voltage + safety - life	+ low temperature performance + safety + higher power compared to graphite - steep characteristic U vs. SOC - life - energy density	+ low temperature performance + limited cooling required + very higher power - low cell voltage - energy density

- *Vanadium redox battery (VRB)*

This is the most mature of all the flow battery systems. Typically, flow batteries store energy in liquid electrolytes as charged ions in two separate tanks. In contrast to the others, vanadium redox uses one common electrolyte. The electrolyte on the anode side and that on the cathode side are separated by a membrane that is permeable to ions. These batteries, as a more complicated system despite being sealed batteries, required a certain amount of auxiliaries to work correctly, in particular a hydraulic subsystem including valves, pipes, and seals.

Actual experience with this technology shows the robustness and reliability of these systems. In particular, suppliers estimate the lifespan to be 15 or more years, with a cycling capability of 10,000 cycles at a 100% depth of discharge. As reported in [3] multiple MW/MWh systems have been installed all over the world, and actual efforts on this

technology aim to increase their notice by electric power companies and achieve a cost reduction to gain market acceptance for grid-scale applications [23].

- *Zinc-Bromine battery (Zn-Br)*

This is another flow battery that is in an earlier stage of development despite the maturity of the vanadium redox battery. The interest is related to the claimed estimated lifetime of up to 20 years and longer cycle lives. Small projects, typically in rural areas, are being used around the world to avoid the installation of new power lines. In addition, in the USA, electric utilities plan to conduct some experiments on a transportable system (0.5 MW/2.8 MWh) for grid support and reliability [3].

1.2.5. SUPERCAPACITOR

These devices are characterized by a greater energy density than traditional electrolytic capacitors (by about two orders of magnitude). As in a traditional capacitor, the energy is stored in an electrostatic field, so that no electrochemical reactions take place during the charging and discharging processes. For this reason, the process is highly reversible and the charge-discharge cycle can be repeated frequently and virtually without limits (today a typical lifespan is up to 1 million cycles).

Today's most common supercapacitors for industrial applications are based on carbon for the electrode materials and an organic solution for the electrolyte. In this way, the typical specific energy and specific power values are 7 Wh/kg and 4 kW/kg, respectively.

An important characteristic of these storage devices is their well-established production process. Thus, over the last 10 years, no significant variations in the chemical and material design have occurred. In this way, much significant experience have been gained in transportation, automotive, and industrial applications, particularly involving stationary applications of supercapacitors for a peak shaving and energy recovery functions on the electric light-train railway system in Dresden (Figure 1.8) and Cologne cities (Germany, since 2002) and Madrid (Spain, since 2003), and the on-board experience gained by Bombardier with its MITRAC energy saver for light-train and diesel-electric train (Diesel Multiple Unit) applications. Much experience has also been gained with the diesel hybrid buses made by Vossloh Kiepe GmbH (Germany), Scania AB Hybrid Bus (Sweden), KAM (China), and ISE Corp. (USA), in addition to the Continental AG Active

Boost for the second generation start & stop PSA vehicles (from 2012). Other important industrial applications are the uninterruptible power supply (UPS) for a wind turbine pitch control system (Enercon GmbH patent) and telecommunication applications, as well as the industrial use with the hybrid fuelcell-supercapacitor forklift solution produced by Still GmbH.

Figure 1.8. **Siemens SITRAS SES full time installation in Dresden (Hellerau).**

In the last years, as shown in [2, 6, 27], a growing interest in using supercapacitor technology for grid applications has arisen. In particular, a supercapacitor's technical performances are especially suitable for transmission support, electric service power quality, and wind generation grid integration (short duration fluctuations), Table 1.1 shows that the typical discharge duration required is in the range of 2 seconds to 2 minutes In this direction, it is important to underline the ongoing U.S. DOE funding on supercapacitor applied research granted to EnerG2, Inc. ($21 million) and to the FastCap System Corp., ($5.35 million) in order to produce a nanotube enhanced ultracapacitor with a higher energy density comparable to standard batteries, yet with a greater power density and a cycle life of thousands of times. The interest is related to the potential cost reduction on hybrid and electric vehicles and on grid-scale storage applications.

1.2.6. SMES

In 1971, Peterson and Boom invented the SMES system used today, which consists of a superconductive storage coil charged and discharged by a power interfaced converter. Superconductivity Inc., USA, has been among the first to develop SMES technology (Superconducting Magnetic Energy Storage) from an industrial point of view.

The energy is stored as magnetic energy using a superconductive material, consisting of ceramic conductor showing the property of superconductivity with a neglectable resistance at a very low temperature, in the range of a few Kelvin up to 134 K. In this way, it

is possible to store energy without losses from the Joule effect, except those related to the cooling system used to maintain the coil in a superconductive phase.

SMES devices, characterized by a specific power in the range of 1–10 kW/kg and a specific energy of 1–2 Wh/kg [29], are suitable for stationary grid applications in order to enhance the power quality by frequency/voltage control, network stability, voltage sag protection, spinning reserve, and short term load leveling.

The first European industrial SMES system was installed in Elettra, the first European "third generation" high brightness synchrotron light source in its range (Trieste, Italy). The solution was designed to store 4 MJ, allowing operation in "islanding mode" for a maximum time of 1 second supplying a load of about 1 MW [30].

There is active interest in developing innovative solutions based on SMES devices, as demonstrated by the consistent funding of $4.2 million granted by the ARPA-E Agency (U.S. Department of energy) to ABB in the period of 2010–2013. The SMES project has the aim to increase the amount of energy that can be stored and to extend the duration during which power is available at a fraction of the cost of actual SMES devices. In this project, the team aims to develop a 20 kilowatt ultra-high field superconducting magnetic energy storage system with a capacity of 3.4 MJ.

1.2.7. FUEL CELL

Fuel cell devices, in contrast to the storage technologies previously described, are not strictly storage systems because the hydrogen used is an energy vector. In addition, in a fuel cell, the fuel and oxidant are supplied continuously from an external source when power is desired. In a direct system, a fuel such as hydrogen (i.e. produced from water by an electrolysis process), methanol, or hydrazine is injected directly into the cell to react and produce electrical energy. In an indirect system, a fuel such as natural gas or another fossil fuel is converted into a hydrogen-rich gas using a reforming process and is then used in the cell.

The main obstacles in using hydrogen are related to the storage and technical-efficiency performances of fuel cells in converting hydrogen into another energy type, typically electric energy.

In principle, the process of any fuel cell could be reversed, allowing the chemical energy contained in the hydrogen to be converted into electrical and vice versa. However,

a given device is usually optimized to operate in one mode and may not be built in such a way that it can be operated backwards.

Until now, many different types of fuel cell technologies have been developed [26]: Solid Oxide (SOFC), Molten Carbonate (MCFC), Phosphoric Acid (PAFC), Alkaline (AFC), Proton Exchange Membrane (PEM), Direct Methanol (DMFC), and Regenerative (RFC) fuel cells, all with a specific power in the range of 10–40 Wh/kg and specific energy of 100–500 Wh/kg.

The main applications are portable applications such as electric generator, transportation, and stationary grid applications. In transportation, much experience has been gained with industrial forklifts (i.e., Still GmbH RX 60 fork lift truck), automotive and bus applications (i.e., the Van Hool GmbH buses delivered in 2010 for the AC Transit-ZEBA Advanced Fuel Cell Bus Project in San Francisco), and scooters. Despite the large amount of activity, there is no real market demand for fuel cell applications. Regarding the stationary grid applications, the interest in using fuel cells is for on-site power generation, cogeneration, and combined heat and power (CHP). These systems are especially suitable for applications with large load requirements such as hospitals, universities, manufacturing facilities, wastewater treatment plants, and grid support.

In Europe, the first fuel cell power plant with an industrial size was located in Milano (Italy), with a nominal power of 1.3 MW, and consisted of 2 PAFC cells with a rated power of 650 kW, Actually, the power plant has been converted using four novel stacks of molten carbonate fuel cells with a nominal power of 500 kW. It is also significant that an announcement was made in February of 2011 by FuelCell Energy, Inc., a leading manufacturer of ultra-clean industrial solutions, that Southern California Edison Company (SCE) has ordered the installation of a 1.4 megawatt (MW) fuel cell power plant as a utility-owned fuel cell on the campus of California State University, San Bernardino.

A growing interest in fuel cell grid applications has also been shown by the U.S. DOE. In 2010, it granted public funding of $2.1 million to devise an advanced energy storage device incorporating a regenerative fuel cell, which means a fuel cell capable of being reversed without a significant loss of efficiency. In fact, as reported in [6], regenerative fuel cell research needs to improve the thermal management of endothermic electrolysis reactions and exothermic fuel cell reactions.

1.3. FUTURE DIRECTIONS OF STORAGE SYSTEMS

The actual potential market for energy storage systems is huge considering both the transportation and grid scale applications. The general overview given above underscores how all of the technology options need further enhancement in order to fulfill the related applications performance requirements. If the common research driver is a lower power and energy cost, from a technical point of view, different technical improvements for transportation and grid applications are needed.

In transportation, the major attention is devoted to supercapacitor and electrochemical storage devices, particularly lithium ion technology. If the main limitation of a supercapacitor is related to the less than brilliant energy density, the main issues related to lithium-ion technology are related to the safety of this technology when used in stressed operating conditions and the acceptable operative working temperature. In grid applications, characterized by a stronger system vision, the main needs concern not only the development of new material and technology options in order to increase the system performances, but, in addition, new methodologies for optimal sizing, placements, and control strategies to maximize the value of the storage [6].

Another common point for storage applications is related to the real potential benefits achievable by the integrated use of storage systems. When analyzing single benefits, it is not typically possible to achieve a consistent economic advantage from the use of storage devices. The highest revenues are obtained when multiple benefits are considered [3]. Furthermore, in grid applications, the policy rules and regulatory framework have to be revised in order to have a significant impact on the allowable cost of energy storage systems. In this way, electric authorities can play an important role to encourage the use of storage devices and to accommodate the benefits of emerging energy storage systems. The market potentiality of the stationary electric network applications can be an important driver for the massive industrial production of storage technologies, matching the industrial system cost requirements for transportation applications.

These general considerations underline why the actual research objectives are not only the development of new innovative storage technologies but also the development of adequate diagnostic and modeling tools, system analyses, advanced control systems, and power electronics, along with demonstrations and deployment experiments, in order to

really understand the potentiality of a single storage technology and the real benefits of using it in actual applications [3, 6, 23].

1.4. BIBLIOGRAPHY

[1]   U.S. Energy Information Administration (EIA), International Energy Outlook, July 2010, DOE/EIA-0484(2010), www.eia.gov/oiaf/ieo/index.html.

[2]   "Electric Energy Storage Technology Options: A White Paper Primer on Applications, Costs, and Benefits", EPRI, Paolo Alto, CA, 2010. 1020676.

[3]   J. Eyer, G. Corey, "Energy Storage for the Electricity Grid: Benefits and Potential Assessment Guide. A study for the DOE Energy Storage System Program", Sandia Report SAND2010-0815, February 2010.

[4]   2009 Progress Report for Energy Storage Research and Development, U.S. Department of Energy Office of FreedomCAR and Vehicle Technologies.

[5]   "Energy Storage System Goals: USABC Goals for Advanced Batteries for EVs", http://www.uscar.org/guest/view_team.php?teams_id=11

[6]   U.S. Department of Energy, Office of Electricity Delivery & Energy Reliability, "Energy Storage Program PlanningDocument", February 2011

[7]   P. F. Ribeiro, M.L. Crow, "Energy Storage Systems for Advanced Power Applications", Proceedings of the IEEE, Vol. 89, NO. 12, December 2001.

[8]   S.Kulkarni, S. Santoso, "Impact of pulse loads on electric ship power system: With and without flywheel energy storage systems," Electric Ship Technologies Symposium, 2009. ESTS 2009. IEEE , vol., no., pp.568-573,20-22 April 2009.

[9]   S. Samineni, B.K. Johnson, H.L. Hess, J.D. Law, "Modeling and analysis of a flywheel energy storage system for voltage sag correction," Electric Machines and Drives Conference, 2003. IEMDC'03. IEEE International , vol.3, no., pp. 1813- 1818 vol.3, 1-4 June 2003.

[10]   N. Hasegawa, K. Fujimoto, T. Matsuyama, T. Ichikawa, K. Yukita, Y. Goto, K. Ichiyanagi, "Suppression of power variation for PV using flywheel and EDLC," Transmission & Distribution Conference & Exposition: Asia and Pacific, 2009 , vol., no., pp.1-4, 26-30 Oct. 2009.

[11]   N. Lu, M.R. Weimar, Y.V. Makarov, F.J. Rudolph, S.N. Murthy, J. Arseneaux, C. Loutan, "Evaluation of the flywheel potential for providing regulation service in California," Power and Energy Society General Meeting, 2010 IEEE , vol., no., pp.1-6, 25-29 July 2010

[12]   X. Chunling, Z. Conghui, "Research on the Ship Electric Propulsion System Network Power Quality with Flywheel Energy Storage," Power and Energy Engineering Conference (APPEEC), 2010 Asia-Pacific , vol., no., pp.1-3, 28-31 March 2010.

[13]   A. Jaafar, C.R. Akli, B. Sareni, X. Roboam, A. Jeunesse, "Sizing and Energy Management of a Hybrid Locomotive Based on Flywheel and Accumulators," Vehicular Technology, IEEE Transactions on , vol.58, no.8, pp.3947-3958, Oct. 2009.

[14]   "Report of the basic energy sciences workshop for electrical energy storage", Basic research needs for electrical energy storage, Office of Basic Energy Sciences, US Department of Energy, April 2007.

[15]   M. Ceraolo, "New Dynamical Models of Lead–Acid Batteries", IEEE Transactions on Power System, Vol. 15, NO. 4, November 2000.

[16]   S. Barsali, M. Ceraolo, "Dynamical Models of Lead-Acid Batteries: Implementation Issues", IEEE Transactions on Energy Conversion, VOL. 17, NO.1, Mars 2002.

[17]   M. F. de Koning, A. Veltman, "Modeling battery efficiency with parallel branches", 35th annual IEEE Power Electronics Specialists Conference, 2004.

[18]   Moubayed Nazih, Kouta Janine, El-Ali Ali, Dernayka Hala, Outbib Rachid, "Parameter identification of the lead-acid battery model", Photovoltaic Specialists Conference, 2008. PVSC '08. 33rd IEEE, ISBN: 978-1-4244-1640-0.

[19]   Y.Yamaguchi, M. Shiotaa, M. Hosokawaa, Y. Nakayamaa, N. Hiraib, S. Hara, "Study of charge acceptance for the lead-acid battery through in situ EC-AFM observation - influence of the open-circuit standing time on the negative electrode", Journal of Power Sources Volume 102, Issues 1-2, 1 December 2001, Pages 155-161.

[20]   M. Thele, J. Schiffer, E. Karden, E. Surewaard, D.U. Sauer, "Modeling of the charge acceptance of lead–acid batteries", Journal of Power Sources Volume 168, Issue 1, 25 May 2007, Pages 31-39.

[21]   S. C. Kim, W. Hi Hong, "Fast-charging of a lead–acid cell: effect of rest period and depolarization pulse", Journal of Power Sources Volume 89, Issue 1, July 2000, Pages 93-101.

[22]   L.T. Lam, N.P. Haigh, C.G. Phyland, A.J. Urban, "Failure mode of valve-regulated lead-acid batteries under high-rate partial-state-of-charge operation", Journal of Power Sources - J POWER SOURCES , vol. 133, no. 1, pp. 126-134, 2004.

[23] Nexight Group, "Advanced Materials and Devices for Stationary Electrical Energy Storage Applications", report by Sandia National Laboratories and Pacific Norwest National Laboratory on behalf of the U.S. Department of Energy Office of Electricity Delivery and Energy Reliability and the Advanced Research Projects Agency-Energy, December 2010.

[24] D. Howell, "Fiscal Year 2009 Annual Progress Report for Energy Storage R&D" , U.S. Department of Energy, January 2010.

[25] D. Howell, "Fiscal Year 2010 Annual Progress Report for Energy Storage R&D" , U.S. Department of Energy, January 2011.

[26] D. Linden, T.B. Reddy, "Handbook of batteries", 2002 McGraw-Hill, ISBN 0-07-135978-8.

[27] EPRI-DOE Handbook of Energy Storage for Transmission &Distribution Applications, EPRI, Palo Alto, CA, and the U.S. Department of Energy, Washington, DC: 2003. 1001834.

[28] C. Polk, R. W. Boom, Y. M. Eyssa, "Superconductive Magnetic Energy Storage (SMES) External Fields and Safety Considerations", IEEE TRANSACTIONS ON MAGNETICS, VOL. 28, NOJ, JANUARY 1992

[29] G. Ries, H. -W. Neumueller, "Comparison of energy storage in flywheels and SMES", Elsevier, Physica C: Superconductivity, Volumes 357-360, Part 2, August 2001, Pages 1306-1310

[30] R. Visintini, S. Quaia, R. Chiumeo, "Voltage Sags Effects on the Operation of a Synchrotron Light Source: Experimental Analysis and Solution Project", 10th International power electronics and motion control Conference, EPE-PEMC September 9-11-2002.

2.   *SUPERCAPACITORS: TECHNOLOGY AND PERFORMANCES*

2.1.   *SUPERCAPACITOR TECHNOLOGY*

In its construction and operation, a supercapacitor differs markedly from an electrolytic capacitor. The latter is a single capacitor comprising two conductors separated by an insulator. Supercapacitors, from a construction point of view, are similar to electrochemical batteries in that each of the two electrodes is immersed in an electrolyte, and they are separated by an ion-permeable membrane (Figure 2.1). In particular, the two electrodes are aluminum foils, upon which a nonporous material, typically activated carbon, is deposited in order to realize a high equivalent conductive surface. The two electrodes are immersed in an electrolyte solution, typically acetonitrile. The anions and cations of the solution are respectively attracted toward the positive and negative electrodes and, without charge transfer, form thin layers, with intermolecular distances between the ions and electrodes. The name Double Layer Capacitors (DLCs) is derived from these two layers, which are where the energy is stored due to the presence of an intense electrostatic field. The separator has the unique function of preventing any direct contact between the electrodes with an evident short circuit effect.
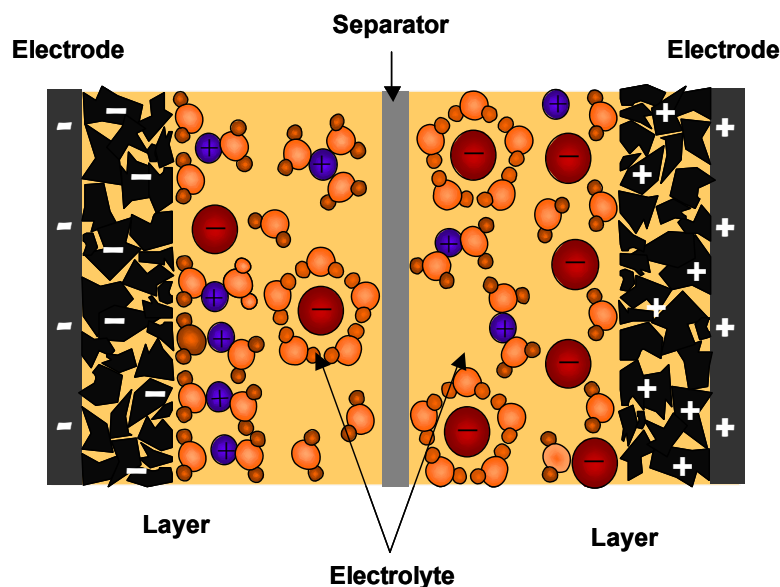

Figure 2.1.   Structure of supercapacitor.

The main difference, compared to electrochemical batteries, is that in DLCs, in principle, no electrochemical reactions or phase changes take place, or they are strongly reduced, and all of the energy is stored in an electrostatic field using the reversible

adsorption of the ions of the electrolyte onto active materials that are electrochemically stable and have high accessible specific surface areas. For this reason, the process is highly reversible, and the charge-discharge cycle can be repeated frequently and virtually without limit. Each electrode-electrolyte interface represents a capacitor; therefore, the complete cell comprises two capacitors in series. The thickness of the double layer depends on the concentration of the electrolyte and on the size of the ions and is on the order of 5–10 Å for concentrated electrolytes. The double layer capacitance is about 100–200 F/m² for a smooth electrode in a concentrated electrolyte solution [1].

The electrode surface area is increased by using porous electrodes with an extremely large internal effective surface of up to 3000 m²/g of activated carbon. These last two construction details make it possible to realize, considering parasitic effects and the total active mass (electrodes and electrolytes), supercapacitor storage devices of up to 75 F/g. The double layer is also called the Helmholtz layer after the physicist who introduced the model to explain this phenomenon in 1853 [1].

2.1.1. SUPERCAPACITOR CLASSIFICATION

The dynamic behaviors of supercapacitors are strongly related to the ion mobility of the electrolyte used and to the porosity effects of the porous electrodes; the storage process in the double layer is a superficial effect, consequently the electrode surface behaviors play an important role. The most common DLCs for industrial applications are based on carbon for the electrode materials and an organic solution for the electrolyte, typically acetonitrile. In order to classify supercapacitors, the electrode material and electrolyte type are extensively discussed in the following.
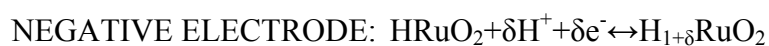
2.1.2. ELECTRODE MATERIAL

As is known, the charge storage process in the double layer interface is greatly influenced by the surface characteristics of the electrodes. Consequently, the electrode materials play a crucial role in determining the properties and cell performances of supercapacitors. The common materials used are:

- Carbon. According to manufacturer's technology, carbon is used in various modifications. The main reasons for choosing this material are related to the low cost (typically coconut shells are used), high surface area, and the fact that it is an established electrode production technology. In addition, the use of carbon

materials make it possible to realize a specific surface area of up to 3000 m2/g and a charge storage in the electrochemical double layer that is predominantly capacitive. There are two main carbon electrodes: activated carbon electrodes and nanostructured electrodes. The first is the most common in industrial applications due to the low cost of its production because of the specific surface area. The carbon forming the electrodes is attached to the metallic collector using a bonding agent. The thermal activation process makes the carbon electrodes highly porous. The interest in nanostructured electrodes is connected to the possibility of realizing a regular porous structure with an average pore diameter of 2 nm. The main problems, actually, are associated with the growth on the conducting current collector, density of tubes, carbon weight per cm2 of collector, and achievable electrolyte molarity [2]. Nowadays, industrial carbon-based electrochemical capacitors mainly store energy in an electrostatic field. Therefore, the pseudocapacitance contributions from surface functional groups, typically redox reactions, can be neglected and controlled in the manufacturer's process.

- Metal oxides. Metal oxide electrodes show good performances related to the capacitive effect, up to 750 F/g, but they are characterized by the presence of a high number of redox reactions in the metallic oxide. Thus, the capacitive effect is mainly related to electrochemical reactions. Favored metal oxides are RuO_2, IrO_2, and other noble metals realized by thermal or electrochemical processes. These materials have excellent electrical conductivity and a surface area of up to 100 m2/g. By applying a sufficient potential difference between electrodes, a redox reaction takes place; for example, when RuO_2 is used as the electrode, the two semi-reactions and global reaction that take place are [3]:

POSITIVE ELECTRODE: $HRuO_2 \leftrightarrow H_{1-\delta}RuO_2 + \delta H^+ + \delta e^-$

NEGATIVE ELECTRODE: $HRuO_2 + \delta H^+ + \delta e^- \leftrightarrow H_{1+\delta}RuO_2$

GLOBAL REACTION: $HRuO_2 + HRuO_2 \leftrightarrow H_{1-\delta}RuO_2 + H_{1+\delta}RuO_2$

The main reason for using RuO_2 as the electrode material is related to the independence of the capacitance on the applied voltage. High capacitance values are obtainable by using IrO_2 as the electrode material, but the strong voltage dependence on the capacitance must be taken into account. Both solutions are

strongly limited from an industrial point of view due to the high cost of the noble metals used.

- **Polymer.** Polymeric materials such as p- and n-doped poly (3-arylthiopene), p-doped poly (pyrrole), poly (3-methylthiophene), or poly (1,5-iaminoanthraquinone) can be used as electrodes for electrochemical redox supercapacitors because the kinetics of the electrochemical charge-discharge processes, known as doping-undoping, are generally fast [4]. Compared to metallic oxides, polymeric electrodes can be realized at a lower cost, which makes them interesting from an industrial point of view. Furthermore, these materials have the peculiarity to be doped, in a way similar to semiconductors, so that the conductivity, according to the oxidation or reduction reaction in which the electrode is interested, can be controlled. Another difference between polymeric and metallic oxides is related to the redox reactions that take place: a unique redox reaction type in polymeric materials and different ones in oxide metallic electrodes. This means that the production process for polymeric electrodes can be easily controlled.

2.1.3. ELECTROLYTE TYPE

The electrolyte selection is as important as the electrode one. The maximum working voltage for a supercapacitor cell is mainly limited by the decomposition voltage of the electrolyte, so that the energy density is strongly limited by it. In addition, the power density, limited by the internal resistance of the device, is mainly related to the electrolyte conductivity.

The choice of the coupled electrode-electrolyte must be carefully evaluated because the dimensions of the pores on the electrodes have to be designed according to the electrolyte ion molecular dimension. There are 2 main electrolyte categories:

- Organic. Organic electrolyte is the one that is most used in commercial devices and is characterized by a higher achievable voltage despite being of the aqueous type. Common cells using these electrolytes reach a unit cell voltage above 2 V, typically in the range of 2.5–3 V. The limitation on the cell voltage is due to the water content of the electrolyte and impurity in the solution. Different research projects have shown the possibility of increasing the maximum operative voltage by purification processes for the electrolyte, but in this case the electrode corrosion must to be

controlled by protective coatings [5]. The main gap is due to the specific resistance, which is greater than the aqueous electrolyte type by at least a factor of 20. This affects the maximum deliverable power and the total efficiency of the device.

- Aqueous. Technically, the advantages in using aqueous electrolytes are related to the higher conductance and the easier purification and drying processes during production [6]. The higher conductance value is obtainable by the lower molecular dimension of the ions, which yields a lower resistance in moving through the electrode's pores. This means higher values of deliverable power are obtainable. Furthermore, the cost of an aqueous electrolyte is lower than that of the organic type. The main disadvantage is related to the lower operating voltage, which is typically 1 V. Thus, the amount of storable energy is significantly lower at the same volume. Common aqueous electrolytes are sulphuric acid and potassium hydroxide.

- Polymer. Polymers, when combined with appropriate salts, show a high ionic conductivity for use as electrolytes. Peter V. Wright, a polymer chemist from Sheffield, and his associates, first showed in 1975 that poly-ethylene oxide (PEO) can act as a host for sodium and potassium salts, thus producing a solid electrical conductor polymer/salt complex [7]. Actual studies on poly-ethylene oxide-based polymer electrolytes and ionic liquid-incorporated poly-vinylidene fluorideco-hexafluoropropylene-based gel polymer electrolytes [8] show a growing interest. The main restriction in using liquid electrolytes is related to the maximum applicable voltage. Thus, only limited values of specific power and energy can be achieved. In addition, the organic electrolytes that are commercially used suffer from safety problems related to their volatility, flammability, and toxicity. PEO-based electrolytes are some of the most promising materials due to their good thermal and electrochemical properties, even if they are hindered by a low room temperature ionic conductivity. For this reason, researchers are investigating the benefits of adding room temperature liquid electrolytes to PEO-based electrolytes to improve the ionic conductivity, as shown in [9,10], which investigated new room temperature molten salts and polymers compatible with the molten salts to achieve high ion-conductive.

2.2. FUTURE DIRECTIONS FOR SUPERCAPACITORS

The supercapacitors that are commercially available can deliver high levels of electrical power and offer long operating lifetimes. These devices are often compared to lithium-ion battery technology, with a continuing debate about the advantage of using high power lithium-ion batteries instead of supercapacitors in transportation and grid applications. From a technical point of view, supercapacitors are characterized by the faster availability of the stored energy compared to a lithium battery, with larger stored energy for the latter. With this motivation, and in order to enlarge and strengthen supercapacitor penetration in all of the typical lithium battery applications, the research aimed toward increasing their specific energy, while maintaining the same characteristics of specific power and lifespan.

Actually, the research is moving in two important directions. The first involves the study of new electrode materials in order to increase the specific surface area and consequently the related specific capacitance, while the second involves realizing hybrid supercapacitors that can exploit pseudo-capacitive metal oxides with a capacitive carbon electrode, or lithium-insertion electrodes with a capacitive carbon electrode. In this way, the cell voltage and specific energy can be improved [11].

In relation to the first direction, it is important to underline the prominent research on the use of nanotube structures for the electrodes to achieve an increased specific surface area, due to a well-ordered and precise realization of the electrode structure, despite the traditional porous one. Niu et al. first introduced the idea of a DLC using entangled multiwalled nanotubes (MWNTs) [12] and achieved prominent results usable for industrial production, as represented by the use of an electrode structure based on vertically aligned carbon nanotubes (VCNT) as the active layer. As shown in [4], specific energy densities up to 21 Wh/kg and 22 Wh/l are obtainable at a voltage of 2.7 V for a packaged DLC cell using the VCNT-based electrodes.

Another important research result regarding the electrode's structure involves the possibility of increasing the capacitance by means of pores smaller than the solvated ion size (micropores). This has been provided by experiments using carbide derived carbons (CDCs) as the active material [13, 14]. As reported in [11], there is a clear lack of understanding of the double layer charging in the confined space of micropores, where there is no room for the formation of the Helmholtz layer and diffuse layer expected at a

solid–electrolyte interface. Some recent studies [15, 16] provided some guidance for developing micropore materials with improved capacitance properties, but further material optimization may take a very long time.

The second research direction aims to improve both the energy and power density of electrochemical supercapacitors by adding an activated carbon structure with pseudo-capacitive materials (Figure 2.2), which can be characterized by fast, reversible redox reactions at the surface of the active materials.
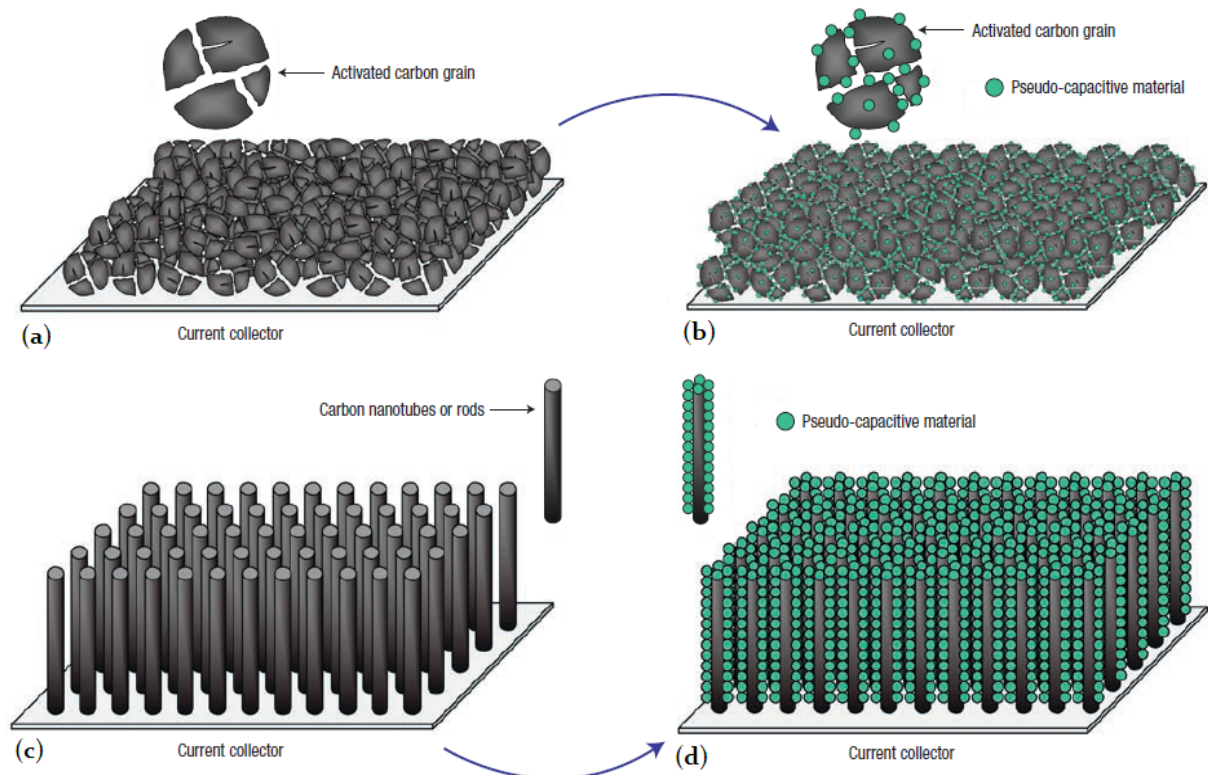
Figure 2.2. **Decoration of activated carbon grains (a) or highly ordered high-surface-area carbon nanotubes (c) with pseudo-capacitive materials, respectively (b) and (d), [11].**

Particularly interesting is the hybrid concept that originated in the Li-ion batteries field. The actual studies and first prototype products combined a lithium-insertion electrode with a capacitive carbon electrode. In particular, the interesting results on nanomaterials, as well as continuing improvements in lithium-ion technology, should lead to the design of high-performance supercapacitors. The gap between lithium-ion batteries and EDLCs could be filled by combining high-rate redox reaction anodes or lithium alloying anodes with a positive supercapacitor electrode. These devices could be very interesting in applications where high power and medium cycle life are needed, such as hybrid automotive applications.

2.3. SUPERCAPACITOR BEHAVIORS AND METHOD ANALYSIS

Commercially available supercapacitor devices are characterized by the typical performances specified in Table 2.1.

Table 2.1. Supercapacitor typical performances

Specific Energy (Wh/kg)	1 - 5
Specific Power (kW/kg)	1 - 8
Self discharge (days)	30
Cycling lifetime (cycles)	1 million
Operative Temperature Range (°C)	-40 +65
Cell operative voltage (V)	2.7 – 3.0
Efficiency	0.7 – 0.95
Specific Energy cost (€/Wh)	30 - 50

The range of collected data, particularly for the specific energy, power, and system efficiency, takes into account the performance variations according to the real condition of use. In order to better understand these aspects Figure 2.3 shows a measured Ragone plot for a real supercapacitor cell.
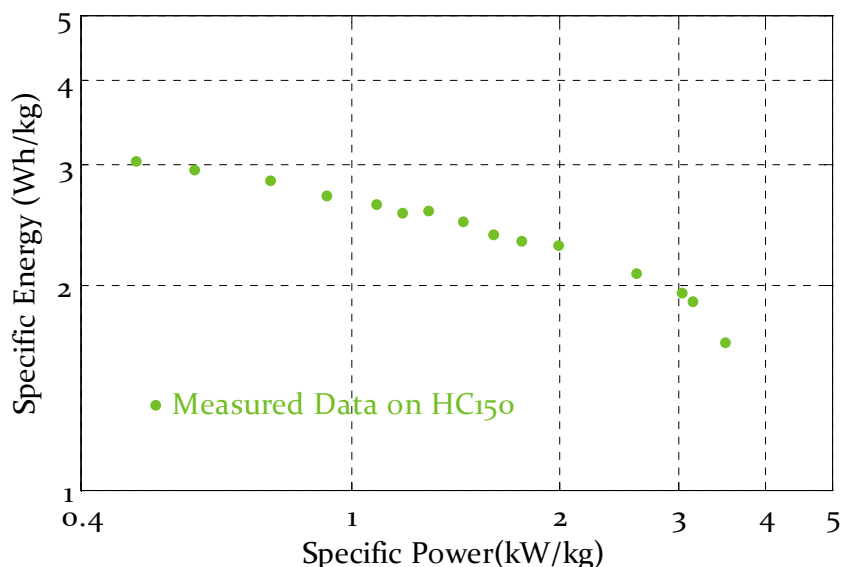

Figure 2.3. Measured Ragone plot for 150F@2.7V Maxwell Technologies cell. The specific power and energy were measured between the nominal voltage and half that value.

According to this, it is clear how the real working conditions influence the technical performances of the device in a consistent way, and how an adequate modeling is necessary in order to correctly implement and integrate the technology in real applications. A first important aspect involves the close relationship between the performances and dynamic use of the device.

The main methods for analyzing the performances of a supercapacitor are:

- Constant Current charge/discharge tests;

- Cyclic Voltammetry;

- Electrochemical Impedance Spectroscopy (EIS).

A constant current charge/discharge test is a common analysis method for evaluating device performances in terms of terminal voltage variation according to the applied charging/discharging current rate. This method, which was especially common in the past, to evaluate the performances of electrochemical batteries, is able to identify the device performances related to the steady state condition of the test. Yet, no information regarding the device dynamic response is identified in a direct way. Particularly for a supercapacitor, the charge or discharge interval is on the order of tens of seconds at a maximum, which means the test is characterized by a harmonic content that is closer to the typical dynamic use of a supercapacitor rather than to a steady state condition. In this way, the results are greatly affected by the dynamic imposed by the test, which could make it very difficult to understand the real device performances due to an overlapping of dynamic effects.

In order to improve this aspect, cyclic voltammetry has been extensively employed [17, 18] because it can analyze the device performances according to the dynamic applied. In particular, considering the relationship between the voltage and current of an ideal capacitance as:

$$i(t) = C\frac{\mathrm{d}u}{\mathrm{d}t},$$
(2. 1)

it is possible to measure the accessible capacitance, C, as the ratio between the imposed current, which is typically constant and equal to I, and the voltage sweep rate, du/dt. In the case of a pure capacitor, the response currents follow (2. 1). At a porous electrode, I increases with du/dt but, owing to the effect of the distributed resistance of the pores and electrolyte, at a rate proportional to a power of du/dt lower than 1 [19]. In other words, due to the dynamic performances of the device, the charge/discharge acceptance decreases with an increase in the voltage sweep rate so that, as shown in Figure 2.4, the area enclosed by the curve increases with the voltage sweep rate.
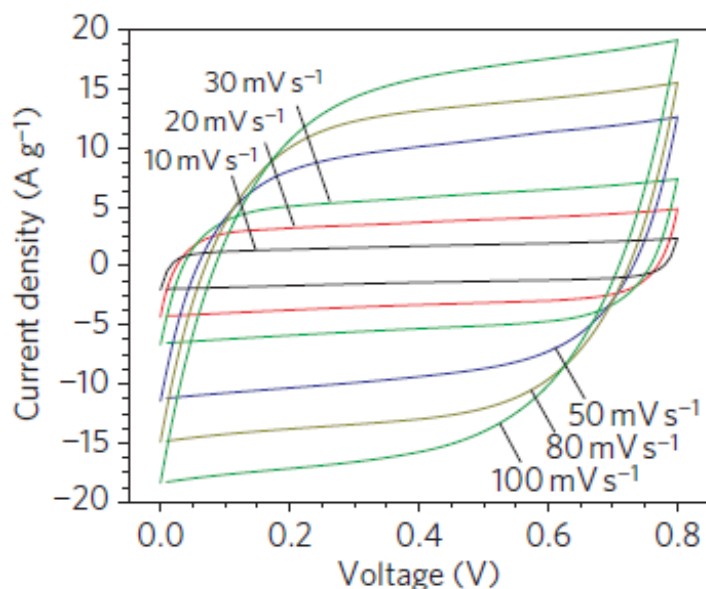
Figure 2.4. **Cyclic voltammograms (current density versus voltage) for nanoporous gold/MnO₂ electrode at six different sweep rates between 10 and 100 mV/s [20].**

Finally, electrochemical impedance spectroscopy (EIS) represents today's most used method to investigate storage device behaviors. There are three different approaches to EIS, but the most common and standard one is to measure the impedance by applying a single-frequency voltage (or current) to the terminal of the device while testing and measuring the phase shift and amplitude, or real and imaginary parts, of the resulting current (or voltage) at that frequency using either an analog circuit or fast Fourier transform (FFT) analysis of the response [21]. In particular, each test can be conducted at different polarization voltages (or currents), which means applying a sinusoidal voltage of a few tens of mV to the device at a mean value, U_{DC}. If the test is current-controlled, which is typical for electrochemical batteries, this means charging or discharging the device with a mean current value, I_{DC}, with a summed sinusoidal current in order to measure the impedance at a specific frequency.

The advantage of this technique is the possibility to investigate the dynamic device performances in the frequency range of greatest interest. In addition, the analysis results consist of the frequency response of the device, so that a direct and immediate indication of the possible electric circuit capable of modeling that dynamic is given. Finally, the punctual information regarding each single explored frequency gives precise details regarding the internal dynamic characterizing the device.

As shown in Figure 2.5, EIS directly shows the electric parameter of a device as a function of the applied frequency of use. This makes it possible to directly notice, for

example, the region in which the device behaves as a supercapacitor or the region in which no capacitance can be found. In particular, referring to a series model of the device, in this figure, the equivalent resistance and capacitance are reported.
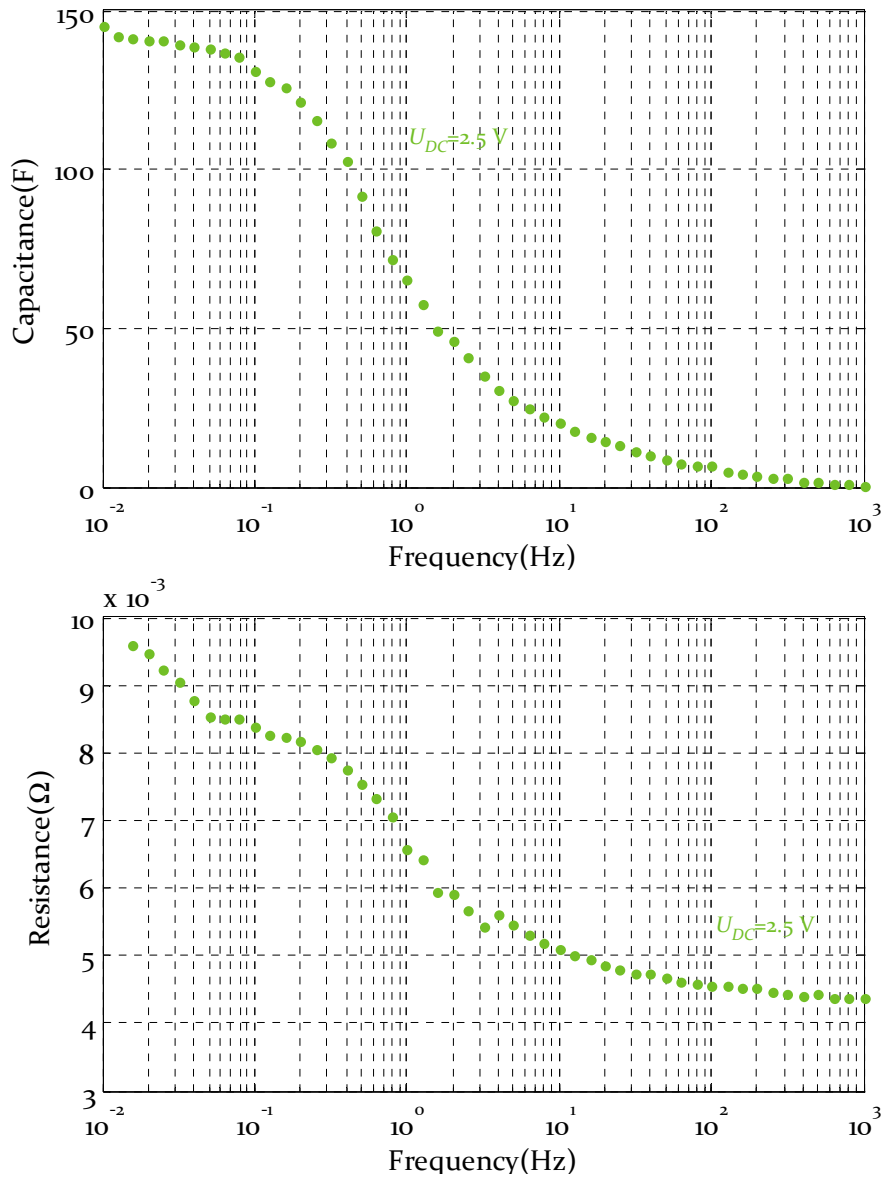

Figure 2.5. **Measured frequency response of a 140F@2.5V rated voltage Maxwell Technology cell.**

In this work, the device analyses of commercially available supercapacitors (carbon activated electrodes in an organic electrolyte) were carried out using electrochemical impedance spectroscopy (EIS) and traditional constant current charge/discharge tests.

43

2.4. SUPERCAPACITOR MODELS

2.4.1. DOUBLE LAYER CAPACITANCE

The theory of the double layer was first treated by Helmholtz in 1853, who discovered charge storage at the boundary between a conductor and ionic solution [1]. It was further investigated by the physicists Gouy, Chapman, and Stern [22 -24] (Figure 2.6). The Helmholtz double layer differential capacitance can be expressed as:

$$C_H = \varepsilon_o \cdot \varepsilon_r \cdot \frac{A}{d},$$

(2. 2)

where $\varepsilon_o \cdot \varepsilon_r$ represent the dielectric constant.

In 1913 Chapman, independently of Gouy, gave a mathematical formulation to this problem in order to describe the casual ion distribution of the "double diffused layer" by means of a Poisson equation and Boltzman distribution. The Gouy-Chapman mathematical formulation defines the double layer differential capacitance as:

$$C_{G-C} = z \sqrt{\frac{2 \cdot q \cdot n_o \cdot \varepsilon}{u_t}} \cosh \frac{z \cdot \psi_o}{2 \cdot u_t},$$

(2. 3)

where ε is the dielectric constant, z is the valence of the ions, n_o is the number of ions per cubic meter, ψ_o is the applied potential drop, q is the elementary charge, and u_t is the thermodynamic potential, which is defined as:

$$u_t = \frac{k \cdot T}{q},$$

(2. 4)

where T is the temperature in K and k is the Boltzman constant.

Finally, in 1924, Stern improved the two previously described theories by also considering the size of the ions in the solution. His theory describes the double layer configuration as consisting of two distinct zones. In the first one, the potential distribution follows a linear dependence, as in the Helmholtz theory, while in the second one, the charge distribution is a double diffusion layer, as in the Gouy-Chapman theory (Figure 2.6). It could be said that this theory is the integration of the previous theories, so that the total capacitance can be expressed as the series connection of the Helmholtz capacitance expression (2. 2) and that of Gouy-Chapman (2. 3):

$$\frac{1}{C_S} = \frac{1}{C_H} + \frac{1}{C_{G-C}}.$$

(2. 5)

From these more electrochemical models, different evolutions have been developed, taking into account also the resistive contributions of the electrodes and electrolyte. This

has produced more electrical models obtained from a network of resistors and voltage-dependent non-linear capacitor branches.
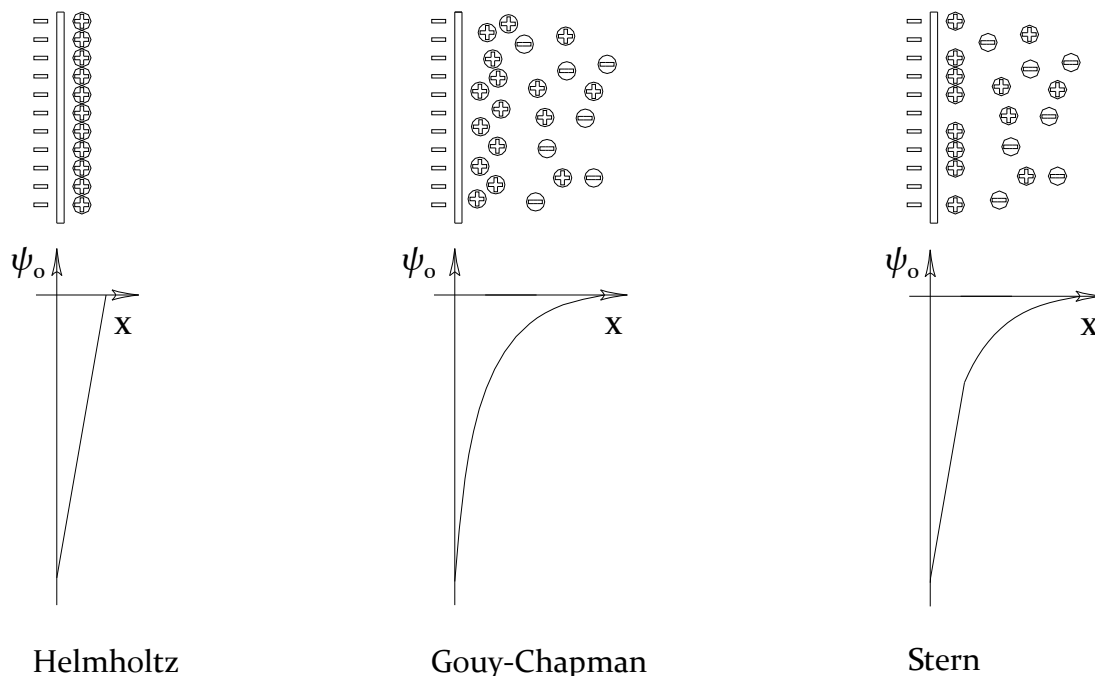

Figure 2.6. **Potential drop distribution at electrode interface according to Helmholtz, Gouy-Chapman and Stern models.**

2.4.2. *THE ROUGH AND POROUS ELECTRODE IMPEDANCE*

The use of rough and porous electrodes is the most common technical solution adopted to greatly increase the double layer surface. De Levie [25, 26] first analyzed and presented a model describing the pores of a porous electrode as essentially circular cylindrical channels of uniform diameter and semi-infinite length. If the series resistance of the electrolyte per unit length is r, and the interfacial capacitance per unit length is c, then the pore behaves as a transmission line with open-circuited output terminals (Figure 2.7). The last condition makes it possible to describe the mass transport impedance due to linear diffusion in a plane sheet with an impermeable boundary (restricted diffusion) [27], which is typical in a double layer interface.
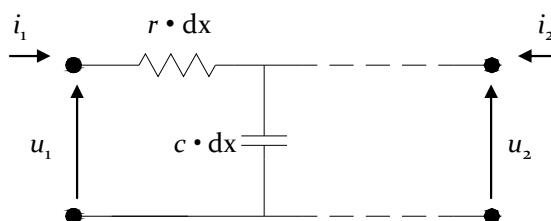

Figure 2.7. **Resistive-Capacitive transmission line circuit representing behavior of semi-infinite diffusion process.**

By solving the electric circuit in Figure 2.7 the equivalent impedance at the input terminals, u_1-i_1, when the abscissa x = l, with l the pore length, can be written as:

$$Z_p(j\text{w}) = \sqrt{\frac{r}{j\text{w} \cdot c}} \cdot \coth\left(l \cdot \sqrt{r \cdot j\text{w} \cdot c}\right) \qquad (2.\,6)$$

As shown in [28,29] the inverse transform of the general expression reported in (2. 7)

$$G(j\text{w}) = \frac{k_1}{\sqrt{j\text{w}}} \coth\left(\frac{k_2}{k_1}\sqrt{j\text{w}}\right) \qquad (2.\,7)$$

is equal to

$$g(t) = \frac{k_1^{\,2}}{k_2} + \frac{2 \cdot k_1^{\,2}}{k_2}\sum_{n=1}^{\infty} e^{\left(-\frac{n^2 \cdot p^2 \cdot k_1^{\,2}}{k_2^{\,2}}\right)t}, \qquad (2.\,8)$$

which means, by comparing the expression in (2. 6) with (2. 7), the inverse transform of $Z_p(j\omega)$ in (2. 6) is equal to:

$$Z_p(t) = \frac{1}{c \cdot l} + \frac{2}{c \cdot l}\sum_{n=1}^{\infty} e^{\left(-\frac{n^2 \cdot p^2}{r \cdot c \cdot l^2}\right)t}. \qquad (2.\,9)$$

It is important at this point to underline the close relationship between the two models represented in Figure 2.8. Figure 2.8(a) is the transmission line model arising from the De Levie theory reported above, while Figure 2.8(b) is the circuit representation of the Z_p impedance in the time domain of (2. **9**). The two circuits can all yield the same impedance for all frequencies when their elements are properly related.
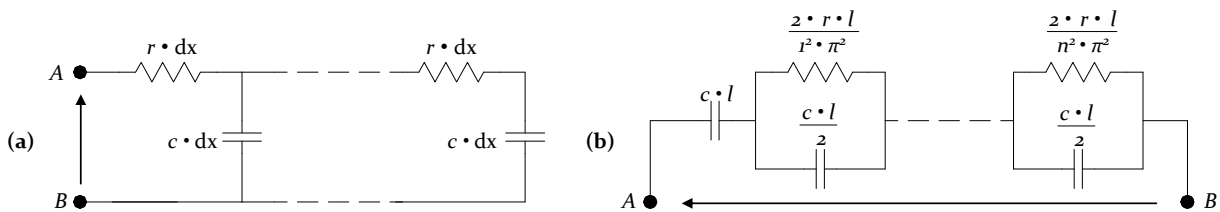

Figure 2.8. Two equivalent circuits when circuit parameters are properly interrelated. The transmission line model (a) for x = l (pore length) is equal to the series model (b).

The benefit of using one model rather than the other is mainly due to the possibility to use the continuity and knowledge of the physical processes involved and to relate the circuit parameters to specific or physical quantities that can be easily measured. As will be shown in the next chapter, the representation in Figure 2.8(b) makes it possible to introduce a simplified parameter identification procedure based on the specific measurements of physical quantities.

2.4.3. SUPERCAPACITOR ELECTRICAL MODELS

Different models have been developed from the above physical approaches (Figure 2.9) [28, 30-35]. These are more or less complicated according to their ability to properly model the DLC behavior. In fact, the majority do not arise from the punctual physical consideration reported above. On the other hand, some of these models, despite their poor accuracy, are characterized by a very simple parameter identification procedure. The easiest and most common simplified model is the classical equivalent model shown in Figure 2.9(a). It consists of an ideal capacitor, C; an equivalent series resistor (ESR), modeling the internal device resistance; and an equivalent parallel resistor (EPR), which takes into account the self-discharge. This model is very easy to use as the parameter identification procedure, but the validity of its results are strictly dependent on the test conditions in which the parameters are identified. As previously introduced, the dynamic behavior of supercapacitors is non-linear. Thus, this model is especially inadequate when the dynamic has to be considered.
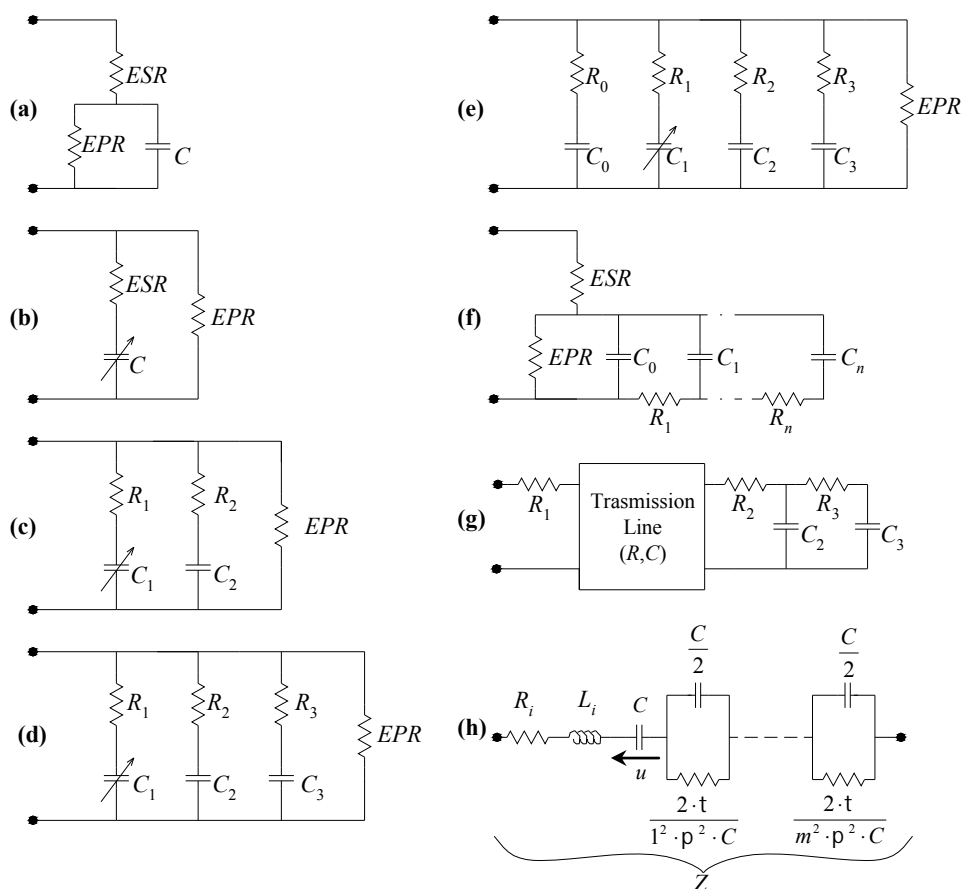

Figure 2.9. Some electrical models taken from literature: (a) classical model, (b) non-linear capacitance model, (c) two-branch model, (d) three-branch model, (e) four-branch model, (f) ladder model, (g) transmission line model, and (h) series model.

A first evolution of the DLC model is the non-linear capacitance model shown in, Figure 2.9(b) [30]. This model takes into account the non-linearity of the equivalent capacitance of the device according to the polarization voltage by means of a non-linear capacitance with its applied voltage. This model, which is easy enough to use, lacks the ability to characterize long-term DLC behavior, due to its lack of additional elements to represent the redistribution phenomena, and the high dynamic of the charge/discharge of the device.

More advanced lumped models are represented by the two-branch model, Figure 2.9(c) [31], three-branch model, Figure 2.9(d) [32], and four-branch model, Figure 2.9(e) [33, 34]. These models, all characterized by a parameter identification procedure based on the constant current charging test, are valid for modeling the low frequency behaviors of a supercapacitor, but they are not accurate at high frequencies. These models differ from each other in the way they represent the DLC's medium- and long-term behaviors. In fact, according to the number of parallel branches, the low dynamic of the device, redistribution phenomena, and self discharge are correctly represented, but the first branch is inadequate to represent the supercapacitor's dynamic behaviors when the charge and discharge frequencies are over 0.1 Hz. In addition, many of these models require precise and accurate measurements in order to identify the first branch parameters.

The ladder model of Figure 2.9(f) and the transmission line model of Figure 2.9(g) [35] are also very difficult to implement due to the parameters identification procedure.

Finally the series model of Figure 2.9(h) is able to represent the high dynamic of the device in a frequency range of tens of mHz to hundreds of Hz [28]. In contrast to the other models, this last one arises from an EIS analysis of the device, so that the aim of the equivalent electric circuit is to model the real frequency response of the device. However, this model, due to its lack of parallel branches, is not able to model either the self-discharge or the charge redistribution that is typical at low frequency. In addition, for the model parameters, it is necessary to identify the complete frequency response of the device (EIS), which means the use of sophisticated laboratory instruments.

The first aim of this work is introducing, in the next chapter, a new supercapacitor model that is:

- capable of representing the full dynamic of the device;

- based on the frequency response of the device;

- characterized by a very simplified parameter identification procedure.

The new model is characterized by a complete modularity so that the equivalent circuit can be tailored according to the desired accuracy in representing the device behaviors. In addition, it will be shown how this model can be reduced to one of the models previously described, and the points that the different models have in common will be shown in terms of modeling and the parameter identification procedure.

Finally, the correlation between specific macroscopic parameters and device performances will be presented, which is very useful both for a comparison between different devices as a guideline and for their construction.

2.5. BIBLIOGRAPHY

[1]   H. Von Helmholtz, Annalen der Physik, 1879.

[2]   R. Signorelli, D.C. Ku, J.G. Kassakian, J.E. Schindall, Electrochemical Double-Layer Capacitors Using Carbon Nanotube Electrode Structures, Proceedings of the IEEE, vol 97, n.11, November 2009.

[3]   Yu. M. Vol'fkovich and T. M. Serdyuk, "Electrochemical Capacitors", Russian Journal of Electrochemistry, Vol. 38, N. 9, 2002, pp. 935-959, DOI: 10.1023/A:1020220425954.

[4]   C. Arbizzani, M. Mastragostino, L. Meneghello: "Polymer-based redox supercapacitors: a comparative study", Electrochim. Acta 41 (1996).

[5]   A. Yoshida, K. Nishida, S. Nonaka, S. Nomoto, M. Ikeda, S. Ikuta, Japanese Patent 9-266143, (to Matsushita Electric), 1997.

[6]   R. Kotz, M. Carlen: "Principles and applications of electrochemical capacitors", Electrochimica Acta, Pages. 2483-2498, Vol.45.

[7]   P. V. Wright, "Electrical conductivity in ionic complexes of poly(ethylene oxide)", British Polymer Journal, Vol 7, 1975, pp. 319–327.

[8]   G. P. Pandey, Y. Kumar, S. A. Hashmi, "Ionic liquid incorporated polymer electrolytes for supercapacitor application", Indian Journal of Chemistry, Vol. 49A, 2010, pp. 743-751.

[9]   A. Noda, M. Watanabe, "Highly conductive polymer electrolytes prepared by in situ polymerization of vinyl monomers in room temperature molten salts", Electrochimica Acta, Vol. 45, 2000, pp. 1265–1270.

[10]   T. Ueki, M. Watanabe, "Macromolecules in Ionic Liquids: Progress, Challenges, and Opportunities", Macromolecules, Vol. 41-11, 2008, pp. 3739-3749.

[11]   P. Simon, Y. Gogotsi, "Materials for electrochemical capacitors", Nature Materials, Vol. 7, 2008, pp. 845-854.

[12]   C. Niu, E. K. Sichel, R. Hoch, D. Moy, and H. Tennent, BHigh, "Power Electrochemical Capacitors based on Carbon Nanotube Electrodes", Appl. Phys. Lett., Vol. 70, 1996, pp. 1480–1482.

[13]   A. Janes, E. Lust, "Electrochemical characteristics of nanoporous carbide-derived carbon materials in various nonaqueous electrolyte solutions", J. Electrochem. Soc., Vol. 153, 2006, A113–A116.

[14]   B. D. Shanina, "A study of nanoporous carbon obtained from ZC powders (Z = Si, Ti, and B)", Carbon, Vol. 41, 2003, pp. 3027–3036.

[15]   J. Chmiola, C. Largeot, P. L. Taberna, P. Simon, Y. Gogotsi, "Desolvation of ions in subnanometer pores, its effect on capacitance and double-layer theory", Angew. Chem. Int. Ed., Vol. 47, 2008, pp. 3392-3395.

[16]   C. Largeot, "Relation between the ion size and pore size for an electric double-layer capacitor", J. Am. Chem. Soc., Vol. 130, 2008, pp. 2730–2731.

[17]   B.E. Conway, Electrochemical Supercapacitors: Scientific Fundamentals and Technological Applications, Kluwer-Plenum, New York, 1999, ISBN 0-306-05736-9 1.

[18]   K. Kinoshita, "Carbon–Electrochemical and Physicochemical Properties", John Wiley Sons, New York, 1988.

[19]   W.G. Pell, B.E. Conway, "Voltammetry at a de Levie brush electrode as a model for electrochemical supercapacitor behaviour", Journal of Electroanalytical Chemistry, Vol. 500, 2001, pp. 121–133.

[20]   X. Lang, A. Hirata, T. Fujita, M. Chen, "Nanoporous metal/oxide hybrid electrodes for electrochemical supercapacitors", Nature Nanotechnology, Vol. 6, 2011, pp. 232-236.

[21]   E. Barsoukov, J. R. Macdonald, "Impedance Spectroscopy Theory, Experiment, and Applications", John Wiley & Sons, Inc, 2005, ISBN: 0-471-64749-7.

[22]   G. Gouy, Compt. Rend. 149 (1910) 654.

[23]   D.L. Chapman, Philos. Mag. 25 (1913) 475.

[24]   O. Stern, Z. Elektrochem. 30 (1924) 508.

[25]   R. de Levie, "Porous Electrodes in Electrolyte Solutions, I", Electrochim. Acta Vol. 8, 1963, pp. 751.

[26]   R. de Levie, "On Porous Electrodes in Electrolyte Solutions, II", Electrochim. Acta Vol. 9, 1964, pp. 1231–1245.

[27]   J.P. Diard, B. Le Gorrec, C. Montella, "Linear diffusion impedance. General expression and applications", Journal of Electroanalytical Chemistry, Vol. 471, 1999, pp. 126–131.

[28]   S. Buller, E. Karden, D. Kok, R. W. De Doncker: "Modeling the dynamic behaviour of supercapacitors using impedance spectroscopy", Industry Applications Conference, Vol. 4, 2001, pp. 2500 – 2504

[29]   P. Mauracher, "Modellbildung und Verbundoptimierung bei Elektrostraßenfahrzeugen," Ph.D. dissertation, RWTH Aachen, Aachen, Germany, 1996.

[30] D. Casadei, G. Grandi, C. Rossi, "A supercapacitor based power conditioning system for power quality improvement and uninterruptible power supply", in Proc. IEEE International Symposium on Industrial Electronics (ISIE 2002), 8-11 July 2002, pp.1247–1252.

[31] R. Faranda: "A new parameters identification procedure for simplified Double Layer Capacitor two-branch model", Elsevier Electric Power Systems Research, Volume 80, Issue 4, April 2010, Pages 363-371, ISSN: 0378-7796.

[32] L. Zubieta, R. Bonert, "Characterization of double layer capacitors for power electronic applications", IEEE Trans. Industry Application, vol. 36, no. 1, pp. 199–204, Jan/Feb 2000.

[33] F. Castelli Dezza, M. Diforte, S. Gervasini, M. Mauri, "An improved model of a double layer capacitor for power electronics applications", Proc. Of. 11th International Power Electronics and Motion Control Conference EPE/PEMC, Riga, Latvia, September 2-4, 2004.

[34] R.N. Nelms, D.R. Cahela, B.J. Tatarchuk, "Modeling double-layer capacitor behaviour using ladder circuits", IEEE Trans. Aerospace Electronic Systems, vol. 39, n.2, Apr 2003, pp.430–438.

[35] F. Belhachemi, S. Raël, B. Davat, "A physical based model of power electric double-layer supercapacitors", in Conf. Record of the 2000 IEEE Industry Applications, 8-12 Oct. 2000, pp.3069–3076.

3. *SUPERCAPACITOR MODEL AND PARAMETER IDENTIFICATION PROCEDURE*

The model adopted and experimentally validated is based on the frequency response of the device in the frequency range of 1 mHz to 10 kHz and the analysis of the open circuit voltage in order to correctly model the full dynamic of the device ranging from the self discharge up to a highly dynamic charge-discharge.

In contrast to other simplified models, the Complete-dynamic model makes it possible to accurately evaluate the supercapacitor efficiency as the terminal voltage variation due to the charge redistribution in the porous electrodes by means of the R-C parallel branches. Each parallel branch represents the device behavior in a certain frequency range and, in order to take into account the full device dynamic, all of the branches have to be parallel connected.

The electric circuit reported in Figure 3.1, consists of a first branch able to model the fast dynamic of the device a certain number of parallel branches, a priori chosen according to the accuracy wanted in modelling the supercapacitor charge redistribution and self-discharge.
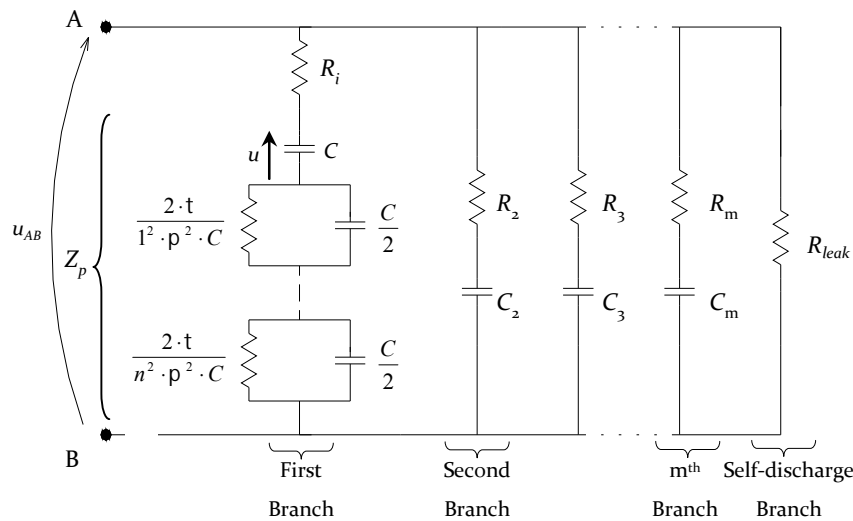

Figure 3.1.   *Complete-dynamic* **supercapacitor model.**

The possibility of estimating parameters using very simple tests is a very important point for the usability of the model. It is clear that the parameter values that give the best match between the model reported in Figure 3.1 and the experimental data can be obtained with least square error minimization. This procedure is too complex to be performed every time and requires the use of dedicated laboratory equipments in order to

conduct the electrochemical impedance spectroscopy (*EIS*) that makes it possible to obtain the experimental curve of impedance versus frequency. Thus, an easier procedure is proposed in the following and the parameters obtained using least square error minimization are used to verify the simplified procedure.

The temperature influence on the supercapacitor behavior is not analyzed because the DLC temperature is assumed to be constant, as in the simplified models described in [1-4], and because this does not affect the proposed simplified procedure for the parameter identification.

3.1. FIRST BRANCH PARAMETERS IDENTIFICATION

The first branch makes it possible to model the short-terms supercapacitor behaviors in the charge-discharge frequency range of 100 mHz–1 kHz. In this time domain a crucial role is played by the porous and rough electrode behaviors and, in particular, it must be taken into account the double layer capacitance dependence with the applied voltage according to the equation (2.3). This means that the constitutive equations for the capacitance between the applied voltage and the storage charge is non linear as reported in (3. 1), Figure 3.2.

$$q = f(u) \tag{3.1}$$

In order to evaluate the equivalent impedance of the supercapacitor in the above reported frequency range, due to the presence of a non linear element, the small signal analysis can be applied. This is a common analysis technique to approximate the behavior of a nonlinear device with linear equations, that means, with reference to the equation (3. 1), to approximate the expression of the stored charge in U_O as the product of the differential capacitance C_d, that is the tangent of the curve in U_O, with the voltage U_O
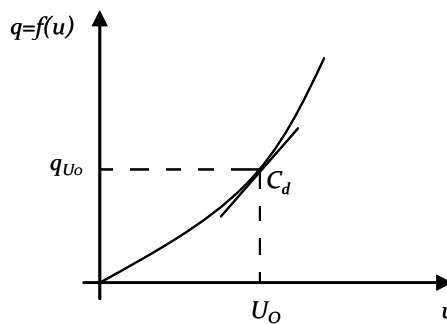

Figure 3.2. **Non linear dependence of the charge stored in a capacitor with the applied voltage.**

In general framework, Figure 3.3, a linear impedance $Z(j\omega)$ series connected to the non linear capacitance C is supplied by a small AC supply $e_{AC}(t)$ in series with the DC supply E_c. Due to the linearity of the circuit with the exception of the capacitance C^*, it's allowed considering the Thevenin equivalent circuit at the capacitance terminals
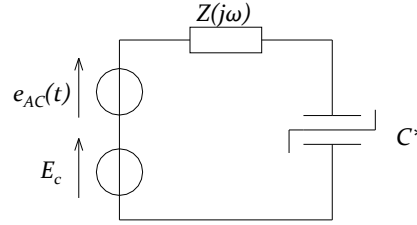
Figure 3.3. **Equivalent circuit of the first two branches during first redistribution interval.**

The solution of the circuit can be written as the sum of the DC solution plus adding terms, in particular:

$$u_Z(t) = U_{Z-DC} + u_{Z-AC}(t);$$
$$u(t) = U_{DC} + u_{AC}(t); \tag{3.2}$$
$$i(t) = I_{DC} + i_{AC}(t).$$

where the "DC" terms representing the solution arising from the evaluation of the working point subjected to the DC supply, or polarization values, while the "AC" terms arising from the AC supply. In particular in DC condition the voltage U_{DC} on the capacitance C^* is equal to E_C. The solution of (3.1) can be written as the sum of the DC solution plus the adding terms and by approximating the non linear characteristic of the capacitance with the first two Taylor series terms it results:

$$q(U_{DC} + u_{AC}) \approx q\big|_{u=U_{DC}} + \frac{dq}{du}\bigg|_{u=U_{DC}} \cdot u_{AC} = q_{DC} + C_d \cdot u_{AC} \tag{3.3}$$

where C_d represents the differential capacitance function of the applied voltage. By subtracting the DC solution to the complete one it results:

$$e_{AC}(t) = u_{Z-AC}(t) + u_{AC}(t) = u_{Z-AC}(t) + \frac{1}{C_d}\int i_{AC}(t) \cdot dt \tag{3.4}$$

The AC supply is sinusoidal by hypothesis and in addition the equation results linear, so it is correct considering the phasor representation at the angular frequency ω imposed by the AC supply, so that it results:

$$\overline{E}_{AC} = \overline{Z} \cdot \overline{I} + \frac{\overline{I}}{jw \cdot C_d}$$

$$\overline{V}_{AC} = \frac{\overline{I}}{jw \cdot C_d} \tag{3.5}$$

The expression in (3. 5) is the approximate solution in sinusoidal regime due to the small signal supply. In particular the approximation arises from the substitution of the non linear characteristic with the tangent in the DC working point. This is possible if the variation despite of the DC value U_{DC} are enough small with respect to the bending of the non linear characteristic in the considered point.

In presence of more than one non-linear elements the linearization procedure to study the circuit is the following:

- the DC solution of the circuit is determined. This is a non linear problem and more than one solutions can be determined;

- the non-linear elements are linearized with the approach reported above; in other words the non linear resistances and capacitances are linearized in the desired DC working point;

- the phasor analysis is introduced in the linearized circuit considering the presence of small signal generators

- the global solution is obtained by summing the DC solution to the sinusoidal one.

This reported theoretical approach is the basis of the Electrochemical Impedance Spectroscopy (EIS) previously introduced in chapter 2, with which it's possible measuring the device impedance for each frequency ω and for each polarization DC voltage U_{DC}. In particular the pore impedance $Z_p(j\omega, U_{DC})$, according to (2.6), can be expressed as:

$$Z_p(j\omega, U_{DC}) = \sqrt{\frac{R(U_{DC})}{j\omega \cdot C(U_{DC})}} \cdot \coth\left(\sqrt{j\omega \cdot R(U_{DC}) \cdot C(U_{DC})}\right) \tag{3.6}$$

where $R(U_{DC})$ and $C(U_{DC})$ are the electrolyte resistance and double layer capacitance respectively, as functions of the polarization voltage U_{DC}. According to (2.9), this impedance in the time domain can be expressed as:

$$Z_p(t) = \frac{1}{C} + \frac{2}{C}\sum_{n=1}^{\infty} e^{\left(-\frac{n^2 \cdot \pi^2}{R \cdot C}\right)t}. \tag{3.7}$$

In other words, Z_p consists of the series connection of the differential capacitance C with, in theory, infinite $R'C'$ parallel branches, where:

$$R' = \frac{2 \cdot R}{n^2 \cdot \pi^2} = \frac{2 \cdot \tau}{n^2 \cdot \pi^2 \cdot C} \qquad \text{and} \qquad C' = \frac{C}{2} \tag{3.8}$$

with $\tau = R \cdot C$. For practical use, the number of $R'C'$ parallel branches can be limited to 4-5 in order to achieve a sufficient accuracy. As explained later, C is the voltage dependent

differential capacitance value, and τ, dimensionally a time, is the time constant of the pore and is strictly related to the dynamic behavior of the supercapacitor.

As reported in (3. 9), C and τ can be expressed as functions of the voltage, u. During the experimental tests, it was verified that C and τ vary almost linearly with the voltage:

$$
\begin{aligned}
C &= C_0 + k_C \cdot u \\
\mathrm{t} &= \mathrm{t}_0 + k_{\mathrm{t}} \cdot u
\end{aligned}
$$

(3. 9)

By analyzing the expression in (3. 6) the following limits, which represents the DC condition, can be easily verified:

$$
\lim_{\mathrm{w}\to 0} R_i + \mathrm{Re}\{Zp\} = R_i + \sum_{n=1}^{\infty} \frac{2 \cdot \mathrm{t}}{n^2 \cdot \mathrm{p}^2 \cdot C} = R_i + \frac{\mathrm{t}}{3 \cdot C} = Ri + \frac{R}{3};
$$

$$
\lim_{\mathrm{w}\to 0} \mathrm{Im}\{\mathrm{w} \cdot Zp\} = -\frac{1}{C}.
$$

(3. 10)

From these two expressions, it is clear that, at very low frequency, the supercapacitor shows its full DC capacitance as a function of the voltage and a resistance as the contribution of the electrolyte resistance, $R(U_{DC})$, and internal ohmic resistance, R_i,. For high frequencies, the following can also easily be verified:

$$
\lim_{\mathrm{w}\to\infty} R_i + \mathrm{Re}\{Zp\} = R_i,
$$

(3. 11)

which indicates that, at high frequencies, the complex pore impedance tends to become zero, and the resistance contribution is related only to the resistance, R_i, which takes into account the ohmic contributions of the electrodes and collectors.

All of the parameters of the first branch can be determined by just measuring the device impedance in a specific frequency region without analyzing the complete frequency response of the device. Due to the presence of other parallel branches, which are responsible for the charge redistribution in the porous electrodes and self discharge, a zero frequency test cannot be performed because, in this case, all of the others parallel branches cannot be ignored. In order to neglect their contribution, the measurement should be made at tens of mHz. As shown in the following (section 3.3 from Figure 3.8 to Figure 3.11), by analyzing the frequency response for different voltages, v, at tens of mHz, the real part of Zp is almost independent of the voltage and equal to R_1, so that it is possible to evaluate $\tau\,(u\,)$ as:

$$
\mathrm{t} = 3 \cdot C \cdot (R1 - R_i);
$$

(3. 12)

measuring the impedance at very low frequency. This means that using the R_1 resistance and capacitance C at tens of mHz, and resistance R_i at a high frequency of some kHz, it is possible to estimate all of the parameters of the first branch for a fixed voltage. Repeating

the tests at different voltages, it is possible to estimate parameter k_c, which takes into account the variability of the capacitance with the voltage.

3.2. PARAMETER IDENTIFICATION FOR MEDIUM-LONG TERM BRANCHES

Using just the first branch, it is not possible to take into account the charge redistribution and self discharge in the porous electrode structure. This aspect is very important to take into account when the efficiency of the device has to be modeled. A fast charge, starting from a fully discharged device, causes an accommodation of a certain amount of charge in the non-uniform structure of the electrodes. Practically, due to the non-uniform structure of the electrodes, there are a certain number of pores that are not easily accessible by ions in order to realize the interface layer where the energy is stored. When the device is charged, the ions first move toward the pores characterized by a lower equivalent resistance, which means easily accessible pores. Consequently, the other pores characterized by higher resistance values, because they are difficult to access due to their geometric disposal, are also reached by other ions. In other words, the full capacitance of the device is not accessible with the same dynamic. Consequently, after stopping a charge phase, started with the device fully discharged, there are a certain number of ions that slowly move toward less accessible pores, which causes a voltage reduction in the device terminal voltage, because increasing the total accessible pores increases the total equivalent capacitance.

This redistribution causes a voltage reduction in the terminal voltage that can be mathematically expressed as the sum of several exponential terms, as reported in the following:

$$u_{a-b}(t) = \sum_{k=1}^{m} A_k \cdot e^{-\frac{t}{t_k}}.$$

(3. 13)

This phenomenon, due to the non-uniformity of the porous electrode structure, causes greater values for the time constants of the pores in certain regions with, in particular, greater values for the equivalent resistance with which ions move in tight pores. This indicates that a certain amount of charge is trapped in these non-uniform zones of the electrode or, in other terms, this charge can be delivered at a very low dynamic and with a very low efficiency.

The number of parallel branches needed to model this phenomenon depends on the amount of non-uniformity in the structure of the porous electrodes. According to the level of accuracy desired, the number of parallel branches can be chosen a priori. The medium-long-term behavior of the device is represented by m RC branches in parallel, the redistribution phenomena for 2 to m branches, and the self-discharge for the last branch. The number of branches, m, can be chosen so that the time constant values vary significantly from one branch to another. Thus, the discharge curve can be split into m intervals. In interval k, only the branches from 1 to k are involved in the energy transfer. All of the other branches, due to their higher time constants, are not affected by the redistribution phenomenon because it is not started yet.

To simplify the parameter identification procedure, the time intervals can be chosen independently from the cell under consideration. According to (3. 13), in this choice, the only restriction is that the time intervals have to be far enough away from each other so that, in each transient, all of the other previous branches can be considered to be in a steady-state condition. Based on an analysis of the experimental data, it has been observed that a good solution in the choice of the time intervals, I, is to use intervals that are equidistant on a logarithmic scale, and in the ith interval, the redistribution phenomenon is mainly related only to the ith time constant, τ_i, with $\tau_i \leq M \cdot \tau_{i+1}$ and M greater than 5.

Considering t_1 as the time instant in which the redistribution starts after the complete charge and defining τ_1 as the time constant responsible for the charge redistribution from the first branch over the second branch, the time instant in which the redistribution, governed by the second branch, can be considered ended is t_2, which is equal to M times τ_1. In this interval, all of the others branches, characterized by consistently greater time constant values, are not affected by the redistribution. At this point, after time instant t_2, the redistribution phenomenon is governed by time constant τ_2, which is responsible for the charge redistribution from the first two branches over the third one and, similarly, time instant t_3 is defined as M times τ_2.

Mathematically it can be written:

$$\begin{cases} t_1 = \text{initial time for the redistribution observation} \\ t_2 = M \cdot t_1 \qquad I_1 : t_1 < t < t_2 \\ t_3 = M \cdot t_2 \qquad I_2 : t_2 < t < t_3 \qquad t_3 = M \cdot t_2 \\ \quad \vdots \qquad\qquad\qquad \vdots \qquad\qquad\quad \vdots \\ t_{m+1} = M \cdot t_m \qquad I_m : t_m < t < t_{m+1} \qquad t_m = M \cdot t_{m-1} \end{cases} \qquad (3.14)$$

subjected to $\tau_i \leq M \cdot \tau_{i+1}$ and letting time constant τ_1 be on the order of tenths of seconds.

For a fixed time window, T_w, during which the self-discharge phenomenon has to be analyzed, parameter M can be easily evaluated as:

$$M = \sqrt[m]{\frac{T_w}{t_1}}. \tag{3.15}$$

This proposed identification procedure is able to estimate all of the parameters of the parallel branches from 2 up to m+1, using m voltage measurements made at the instants given by (3. 14). In the first interval of the redistribution period, the equivalent circuit is reported in Figure 3.4.
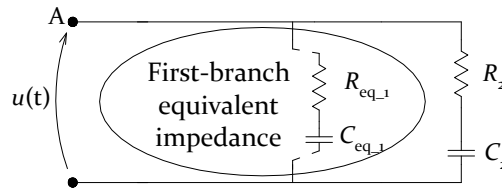

Figure 3.4. **Equivalent circuit of first two branches during first redistribution interval.**

If $u(t_1)$ and $u(t_2)$ indicate, for the considered interval, the initial and final voltages at terminals A and B, respectively, for the circuit in Figure 3.4, using the charge conservation law, it is possible to write:

$$C_2 = \frac{u(t_1) - u(t_2)}{u(t_2)} \cdot C_{eq\_1} \tag{3.16}$$

It is worth noting that when considering the first interval, capacitance C_{eq_1} is not constant. The capacitance varies when the voltage changes according to (3. 9). However, a mean constant value of capacitance between $u(t_0)$ and $u(t_1)$ can be taken into account for the parameter calculation.

Resistance R_1 can be calculated as follows:

$$R_2 = \frac{t_2}{C_2}. \tag{3.17}$$

After time interval I_1, the second redistribution interval, characterized by time constant τ_2, can be taken into account. At this point, all of the previous branches, which are in a steady-state condition, start to discharge over the $R_3 C_3$ branch.

By considering the equivalent impedance of these two branches, the expressions in (3. 16) and (3. 17) can be iteratively repeated so that parameters R_3 and C_3 can be evaluated. In a general form, the equivalent circuit at the kth interval is reported in Figure 3.5.
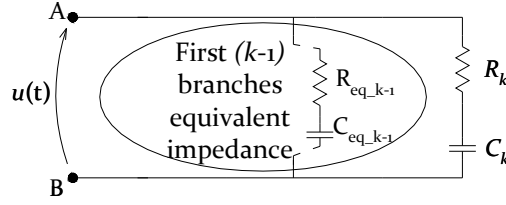
Figure 3.5. Equivalent circuit of first k branches during the kth redistribution interval.

The general expressions for parameters C_k and R_k become:

$$C_k = \frac{u(t_{k-1}) - u(t_k)}{u(t_k)} \cdot \sum_{j=1}^{k-1} C_j$$

$$R_k = \frac{t_k}{C_k}.$$

(3. 18)

If a longer time interval needs to be simulated, the general approach allows the addition of a certain number of parallel branches according to the desired accuracy to be represented.

By increasing the observation time, the parallel branches tend to increasingly represent the self-discharge phenomena only and, in particular, the resistance value is continuously increasing. In this branch, it is possible to neglect the C_{m+1} term and represent this branch using only the equivalent parallel resistance (*EPR*), Figure 3.6.
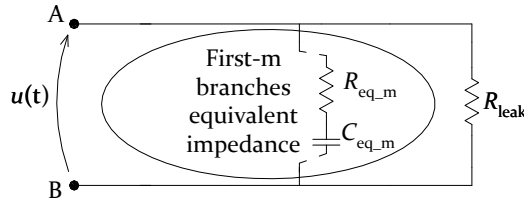

Figure 3.6. Equivalent circuit during self discharge interval.

Therefore, it is possible to determine this parameter by observing the last time interval characterized by time constant τ_m. Considering the same voltage variation at each of the m time intervals observed, the R_{leak} resistance can be evaluated as:

$$R_{leak} = \frac{t_m}{\dfrac{u(t_{k-1}) - u(t_k)}{u(t_k)} \cdot C_{eq\_m}}$$

(3. 19)

where C_{eq_m} is the equivalent capacitance of the previously evaluated m branches.

The R_{leak} value varies according to the time interval observed, because of the variation of the equivalent capacitance, C_{eq_m}. This is due to the fact that this branch should not be merely the physical resistance but, according to the number (m) of branches chosen, it also has to take into account the redistribution phenomenon of the supercapacitor device.

Using (3. 18) and (3. 19) to estimate the parameters of the parallel branches, only *m* voltage measurements are necessary: *m-1* voltage measurements in the instants t_k by means of (3. 9) plus one at the initial instant of discharge, t_1. Moreover, a simpler way to model the self-discharge behavior with the R_{leak} value is using the following equation [2].

$$R_{leak} = \frac{U_n}{I_{leakage}} \qquad\qquad (3.\,20)$$

where the nominal voltage, U_n, and the leakage current, $I_{leakage}$, are reported in the DLC manufacturer's datasheet. It is important to underline that this value of resistance is normally different from the one evaluated with (3. 19) because the leakage current reported in the manufacturer's datasheets is typically a mean value referring to a time interval of 72 hours when the charge distribution is again predominant.

3.3. EXPERIMENTAL ANALYSIS

In order to prove the generality of the complete model, as the parameters procedure, the experimental activities were performed using other supercapacitor cells that were different in size, shape (rectangular and cylindrical), and device generation. In particular, the following reports the experimental results for four different types of supercapacitor cells, whose data are reported in Appendix 7.1:

- BCAP0140, a supercapacitor cell of 140 F at 2.5 V nominal voltage;

- BCAP0150, a supercapacitor cell of 150 F at 2.7 V nominal voltage;

- PC10-old version, a supercapacitor cell of 10 F at 2.5 V nominal voltage;

- PC10-new version, a supercapacitor cell of 10 F at 2.5 V nominal voltage.

The second cell represents the evolution of the first one; in fact, it is characterized by a greater capacitance and nominal voltage values. From a geometric point of view, the cylindrical cells are characterized by different terminal configurations: axial vs. radial. Similarly, the fourth cell represents the evolution of the third one, even if the nominal specified data from the manufacturer are the same. In addition, these cells have a rectangular shape. Using these cells, it is possible to verify whether different geometric and constructive solutions influence the device behaviors. In addition, considering the EIS analysis conducted on other supercapacitor cells in the available literature [5-6], with different sizes and manufacturers, along with the EIS data on innovative supercapacitors with nanotube electrode structures that are not currently available on the market [7], it

can be seen that the frequency response of these devices is qualitatively the same as that reported in the following for the tested cells. This again proves the general validity of the supercapacitor model introduced with different electrode structures.

The EIS data of the supercapacitor devices in the frequency range of 10^{-2}–10^3 Hz make it possible to obtain a typical frequency response, as reported in Figure 3.7, where the trends of capacitance and resistance are measured for different polarization voltages.
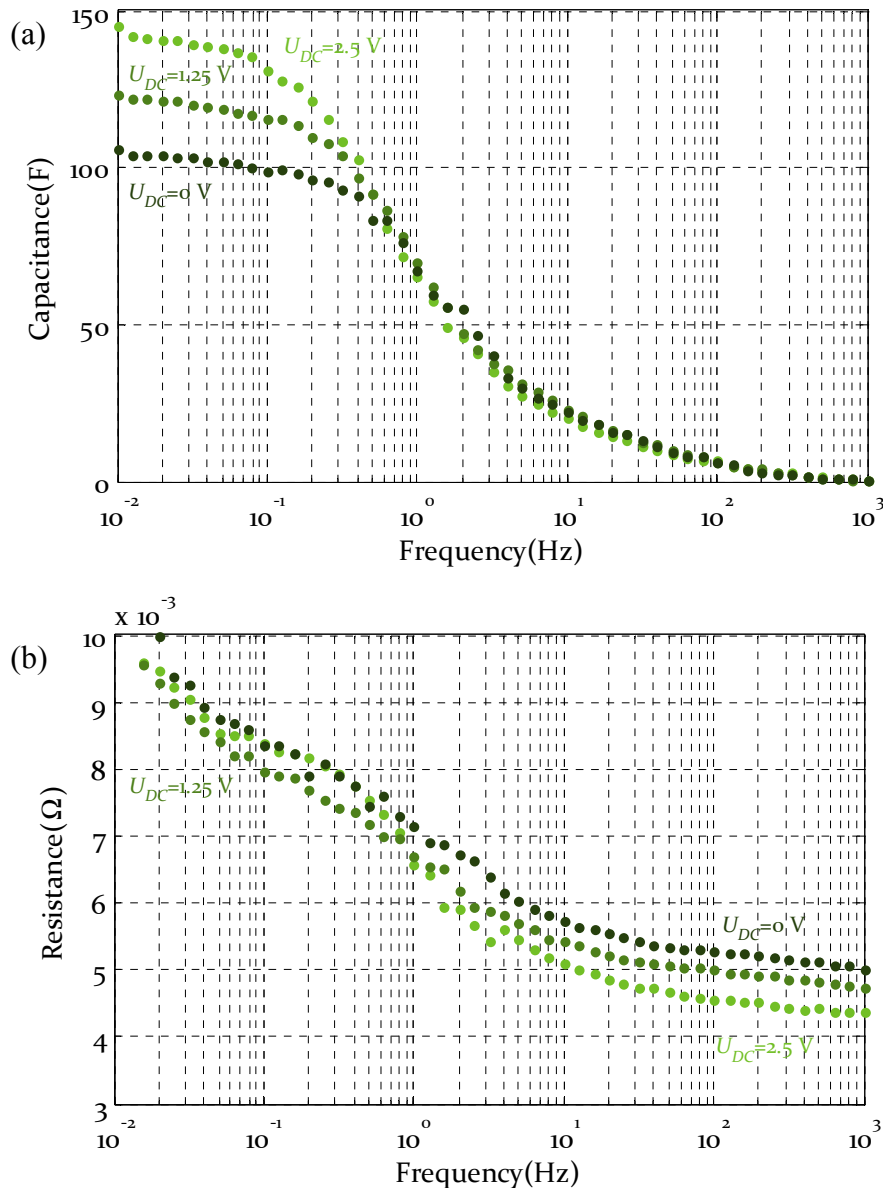
Figure 3.7. **Frequency response: (a) capacitance and (b) resistance of 140 F @ 2.5 V Maxwell supercapacitor (BCAP0140) cell at three different polarization voltages: 0, 1.25, 2.5 V.**

In the first analysis, it can be noticed that, according to DeLevie theory [9,10], the EDLCs behave as supercapacitors in the low frequency range up to several tens of mHz, where in this region the equivalent capacitance is linearly voltage dependent. For greater

frequencies, the equivalent capacitance starts to decrease down to zero for frequencies greater than some hundreds of Hz. This is related to the ion mobility; in fact, the ions, due to their mass, are not able to migrate when subjected to an electrostatic field of high frequency. Consequently, the double layer, where the energy is stored, does not change because ions do not move, and it is unable to store or deliver energy. For the resistance, a continuous decrease can be observed with an increase in frequency. In particular, it can be observed that the resistance in the high frequency region (10^1-10^3 Hz), normally reported on the manufacturer's datasheet as *high-frequencies resistance*, is lower than the resistance in the typical frequency range of usage of supercapacitor devices (10^{-1}-1 Hz) and normally reported on manufacturer's datasheet as *DC resistance.* In addition, in each of these specific regions, the trend is quite constant. It is worth highlighting that, in the DC condition, or a frequency of 0 Hz, the device resistance tends to be the self-discharge resistance, R_{leak}. Finally, another important consideration involves the effect of the charge redistribution, which can only partially be observed in the EIS plot reported in Figure 3.7. For frequencies lower than some tens of Hz, the equivalent measured capacitance continuously increases with the equivalent resistance, which shows greater values than the *DC resistance.*

3.3.1. FIRST BRANCH PARAMETERS BY MEANS OF COMPLETE PROCEDURE BASED ON EIS OF DEVICE

First, the parameters of the first branch, shown in Figure 3.8, are evaluated using a least square minimization, considering the frequency response in the frequency range of 10^{-1}–10^3 Hz, the region where the first branch well represents the device dynamic. In fact, for lower frequencies, the redistribution phenomenon takes place, as confirmed by the increase in the measured capacitance with decreasing frequency shown in Figure 3.7. Because the first branch has to represent only the fast dynamic of the device, the lower frequency of the frequency response considered is 10^{-1} Hz. The parameters obtained are consequently used as reference values to assess the goodness of those obtained with the simplified procedure described above.

Figure 3.8. Comparison between measured and modeled frequency responses by least square minimization of 140 F @ 2.5 V Maxwell supercapacitor (BCAP0140) cell at three different polarization voltages: 0, 1.25, 2.5 V: (a) capacitance and (b) resistance.
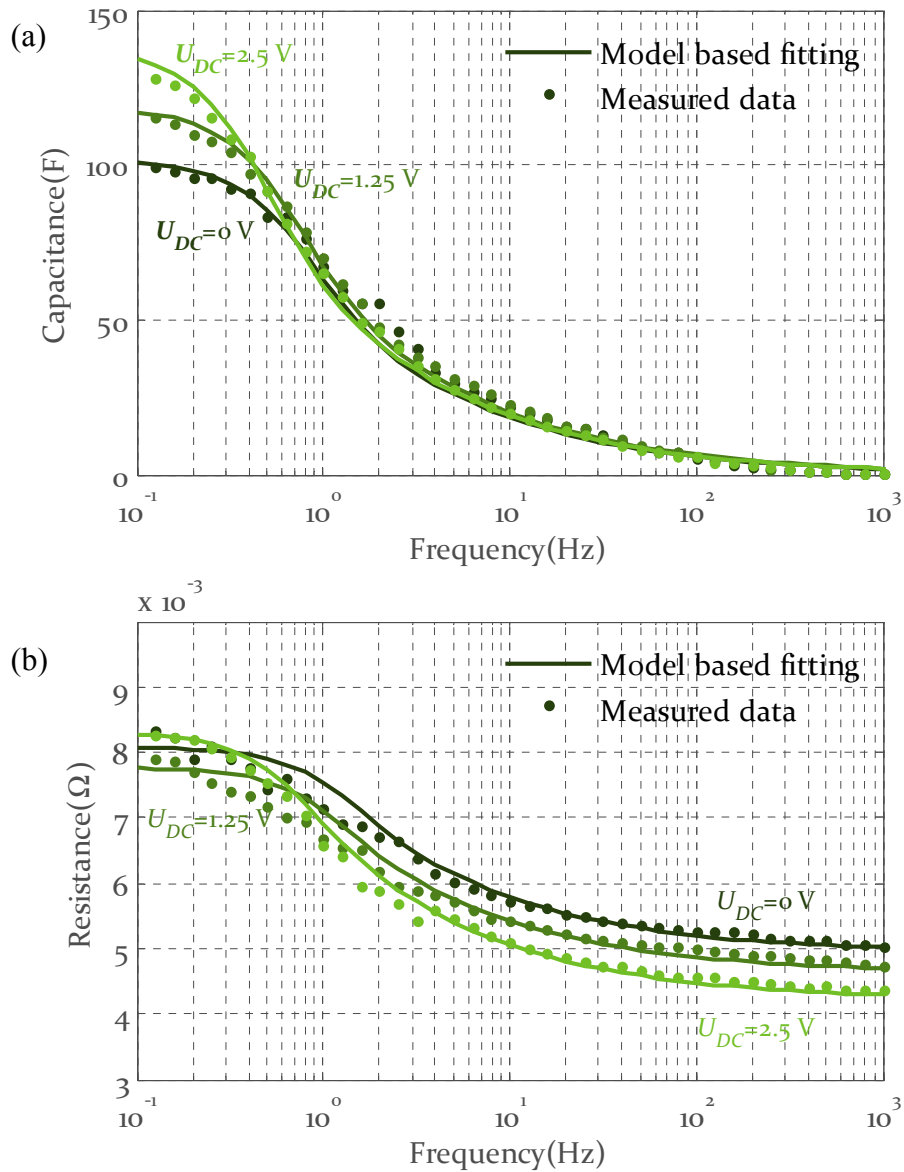
Figure 3.9. **Comparison between measured and modeled frequency responses by least square minimization of 150 F @ 2.7 V Maxwell supercapacitor (BCAP0150) cell at three different polarization voltages: 0, 1.35, 2.7 V: (a) capacitance and (b) resistance.**
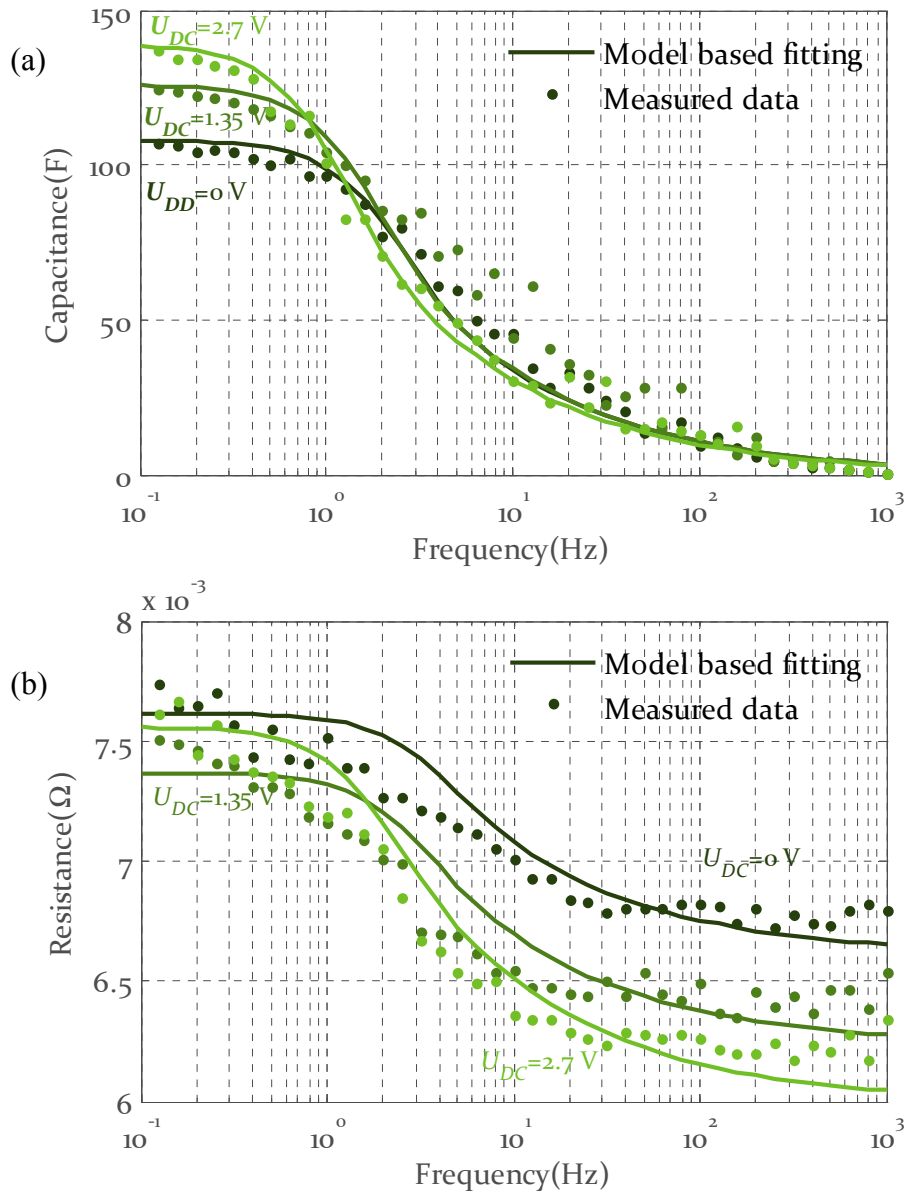
A comparison between Figure 3.8 and Figure 3.9 shows how the two tested devices are dynamically different. In fact, the old version of the supercapacitor, that is the 140 F rated capacitance at a nominal voltage of 2.5 V, shows a lower value of capacitance at each frequency compared to the new version, which is a 150 F rated capacitance at a nominal voltage of 2.7 V. From the dynamic point of view, as reported in Table 3.1, the new version is characterized by a consistently lower value for the time constant, τ, which indicates a greater availability to deliver energy at a high frequency. Finally, greater values of resistance at high frequency are measured for the new version.

Figure 3.10.　Comparison between measured and modeled frequency response by least square minimization of 10 F @ 2.5 V Maxwell supercapacitor cell (PC10 old version) at three different polarization voltages: 0, 1.25, 2.5 V: (a) capacitance and (b) resistance.
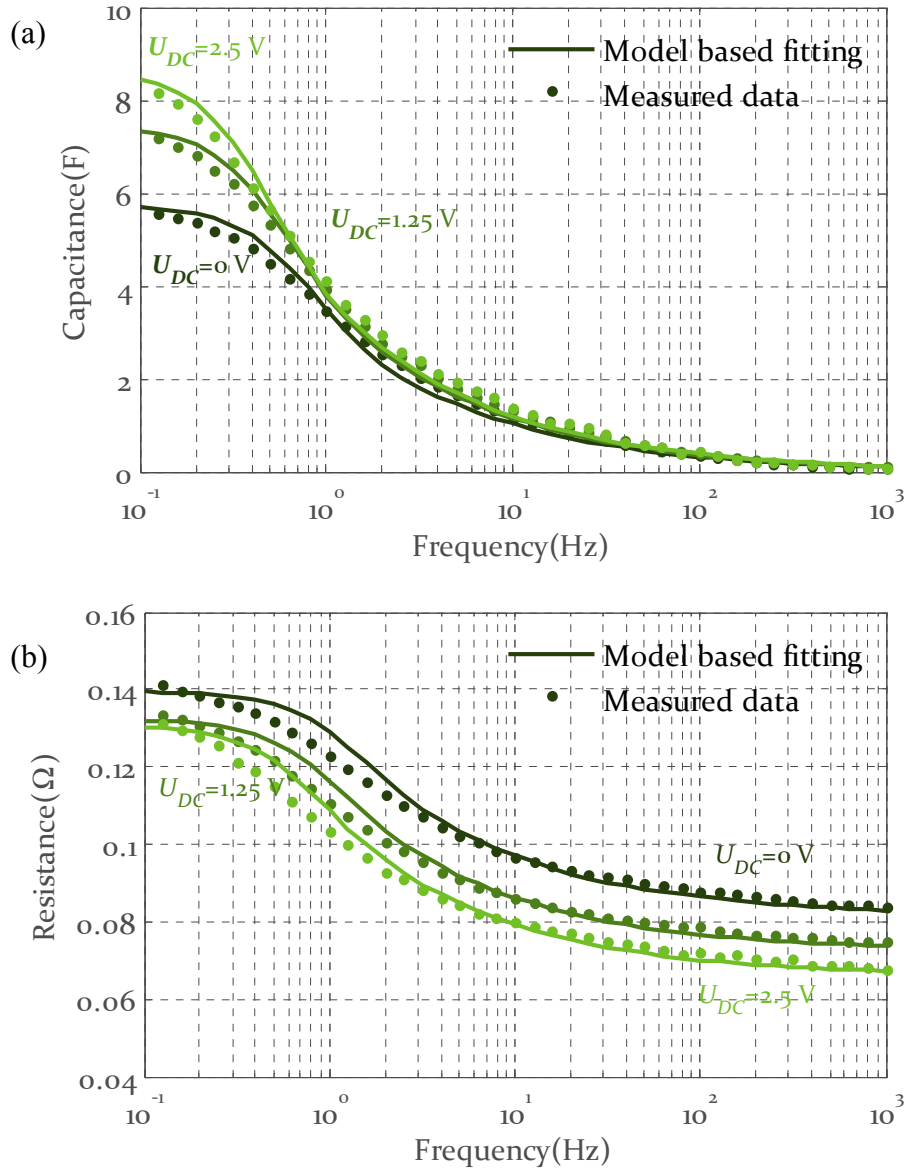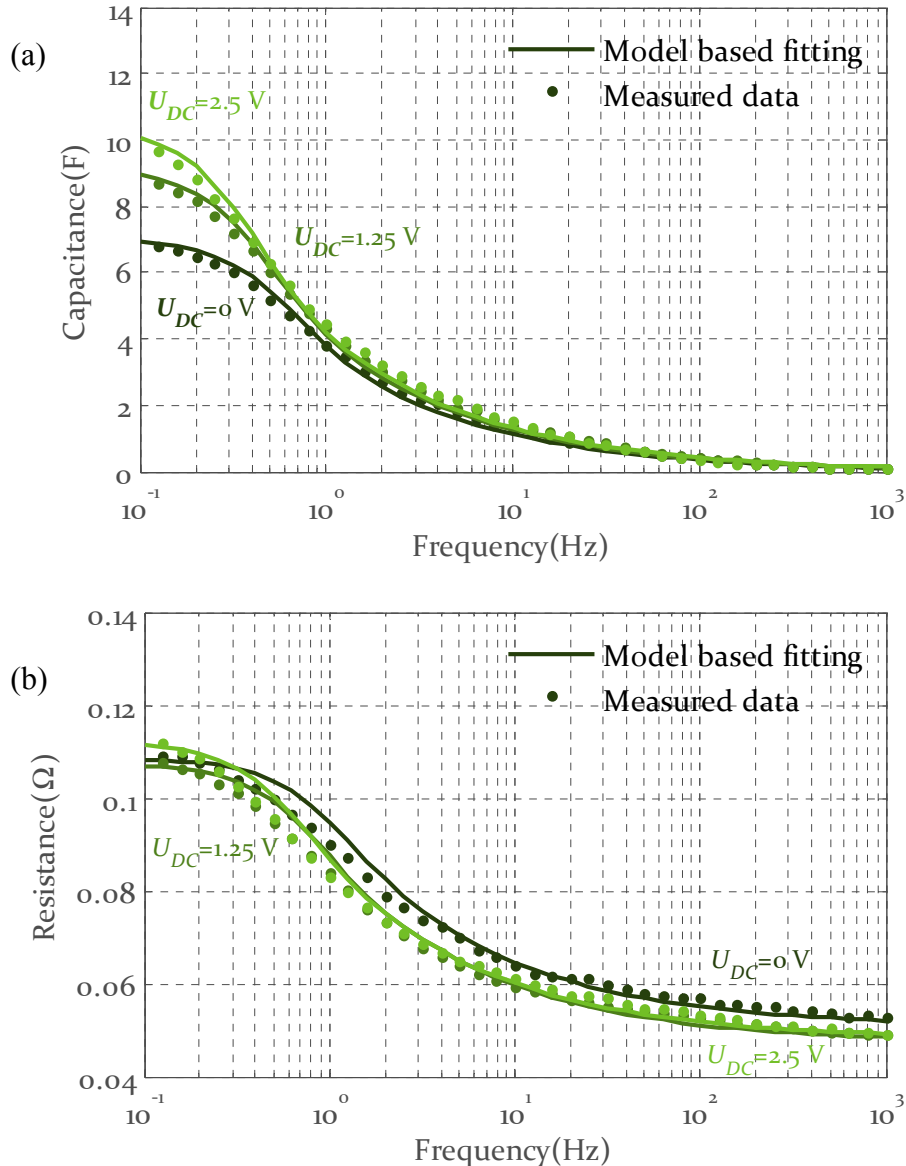
Figure 3.11. Comparison between measured and modeled frequency response by least square minimization of 10 F @ 2.5 V Maxwell supercapacitor cell (PC10 new version) at three different polarization voltages: 0, 1.25, 2.5 V: (a) capacitance and (b) resistance.

Different observations can be made in the comparison of Figure 3.10 and Figure 3.11 where the old and new versions of a 10 F rated capacitance at a nominal voltage of 2.5 V are analyzed. The technological improvement in these rectangular cells is evident by greater values of capacitance in the region of 10^{-1}–1 Hz and a consistent reduction in resistance across the entire analyzed frequency range. The two devices are dynamically similar considering the frequency region in which the supercapacitor behavior starts to decrease (approximately at 0.2 Hz).

In order to evaluate the correlation between the modeled and simulated data, in Table 3.1, where the first branch parameters are reported, the coefficient of determination, R2, has been evaluated as:

$$R^2 = 1 - \frac{\sum_j \left(y_{j,ex} - y_{j,mod}\right)^2}{\sum_j \left(y_{j,ex} - \overline{y}_{ex}\right)^2}$$

(3. 21)

Where the suffixes *ex* and *mod* refer to experimental- and model-based data, respectively, and the mean value is indicated with an overbar.

Table 3.1. **Referring to the equivalent circuit of Figure 3.1, first branch parameters determined by fitting device's EIS data with impedance expression reported in (3.3). The coefficients of determination, R^2 (considering the resistance and capacitance of the device), for different supercapacitor cells determined by means of least square minimization are evaluated in order to verify the mathematical validity of the proposed model in representing the dynamic response of the device.**

	U_{dc}	Ri	C	τ	Coefficient of determination R^2	
	[V]	[mΩ]	[F]	[s]	Resistance	Capacitance
BCAP0140	0	4.89	100.91	0.95	0.971	0.991
	1.25	4.59	117.64	1.10	0.973	0.997
	2.5	4.20	136.38	1.66	0.991	0.998
BCAP0 150	0	6.72	107.35	0.27	0.945	0.992
	1.35	6.37	125.27	0.36	0.931	0.971
	2.7	6.13	138.02	0.57	0.946	0.978
PC 10 OLD	0	81.36	5.69	0.98	0.985	0.996
	1.25	72.33	7.41	1.31	0.988	0.997
	2.5	65.83	8.61	1.65	0.986	0.997
PC 10 NEW	0	50.60	6.99	1.20	0.990	0.998
	1.25	47.14	9.09	1.62	0.992	0.998
	2.5	47.78	10.34	1.97	0.991	0.997

3.3.2. *FIRST BRANCH PARAMETERS BY MEANS OF THE PROPOSED SIMPLIFIED PROCEDURE*

In the following, a comparison with the simplified procedure is reported. Similar to the complete procedure, the following figures report the comparison between the modeled and measured data. In particular, resistance measurements at low frequency (0.1 Hz) and high frequency (1 kHz), in order to identify parameters R_1 and R_i, see (3. 12), which are necessary to indentify time constant τ of the first branch, are conducted at a polarization voltage equal to half the rated one, while capacitance measurements at 0.1 Hz, in order to identify C_o and k_C, see (3. 9), are conducted at a polarization voltages of 0 V and the nominal voltage.

Figure 3.12. Comparison between measured and modeled frequency responses using simplified procedure for 140 F @ 2.5 V Maxwell supercapacitor cell (BCAP0140) at three different polarization voltages: 0, 1.25, 2.5 V: (a) capacitance and (b) resistance.
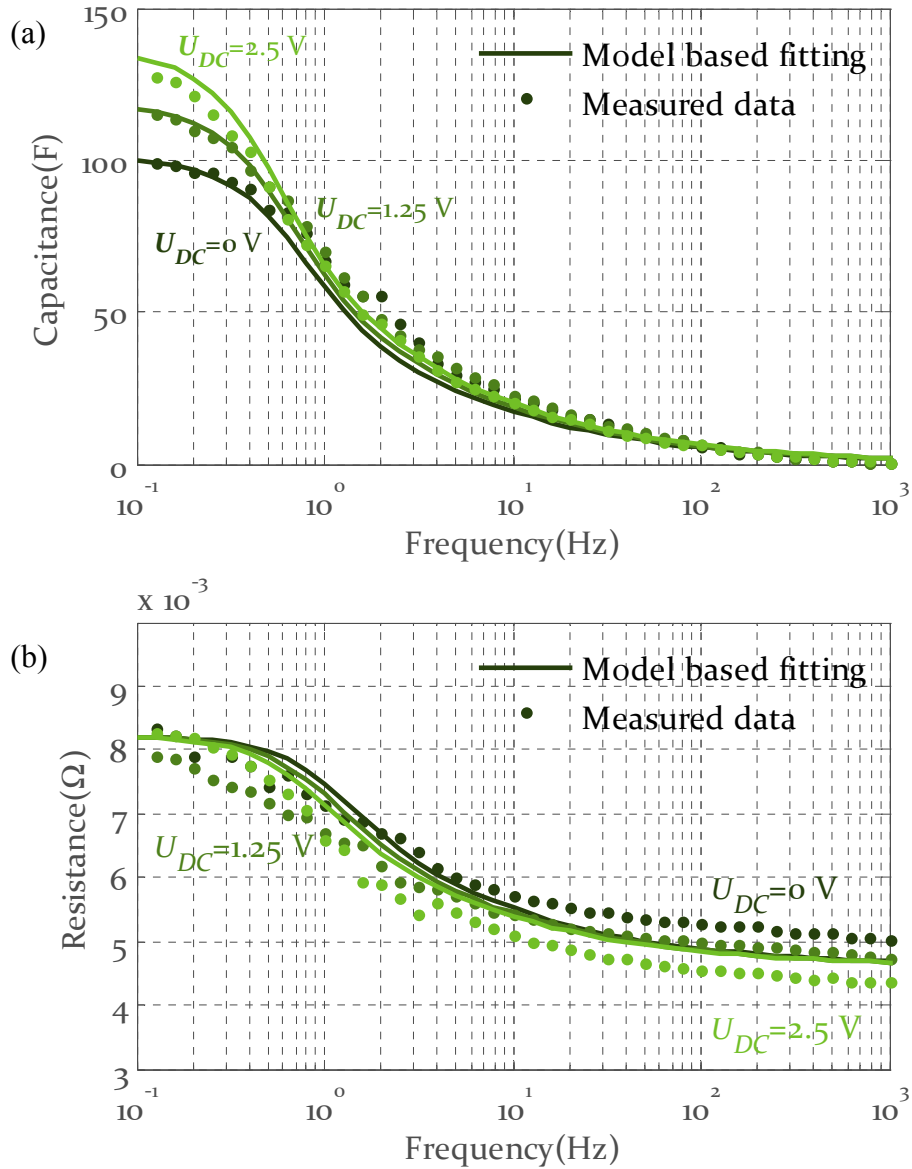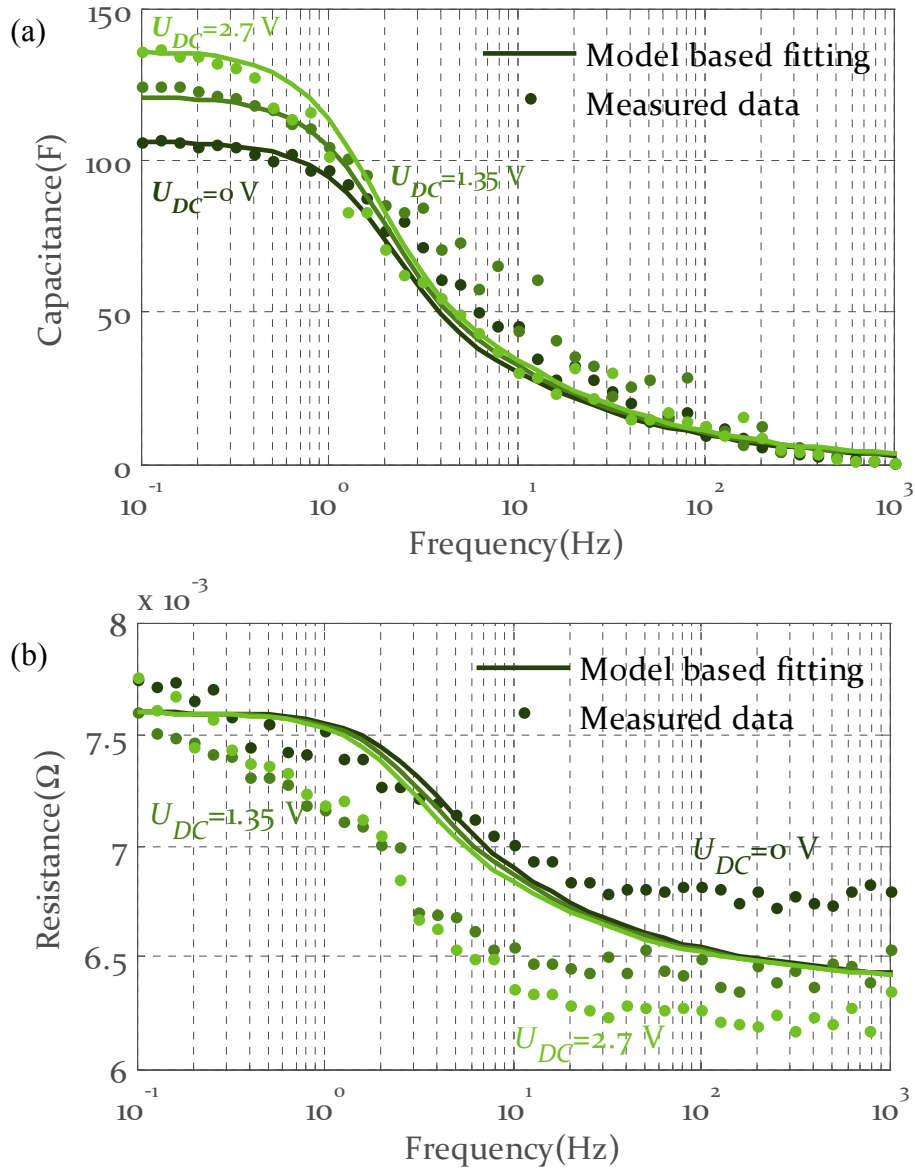
Figure 3.13. Comparison between measured and modeled frequency responses using simplified procedure for 150 F @ 2.7 V Maxwell supercapacitor cell (BCAP0150) at three different polarization voltages: 0, 1.35, 2.7 V: (a) capacitance and (b) resistance.

In order to verify the validity of the simplified proposed procedure, Table 3.2 reports the coefficients of determination, R^2.

Table 3.2. **First branch parameters and coefficient of determination, R² (considering resistance and capacitance of device) for different supercapacitor cells determined using simplified procedure**

	U_{dc}	Ri	R_1	C_0	k_C	Coefficient of determination R^2	
	[V]	[mΩ]	[mΩ]	[F]	[F]	Resistance	Capacitance
BCAP0140	0	4.6	8.2	100.9	13.14	0.945	0.9822
	1.25					0.939	0.993
	2.5					0.946	0.997
BCAP0 150	0	6.5	7.4	107.3	11.2	0.990	0.882
	1.35					0.969	0.924
	2.7					0.967	0.850
PC 10 OLD	0	72.3	138.0	5.68	1.08	0.880	0.994
	1.25					0.967	0.994
	2.5					0.901	0.996
PC 10 NEW	0	47.1	111.7	6.98	1.24	0.969	0.994
	1.25					0.979	0.997
	2.5					0.990	0.999

It is clear from the quantitative analysis reported in Table 3.2, where the estimation error is always lower than 10%, that the first branch parameters based only on specific measurement points (3 measurements at 0.1 Hz and 1 measurement at 1 kHz) lead to a model with very high confidence for the dynamic behaviors of the supercapacitors devices.

3.3.3. MEDIUM-LONG TERM BRANCHES PARAMETERS BY MEANS OF THE PROPOSED PROCEDURE

An evaluation of the parameters of medium-long term branches was conducted by measuring the device open circuit voltage starting from the nominal voltage and considering an observation time of 1.7×106 s. Previous to being fully charge, the devices were left in a short circuit for at least 48 h in order to guarantee a full discharge.

In order to validate the procedure, in the following figures, comparisons are reported between the measured data and simulated data, considering different numbers of medium-long term branches. According to the number of branches used, different estimation error values are obtained. In Figure 3.14 the modeling results with only 3 medium-long term parallel branches and, in Figure 3.154 with 5 branches, are reported on two different types of supercapacitor devices. It is worth noting that the choice of the time constants, according to (3. 14) and (3. 15), is independent of the cells and depends only on the observation time and on the number of medium-long term branches. Thus, with the same time constants, two different cells have been modeled.

Figure 3.14. Redistribution and self-discharge open circuit voltage comparison between measured and simulated data modeled using 3 medium-long term branches: (a) 140 F @ 2.5 V cell (BCAP0140), (b) 150 F @ 2.7 V cell (BCAP0150).

Figure 3.15   **Redistribution and self-discharge open circuit voltage comparison between measured and simulated data modeled using 5 medium-long term branches: (a) 140 F @ 2.5 V cell (BCAP0140), (b) 150 F @ 2.7 V cell (BCAP0150).**

The coefficient of determination, R^2, as a measure of the goodness of the fit, and the parameters of the three medium-long term branches were evaluated and collected in Table 3.3.

Table 3.3.   **Parameters of three medium-long term branches and coefficients of determination, R^2, considering measured and simulated open circuit voltages.**

	R_2	R_3	C_2	C_3	R_{leak}	Coefficient of determination R^2
	[Ω]	[kΩ]	[mΩ]	[F]	[kΩ]	
BCAP0140	185.4	4.5	13.9	14.7	64.04	0.8625
BCAP0150	72.5	3.18	35.5	20.8	47.8	0.9136

The data collected in Table 3.4 show the approximation done with 5 medium-long term parallel branches. It is clear in this way that the R^2 coefficient of determination is better and very close to 1, but the compromise between the accuracy and model complexity depends on the application needs. The possibility to improve the accuracy independently from the cell topology merely by using a different choice of parallel branches is surely a strong benefit in modeling the device.

Table 3.4. **Parameters of five medium-long term branches and coefficients of determination, R^2, considering measured and simulated open circuit voltages.**

	R_2	R_3	R_4	R_5	C_2	C_3	C_4	C_5	R_{leak}	*Coefficient of determination R^2*
	[Ω]	[Ω]	[kΩ]	[kΩ]	[F]	[F]	[F]	[F]	[kΩ]	
BCAP0140	80.6	587.1	3.84	3.07	8.7	8.4	9.0	7.9	10.3	0.9911
BCAP0150	28.4	329.9	3.07	12.4	24.7	14.9	11.2	19.5	74.2	0.9723

In order to further validate the parameter identification procedure, in Figure 3.16 comparison between the measured and simulated open circuit voltages of the two devices for an observation time of 1.7×10^5 s, an order of magnitude lower than the previous case, is reported. In this case, the same procedure considering 3 medium-long term parallel branches, leads to different parameter values as the coefficient of determination, R^2, collected in Table 3.5. By reducing the observation time, the number of parallel branches needed to correctly model the device with high accuracy is consequently lower.
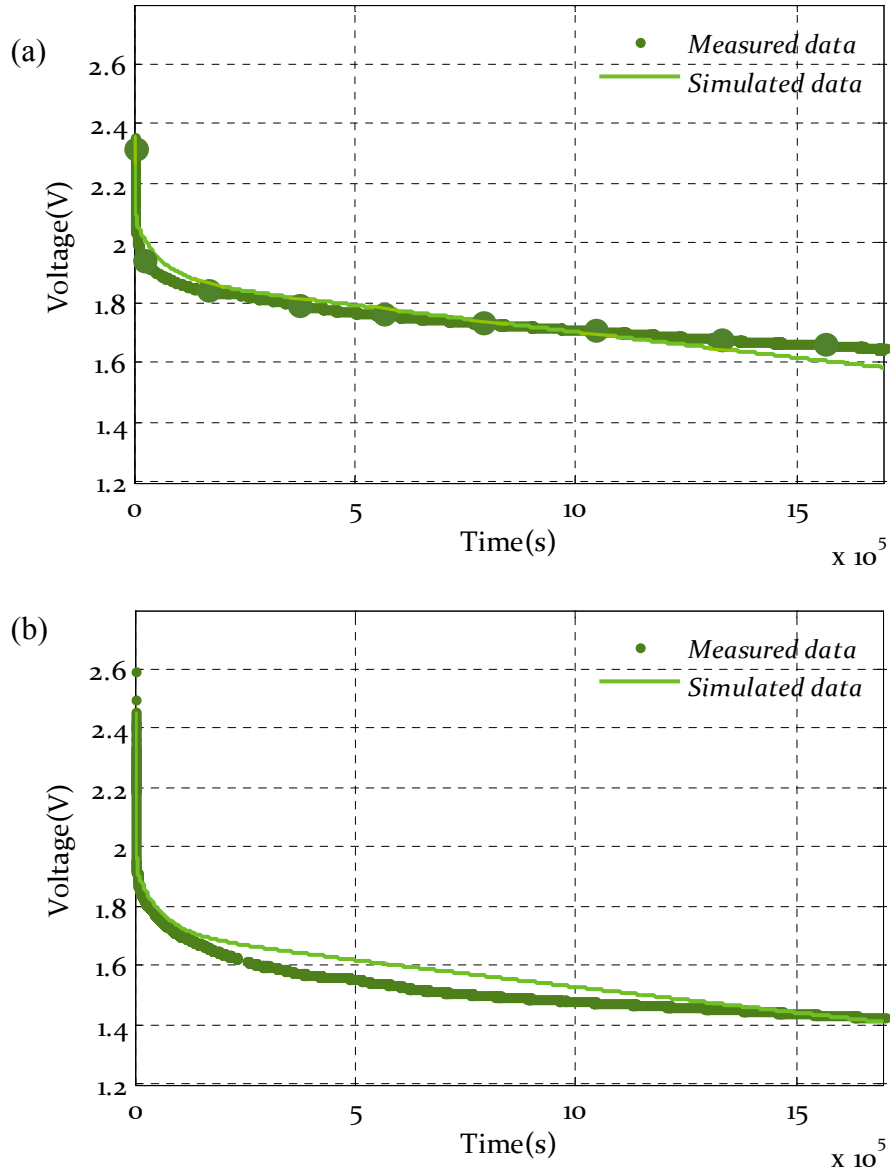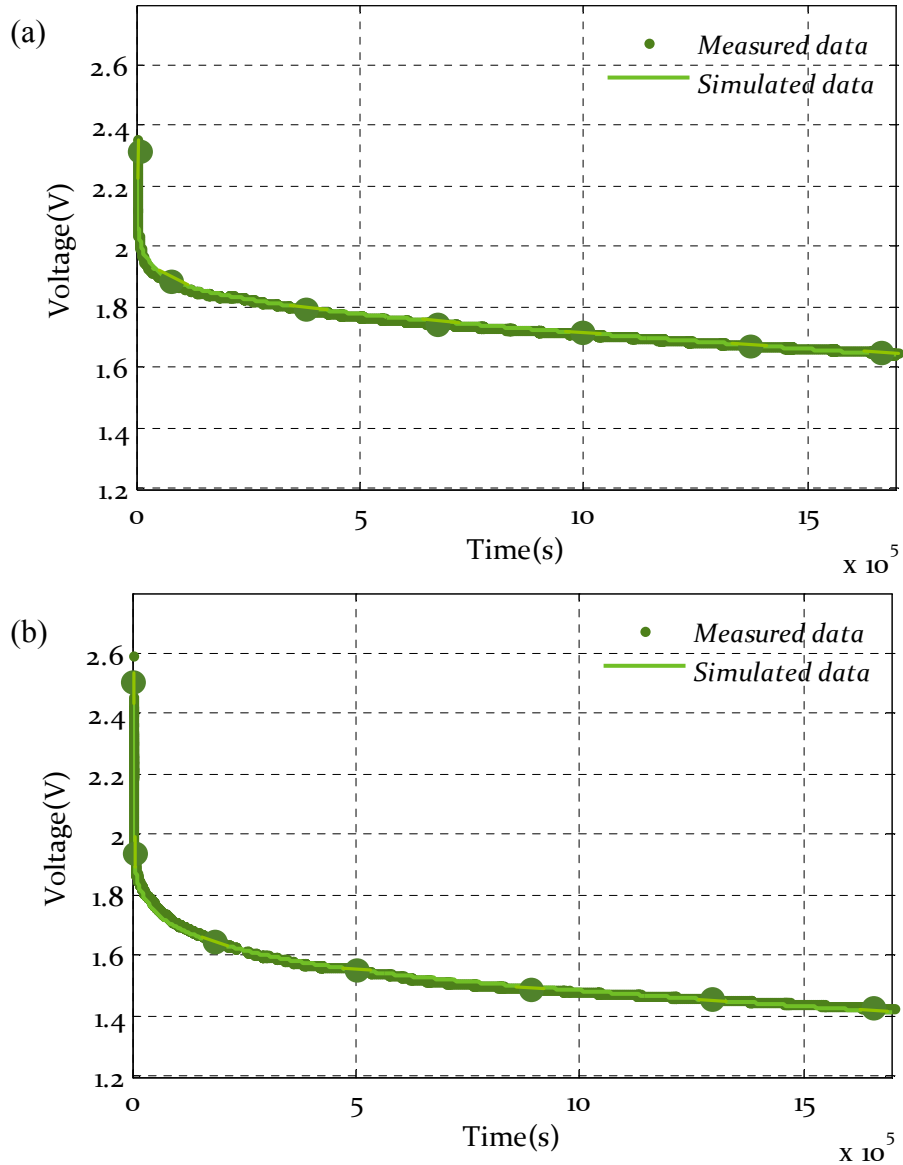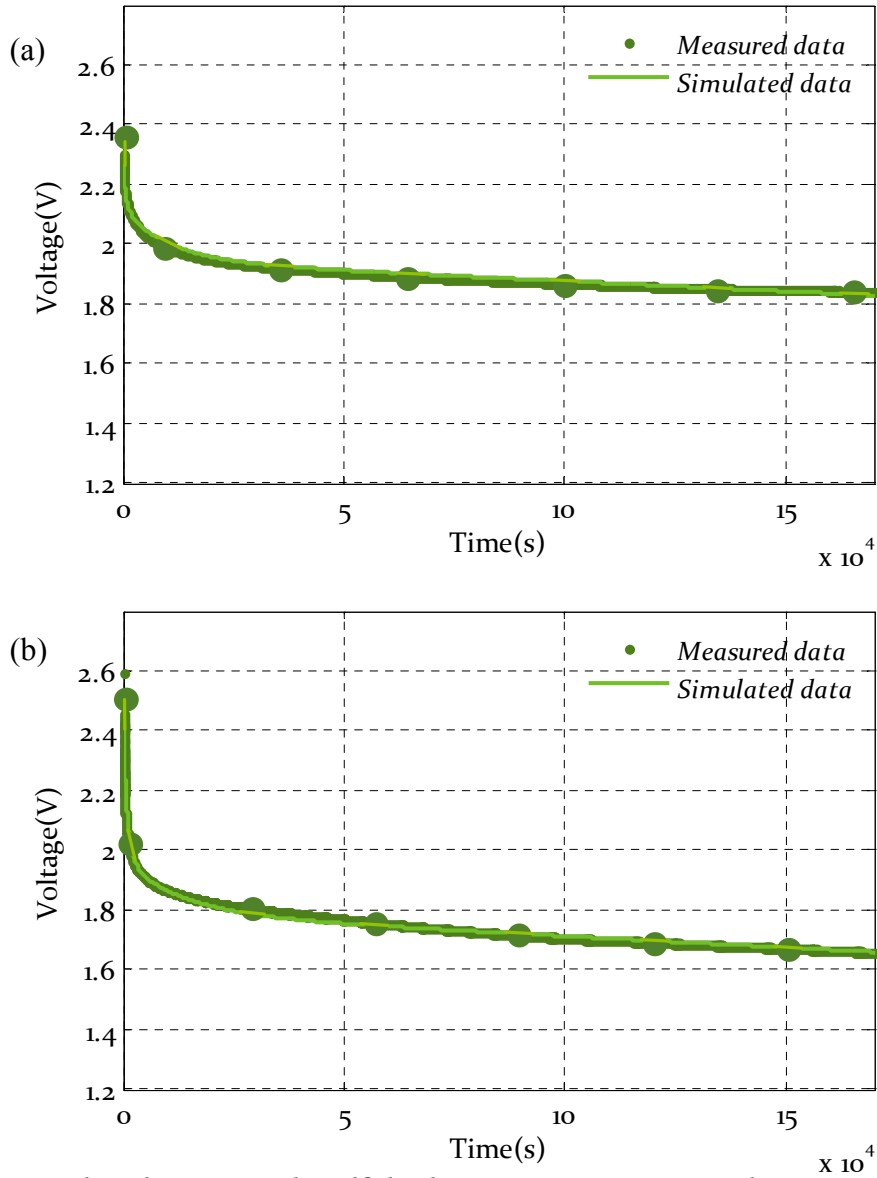
Figure 3.16 Redistribution and self-discharge open circuit voltage comparison between measured and simulated data modeled using 3 medium-long term branches and considering time window of 1.7×10^5 s: (a) 140 F @ 2.5 V cell (BCAP0140), (b) 150 F @ 2.7 V cell (BCAP0150).

Table 3.5. Parameters of five medium-long term branches and coefficients of determination, R^2, considering measured and simulated open circuit voltages.

	R_2	R_3	C_2	C_3	R_{leak}	Coefficient of determination R^2
	[Ω]	[kΩ]	[mΩ]	[F]	[kΩ]	
BCAP0140	111.0	1.23	10.7	11.5	20.3	0.9920
BCAP0150	41.7	0.87	28.6	16.3	13.1	0.9613

3.4. BIBLIOGRAPHY

[1]   M.F. Rose, S.A. Merryman, "Electrochemical capacitor technology for actuator applications" Proc. of the IEEE Energy Conversion Engineering Conference (IECEC 96), Vol. 1, 11–16 Aug. 1996, pp.245–250.

[2]   L. Zubieta, R. Bonert, "Characterization of double layer capacitors for power electronic applications", IEEE Trans. Industry Application, Vol. 36, no. 1, Jan/Feb 2000, pp. 199–204.

[3]   F. Rafik, H. Gualous, R. Gallay, A. Crausaz, A. Berthon, "Supercapacitors characterization for hybrid vehicle applications," Power Electronics and Motion Control Conference, 2006. IPEMC 2006. CES/IEEE 5th International , vol.3, no., pp.1-5, 14-16 Aug. 2006.

[4]   F. Castelli Dezza, M. Diforte, S. Gervasini, M. Mauri, "An improved model of a double layer capacitor for power electronics applications", Proc. Of. 11th International Power Electronics and Motion Control Conference EPE/PEMC, Riga, Latvia, September 2-4, 2004.

[5]   P. Kurzweil, B. Frenzel, R. Gallay, "Capacitance Characterization Methods and Ageing Behaviour of Supercapacitors", 15th International Seminar On Double Layer Capacitors, Deerfield Beach, FL., U.S.A., December 5-7, 2005.

[6]   O. Bohlen, J. Kowal, D. Uwe Sauer, "Ageing behaviour of electrochemical double layer capacitors: Part I. Experimental study and ageing model", Journal of Power Sources, Volume 172, Issue 1, Pages 468-475, 11 October 2007.

[7]   R. Signorelli, D.C. Ku, J.G. Kassakian, J.E. Schindall, "Electrochemical Double-Layer Capacitors Using Carbon Nanotube Electrode Structures," Proceedings of the IEEE , vol.97, no.11, pp.1837-1847, Nov. 2009.

[8]   R.N. Nelms, D.R. Cahela, B.J. Tatarchuk, "Modeling double-layer capacitor behaviour using ladder circuits", IEEE Trans. Aerospace Electronic Systems, Vol. 39, n.2, Apr 2003, pp.430–438.

[9]   R. de Levie, "Porous Electrodes in Electrolyte Solutions, I", Electrochim. Acta Vol. 8, 1963, pp. 751.

[10]   R. de Levie, "On Porous Electrodes in Electrolyte Solutions, II", Electrochim. Acta Vol. 9, 1964, pp. 1231-1245.

4. MODEL VALIDATION

In order to demonstrate the effectiveness of the supercapacitor model introduced in chapter 3, a general discussion, supported by an experimental analysis, will be reported in the following. In particular, an analysis will be made of the accuracy of the model in simulating, not only the dynamic of the device, that is the voltage vs. current profile, but also its macroscopic performances such as the device efficiency and specific energy vs. specific power. Finally, a discussion regarding the correlation between model parameters and device performances, which will be useful to understand the physics of the device, will be presented.

4.1. DYNAMIC ANALYSIS

First, the suitability of the model will be proved by analyzing its ability to simulate the supercapacitor dynamic when the device is cycled with different current profiles. In particular, the supercapacitor cells were charged and discharged with a set of different current values in order to change the dynamic of usage, verify the absence of non-linearity according to the current injected, and, consequently, prove the model validity in this wide range of operating conditions.

A pulse load condition was used for the tests. Using a controlled DC source, EA-PSI 8240-170, and a controlled electronic load, EA-EL 9400-150 (Figure 4.1), a pulsing current of different values was injected into the supercapacitor cells, and the measured terminal voltage was compared with the simulated data.

Figure 4.1   **Test equipment: a controlled DC source EA-PSI 8240-170 and a controlled electronic load EA-EL 9400-150. The equipment is controlled via interface cards with a control program written in Labview environment.**

The working cycles are characterized by different values of constant current during the charging and discharging phases, so that the cell is cycled in different dynamics:

because the same maximum and minimum voltage limits are considered, the cells are charged and discharged in different time intervals.

In Figure 4.2 different comparisons between the simulated and measured voltages, according to the different values of pulsing current injected in the Maxwell supercapacitor cell of 140 F @ 2.5 V, are reported. To evaluate the correspondence between the simulated and experimental data, the coefficient of determination, R^2, was evaluated. Its definition is as follows:

$$R^2 = 1 - \frac{\sum_j \left(y_{j,ex} - y_{j,mod}\right)^2}{\sum_j \left(y_{j,ex} - \bar{y}_{ex}\right)^2} \tag{4.1}$$

where suffixes *ex* and *mod* refer to experimental- and model-based data, respectively, and the mean value is indicated with an overbar.
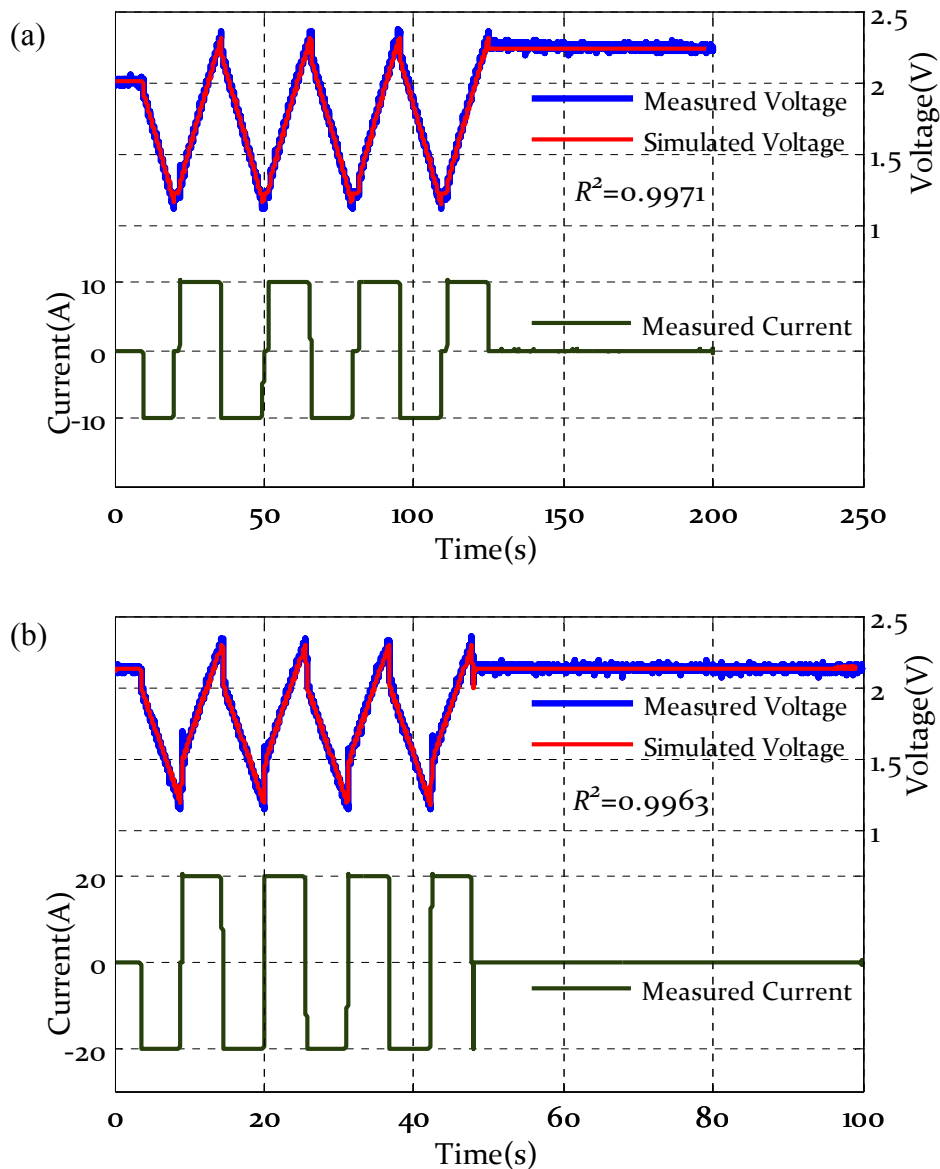
Figure 4.2 **Comparison between measured and simulated cell terminal voltages under different conditions of injected current: (a) 10 A, (b) 20 A, (c) 60 A, (d) 110 A. The cell under consideration is a 140 F @ 2.5V - BCAP0140 cycled between the nominal voltage and its half.**

Similar results are reported in Figure 4.3, where the cell being analyzed is a Maxwell supercapacitor cell of 150 F @ 2.7 V. It can be seen that the internal resistance of the device significantly influences the total exchangeable energy when the device is cycled between fixed voltage limits, as shown in Figure 4.2(d) and Figure 4.3(d). At high current, in fact, the terminal voltage is subjected to a high voltage drop that is comparable to the voltage variation admitted for a supercapacitor device, which is between the nominal voltage and its half. Consequently, the real exchange of energy is related to a very reduced voltage range.
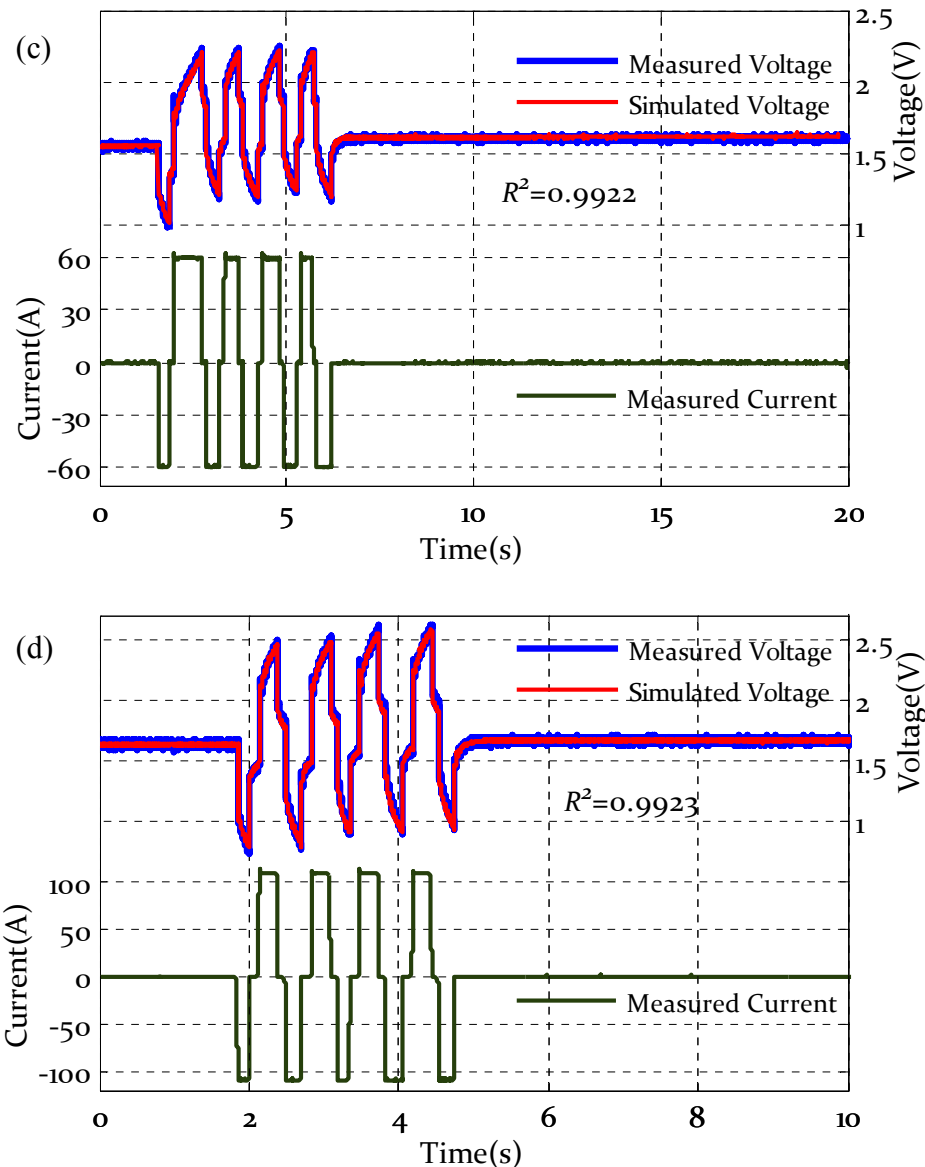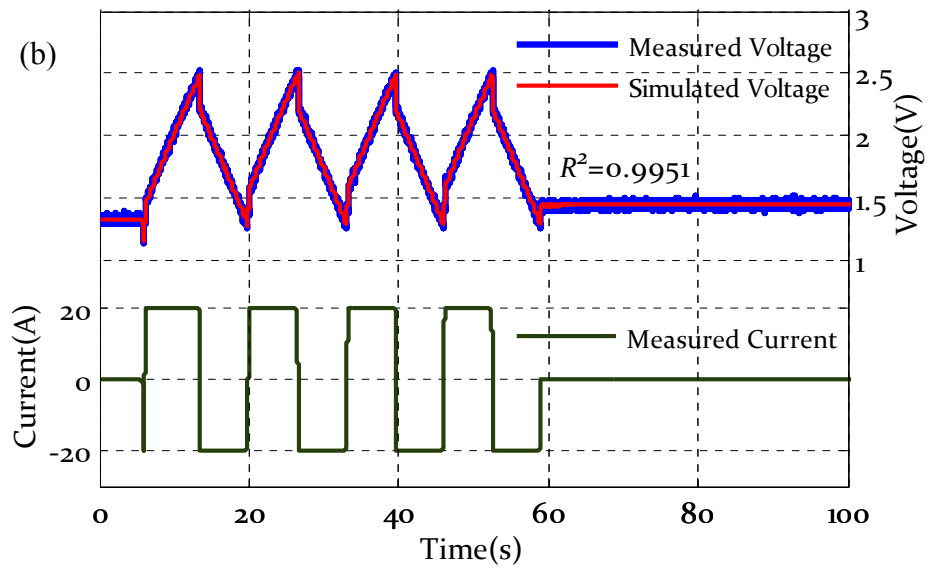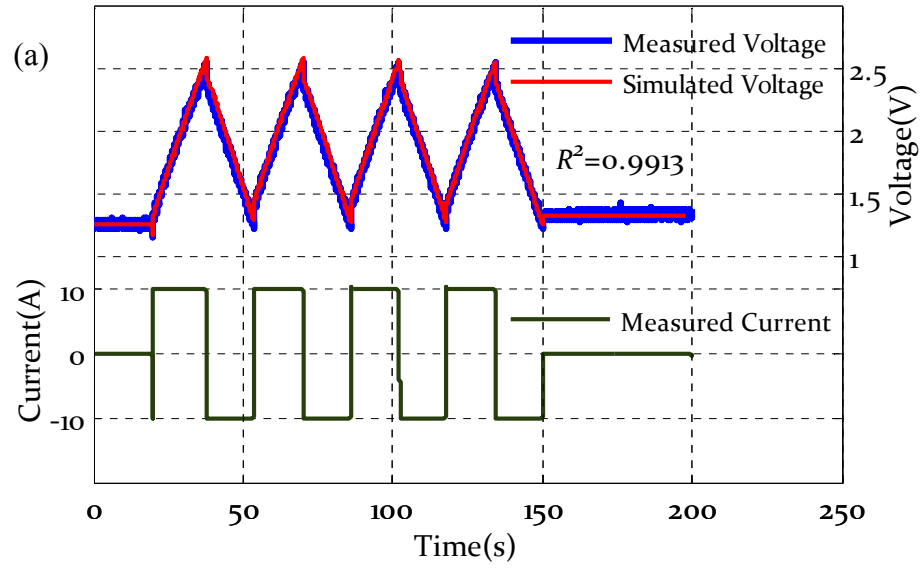
(a)

(b)

$R^2=0.9913$

$R^2=0.9951$
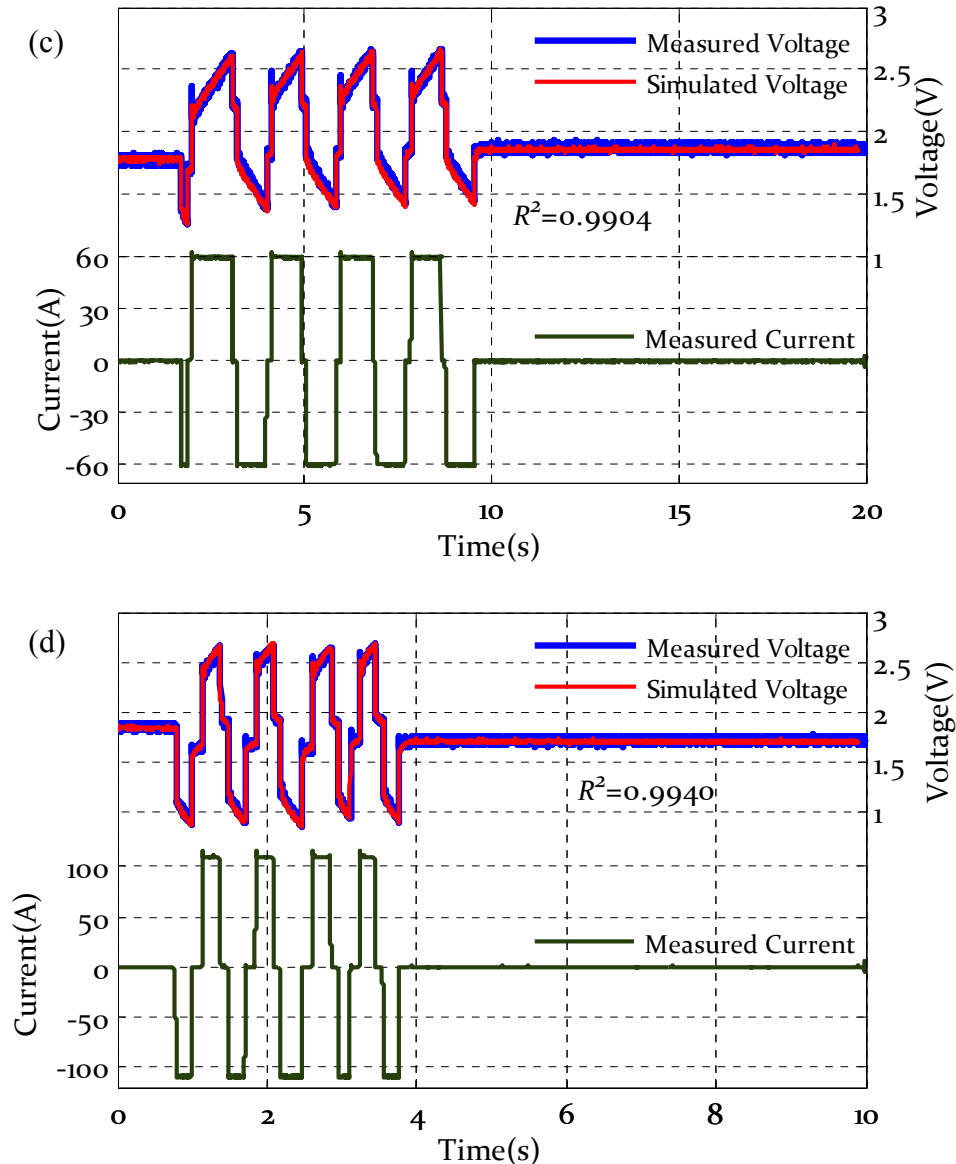
Figure 4.3 **Comparison between measured and simulated cell terminal voltages under different conditions of injected current: : (a) 10 A, (b) 30 A, (c) 60 A, (d) 110 A. The cell under consideration is a 150 F @ 2.7 V - BCAP0150 cycled between the nominal voltage and its half.**

The experimental data of Figure 4.2 and Figure 4.3 show how the cells are charged and discharged repetitively for four complete cycles, after which the current is set to zero. In all operative working conditions, in both high dynamic and slow dynamic operations, as well as when the current is set to zero at the end of the four cycles, the agreement between the simulated and measured data is evident. This indicates the ability of the model to simulate the device dynamic in terms of equivalent voltage at the cell terminals, but does not imply the ability of the model to simulate either the device performances in terms of the specific energy density versus power density or the ability to simulate the device

efficiency. These aspects are taken into account in the following in order to prove the suitability of the model.

4.2. RAGONE PLOT ANALYSIS

An ideal storage device has a specific energy that is independent of the specific power with which the device is charged or discharged. Due to the internal resistance of supercapacitors and the electrochemical behavior of the electrolyte, in practice, it is impossible to use the full store of energy. This is especially true with an increase in the specific charge or discharge power. Supercapacitor devices are normally operated between the nominal voltage and half this value in order to use, in the case of an ideal capacitance, 75% of the stored energy. As reported in Figure 4.4, the presence of the internal resistance primarily causes a voltage drop directly proportional to the current flowing. Thus, with the same maximum and minimum voltage limits, a lower energy can be used. In addition, due to the electrolyte mobility, the equivalent capacitance of a supercapacitor, as reported in chapter 3, is strictly related to the frequency with which the device is charged and discharged. In practice, increasing the dynamic of use, which means increasing the operating power of the device, a lower equivalent capacitance is available, which causes a lower usable specific energy. For these two reasons, the specific energy decreases with an increase in the specific power. It is important to emphasize that the effect of the internal resistance in reducing the specific energy is strictly related to a certain amount of energy wasted on it, while the effect of a reduced internal capacitance with frequency causes a reduction in the specific energy because the device is not able to deliver that energy, which remains trapped in it but is not wasted. The global effect at the device terminals is a combination of these phenomena, which is particular evident in Figure 4.2-(d) and Figure 4.3-(d), where the supercapacitor devices are cycled with high current rates. In these figures, considering the fourth cycle when the cell is charged for the last time, it can be noticed that the voltage, due to the high voltage drop on the internal resistance, after reaching the nominal value (2.5 V in Figure 4.2-(d) and 2.7V Figure 4.3-(d)) falls to approximately 2 V as soon as the charging current is set to zero. For the same reason, in the consecutive discharge phase, a significant voltage drop down to 1.2 V is measured, and the device delivers energy in a relatively short time, until the voltage decreases to 1 V, which is the voltage limit for that cycle. As soon as the discharge current is again set to zero, the terminal voltage increases to approximately 1.7 V. This means the device again

has a certain amount of energy stored in it. Yet, this is cannot be delivered with a high dynamic because of the high voltage drop and the fact that the equivalent capacitance in that condition is significantly lower.

At this point, the supercapacitor performances are experimentally evaluated in order to draw the well-known Ragone plot. This diagram is normally used to compare different storage technologies in terms of specific energy versus specific power. In a sense, the diagram provides information regarding the amount of energy the storage device is able to deliver when operated with a specific power. Generally, the curve is normally plotted as the area in which the device can operate. However, in reality, the curve is well defined and shows the dynamic performances of the device.

In order to correctly draw the Ragone plot, the device has to be charged or discharged using different values of constant power, according to the operating voltage limits and, for each experiment, the total absorbed or delivered energy has to be computed. In Figure 4.4, using the same test equipment as shown in Figure 4.1, an example is reported of the measured voltage profile (from 2.5V down to 1.2V) of the Maxwell supercapacitor cell of 140 F @ 2.5V discharged with a constant power of 40 W.
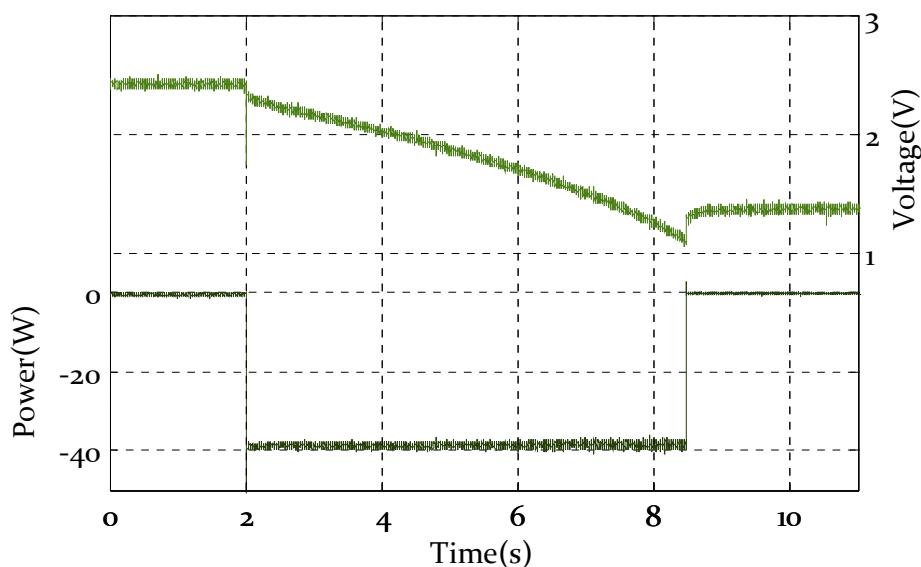
Figure 4.4   **Measured voltage profile on Maxwell supercapacitor cell of 140 F @ 2.5 V when discharged at constant power of 40 W.**

In Figure 4.5 the measured and simulated Ragone plots of two supercapacitor devices are reported. The two cells are the Maxwell supercapacitor cell BCAP0140 (140 F @ 2.5 V nominal voltage) and the BCAP0150 (150 F @ 2.7 V nominal voltage) with weights of 29 g and 35 g, respectively.

It is important to note that the typical energy densities that supercapacitors are capable of delivering and are normally reported in the literature are really exploitable at a specific power of up to 1 kW/kg. Greater specific power values cause significant decreases in the usable energy. In fact, with a value of 4 kW/kg as the specific power in discharge, the usable energy is about halved.
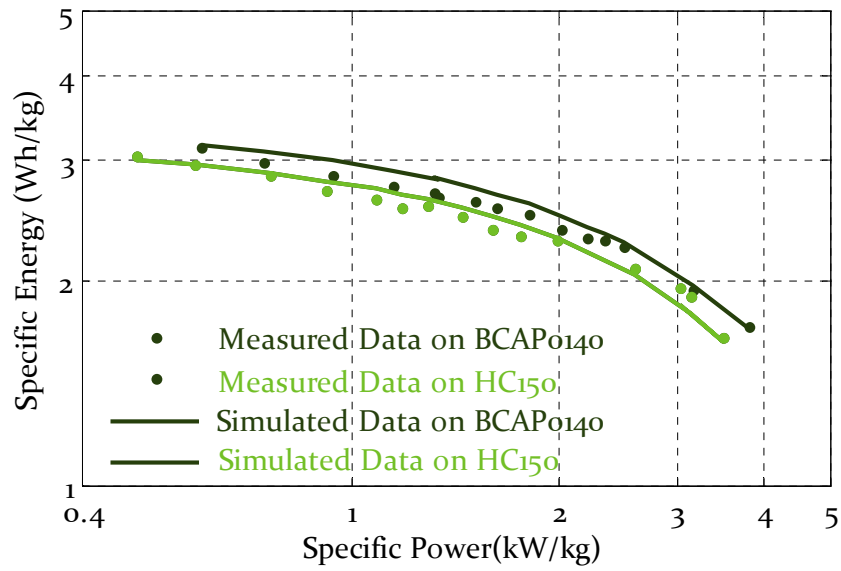
Figure 4.5   **Comparison between measured and simulated Ragone plots on two Maxwell supercapacitor cells: BCAP0140 (140 F @ 2.5 V nominal voltage) and BCAP0150 (150 F @ 2.7 V nominal voltage).**

Figure 4.5 shows the ability of the model introduced in chapter 3 to simulate the dynamic performances of the supercapacitor cells over the complete operating range for these devices. This shows the value of the model and simplified parameter procedure that was introduced because the macroscopic quantity can be correctly evaluated, avoiding the need for measurements that require specific laboratory equipment.

4.3. EFFICIENCY ANALYSIS

The last aspect considered in this set of experiments is the ability of the model to correctly simulate the efficiency of supercapacitor devices.

This aspect has a double valence because it not only represents the ability of the model to simulate another macroscopic physical quantity, but also means that the losses inside a supercapacitor are all related to the joule losses that are taken into account by the resistive elements of the model.

In addition, the availability of a model that is able to correctly simulate the device efficiency is very useful in all operating conditions under which control strategies have to be set in order to minimize the overall storage losses.

In order to accomplish this, starting from the same analysis reported in paragraph 4.1, in which the supercapacitor devices are cycled under different dynamic conditions with different values of injected current, the experimental efficiency is computed as the ratio between the total delivered energy and total absorbed energy, taking into account the energy variation between the initial and final time instants of the cycle in the analysis.

In the simulation, the device is operated with the same experimentally measured current profile, and the device efficiency is calculated as:

$$h = \frac{W_{out}}{W_{in} + \Delta W} \tag{4.2}$$

where:

W_{out} is the total delivered energy by the supercapacitor device;

W_{in} represents the total energy injected in the supercapacitor device;

ΔW is the variation in the stored energy between the initial and final time instants of the cycle.

It should be noted that ΔW is a corrective term that has been introduced to take into account the fact that the device is not at the same voltage, and consequently at the same energy, between the initial and final time instants of the considered cycle.

In Figure 4.6 the measured efficiencies of the two Maxwell supercapacitor cells (BCAP0140-140F@2.5V and BCAP0150-150F@2.7V) are compared with the simulated ones.
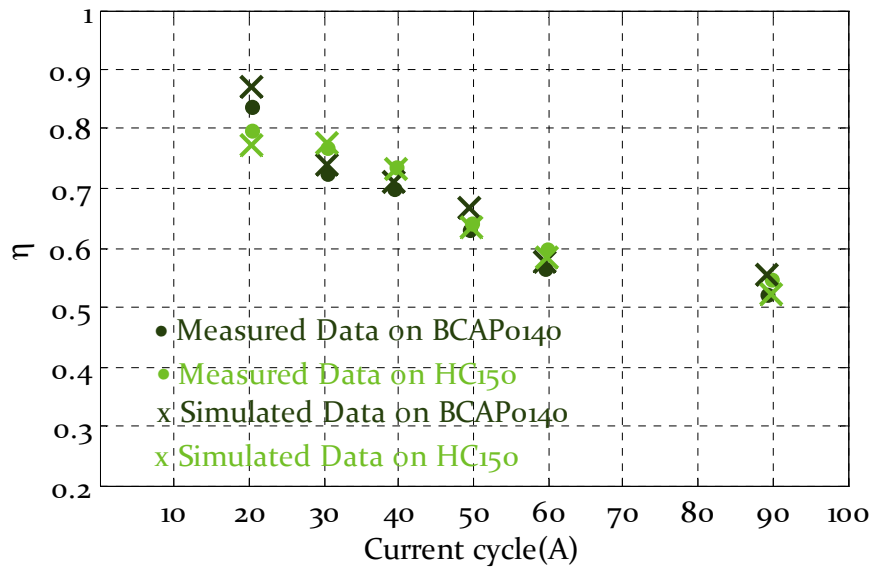
Figure 4.6   **Comparison between measured and simulated efficiencies of two Maxwell supercapacitor cells when cycled at different values of constant current in charge and discharge phases. The devices considered are the BCAP0140 (140 F @ 2.5 V nominal voltage) and BCAP0150 (150 F @ 2.7 V nominal voltage).**

It is important to note that there is no clear linear tendency for the measured efficiency versus the constant current values used in the charge and discharge phases because the control logic of the test equipment used is not able to guarantee the repeatability of the different cycles with which the device is operated. Especially at high current rates, as can be seen in Figure 4.2 and Figure 4.3, the voltage control loop of the test equipment is not sufficiently quick, causing variations in the voltages limits under which the cell is operated. This changes, in a sensible way, the boundary condition under which the device is operated with a certain value of cycle current compared to a different value. However, it is important to note the accuracy of the model in simulating the device efficiency.

Having proved this ability of the model, the efficiencies of supercapacitor devices are simulated as a function of the specific power with which the device is operated. In particular, two operative working conditions are considered: first the device is operated with continuous charge and discharge cycles without any time interval at zero current between the different charge/discharge phases (Figure 4.7 (a)). Then, the power cycle is operated with the same power values during the charge/discharge phases, but, between them, a time interval of 30 s at zero current is considered in order to verify the effect of redistribution and self discharge on the device efficiency (Figure 4.7(b)).
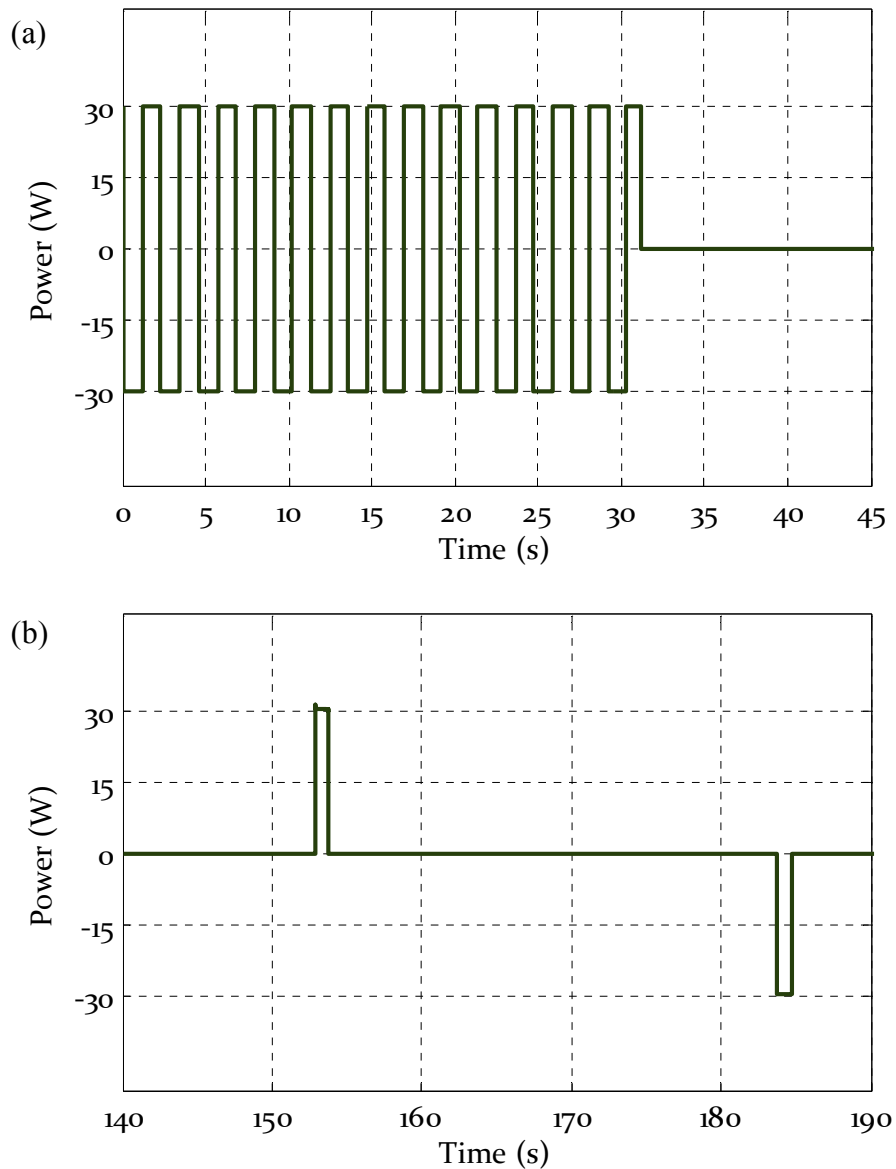
Figure 4.7   **Reference power cycle: (a) without any time interval at zero current between charge phase and consequential discharge one, (b) with time interval of 30 s.**

In particular, as shown in Figure 4.7, 14 complete cycles at constant power are considered, and the simulations are conducted in order to operate the device with the same voltage limits, which are the nominal voltage and half this value. The results for the simulated efficiency are reported in Figure 4.8.
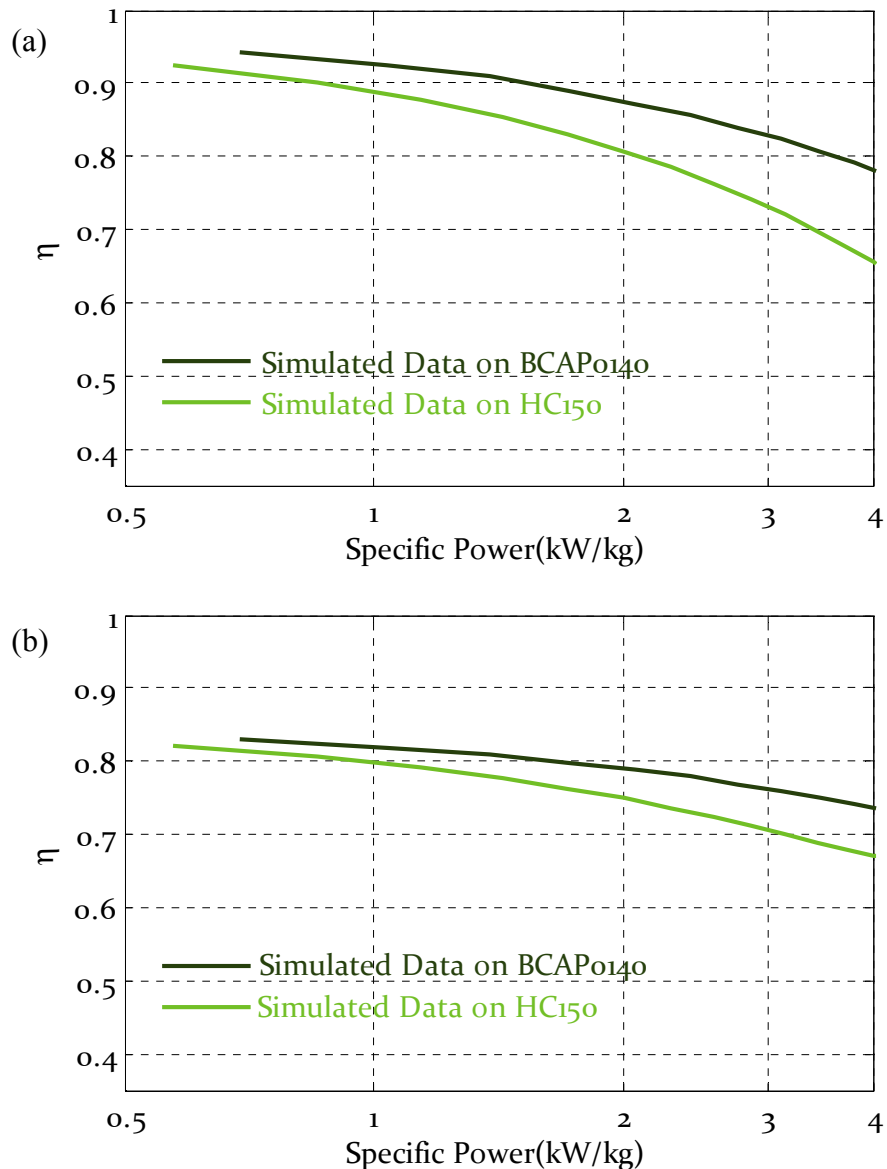
Figure 4.8   **Simulated efficiency of two Maxwell supercapacitor cells cycled at different values of constant power with same fixed voltage limits (nominal voltage and its half) for different cycles. The devices considered are the BCAP0140 (140 F @ 2.5 V) and BCAP0150 (150 F @ 2.7 V). (a) Simulated efficiency according to the power profile of Figure 4.7(a), (b) Simulated efficiency according to the power profile of Figure 4.7(b).**

As shown in Figure 4.8 the supercapacitor efficiency is strictly related to the dynamic of usage. In the typical specific power of usage (0.5–4 kW/kg), the efficiency varies in the range of 0.65–0.95. It is important to underline how the redistribution and self discharge significantly affect the device efficiency. In Figure 4.8(b), where the device, in order to emphasize the redistribution and self discharge phenomena, is cycled between the nominal voltage and its half with a time interval of 30 s at zero current, the supercapacitor efficiency is about 10% lower than the value obtained when the device is cycled continuously without the rest period (Figure 4.8(a)). This aspect is related to the energy

wasted on the modeled resistance elements of parallel branches when the redistribution takes place. The availability of the complete model, capable of representing the self discharge and redistribution phenomena, provides another important key aspect to also correctly simulate the supercapacitor performances under the efficiency profile.

By increasing the specific power, the efficiency values (Figure 4.8(a) vs. Figure 4.8(b)) tend to overlap. As shown in Figure 4.5, under these conditions, the usable energy continues to decrease, which means the effective voltage variation on the capacitive elements of the first branch of the model (Figure 1 in chapter 3) is reduced and consequently, the redistribution phenomenon and its negative effect on the device efficiency are strongly reduced.

4.4. MODEL SCALABILITY

In order to prove the generality of the model, comparisons between the simulated and measured data were conducted, not only at the cell level, but also at the model level. In particular, the experimental data reported in the following were taken, not directly from the Electrical Department of the Politecnico di Milano, but from ENEA–the Italian National agency for new technologies, energy, and sustainable economic development.

The activity involves a supercapacitor module, whose specifications are reported in Appendix 7.1, which is characterized by a nominal capacitance of 63 F and a nominal voltage of 125 V. This module, designed for stationary and traction applications, consists of a series connection of 48 elementary cells of 3000 F @ 2.7 V (Maxwell BCAP3000). The module parameters used for the simulations are reported in Table 4.4.

Table 4.4.   **Model parameters of supercapacitor module: Maxwell BMOD0063 (63 F @ 125 V), considering equivalent electrical model of Figure 3.1 with only three branches.**

	R_i	R_1	C_0	k_C	R_2	C_2	R_3	C_3	R_{leak}
	[mΩ]	[mΩ]	[F]	[F]	[Ω]	[F]	[kΩ]	[F]	[kΩ]
BMOD0063 module	11.82	12.7	45.4	0.156	24	2.54	45	7.23	185

In particular, the activity conducted by ENEA had the aim of characterizing the module for vehicular application. To this end, different tests were performed according to the FreedomCar Ultracapacitor Test Manual [1], which defines a series of tests to characterize aspects of the performance or life behavior of supercapacitors for hybrid electric vehicle (HEV) applications.

Among the different tests Figure 4.9 and Figure 4.10 report the current profile used to characterize the module and verify its performances during the current discharge and charge profiles.
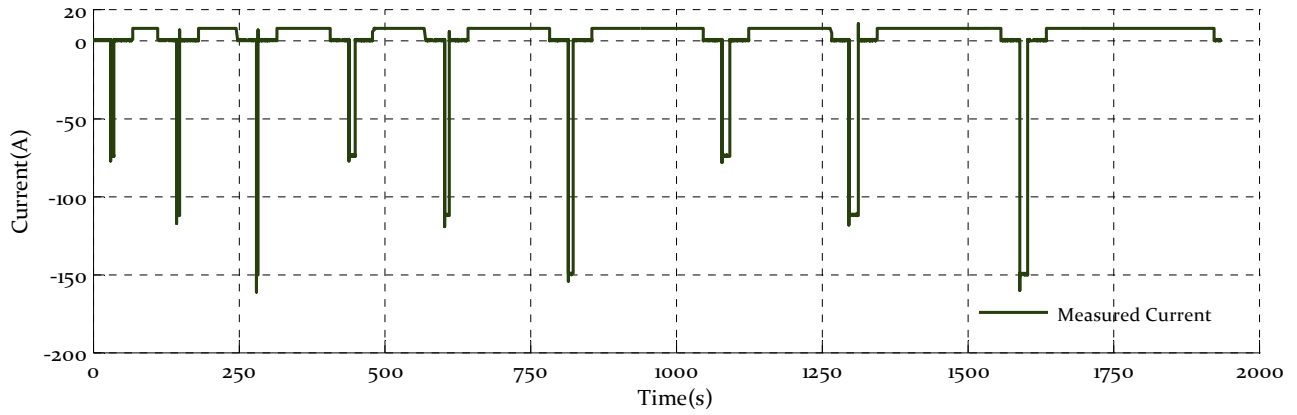
Figure 4.9 **Discharge pulse current characterization profile.**
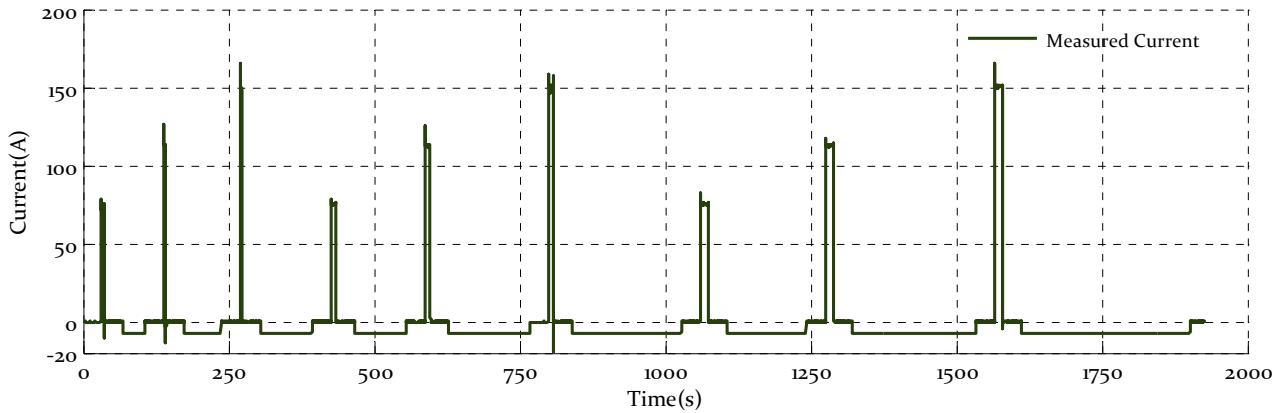
Figure 4.10 **Charge pulse current characterization profile.**

The current profiles are listed according to the data in Table 4.5(a) for the discharge characterization and in Table 4.5(b) for the charge characterization.

Table 4.5. **Supercapacitor module pulse current characterization profile. The cycle described is repeated consequentially three times with different values of t*: 5s, 10s and 15s. (a) Pulse discharge profile, (b) Pulse charge profile.**

(a) Current discharge profile			(b) Current charge profile		
Time increment [s]	Current Value	Voltage Value	Time increment [s]	Current Value	Voltage Value
30	$0 \cdot I_{max}$	U_n	30	$0 \cdot I_{max}$	$U_n/2$
t*	$-0.5 \cdot I_{max}$	Not controlled	t*	$0.5 \cdot I_{max}$	Not controlled
30	$0 \cdot I_{max}$	Not controlled	30	$0 \cdot I_{max}$	Not controlled
to reach U_n	$0.05 \cdot I_{max}$	U_n	to reach $U_n/2$	$-0.05 \cdot I_{max}$	$U_n/2$
30	$0 \cdot I_{max}$	Not controlled	30	$0 \cdot I_{max}$	Not controlled
t*	$-0.75 \cdot I_{max}$	Not controlled	t*	$0.75 \cdot I_{max}$	Not controlled
30	$0 \cdot I_{max}$	Not controlled	30	$0 \cdot I_{max}$	Not controlled
to reach U_n	$0.05 \cdot I_{max}$	U_n	to reach $U_n/2$	$-0.05 \cdot I_{max}$	$U_n/2$
30	$0 \cdot I_{max}$	Not controlled	30	$0 \cdot I_{max}$	Not controlled
t*	$-1 \cdot I_{max}$	Not controlled	t*	$1 \cdot I_{max}$	Not controlled
30	$0 \cdot I_{max}$	Not controlled	30	$0 \cdot I_{max}$	Not controlled
to reach U_n	$0.05 \cdot I_{max}$	U_n	to reach $U_n/2$	$-0.05 \cdot I_{max}$	$U_n/2$

The simulation results and the comparison with the simulated data are reported in Figure 4.12 and Figure 4.13. It is also evident in these simulations that the model is able to correctly simulate the device dynamic under both charge and discharge conditions, as in the low and high dynamic (the correlation factor is higher than 99%).
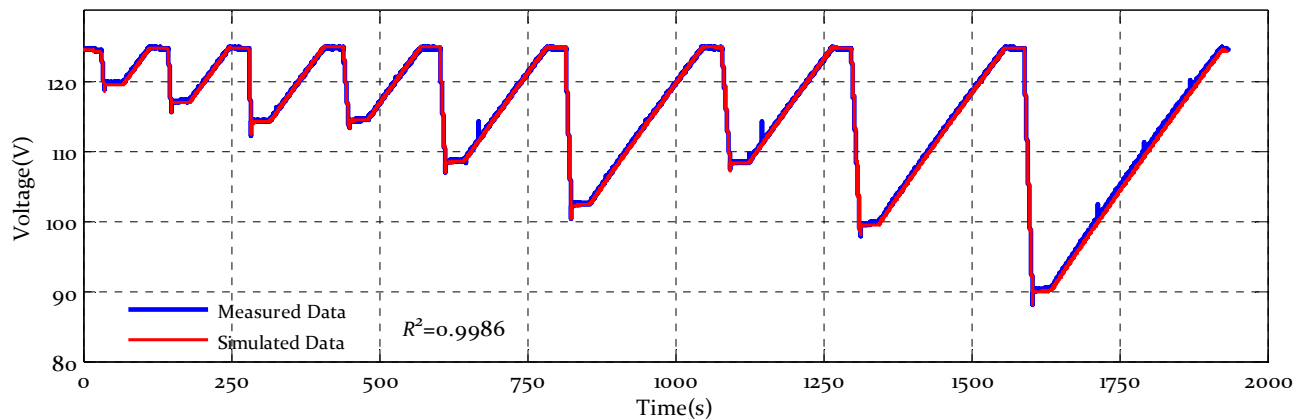
Figure 4.11   **Comparison between measured and simulated module terminal voltages when discharging current profile of Figure 4.9 is applied. The module under consideration is a 63 F @ 125 V–Maxwell BMOD0063.**
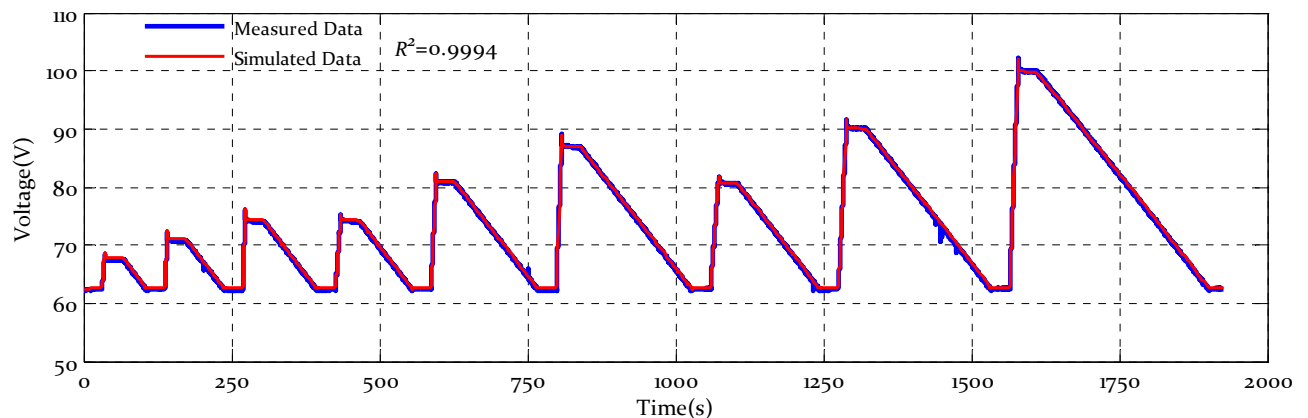
Figure 4.12   **Comparison between measured and simulated module terminal voltages when discharging current profile of is applied. The module under consideration is a 63 F @ 125 V–Maxwell BMOD0063.**

Under the working conditions considered, the comparison between the simulated and measured efficiency, Table 4.6, again shows the validity of the model.

Table 4.6.   **Comparison between measured and simulated efficiency of the Maxwell module BMOD0063 cycle according to the current profile of Figure 4.9 and Figure 4.10.**

(a) Current discharge profile		(b) Current charge profile	
η measured	η simulated	η measured	η simulated
93.3	93.8	93.0	93.4

To complete the dynamic investigation of the module, Figure 4.15(a) shows the simulated efficiency, considering both continuous charge/discharge cycles and a rest

period of 30 s between consecutive charge/discharge phases. Figure 4.15(b) shows the Ragone plot. In order to compare these results with those of the cells reported above, the specific power is calculated considering the total cell mass of 24 kg as a reference rather than the module mass of 59.5 kg. The difference is the result of the module's external case.
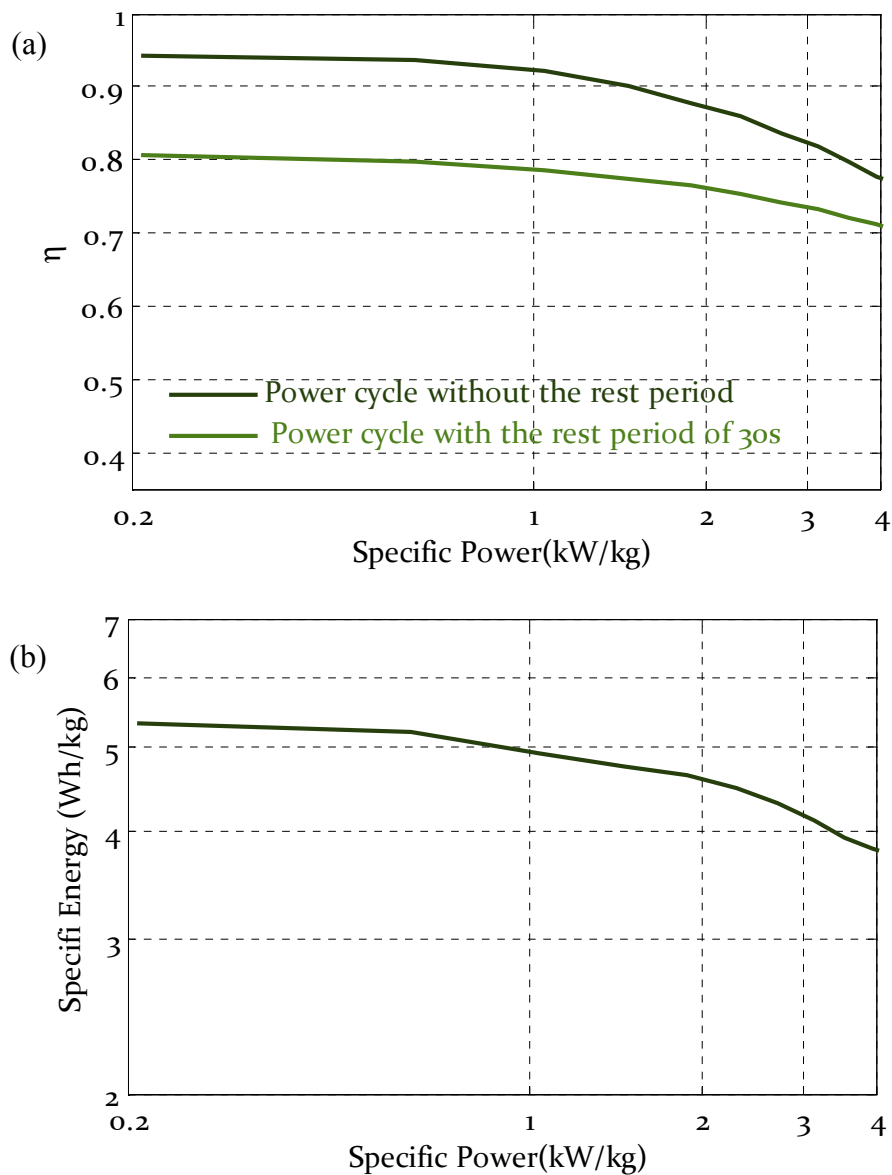
Figure 4.13   **Dynamic performances of Maxwell supercapacitor module BMOD0063 (63 F @ 125 V). (a) Module efficiency versus specific power, (b) Ragone plot.**

Comparing the module results, based on the 3000 F @ 2.7 V cell, it is evident that the system efficiency is very close to that of the cells, 140 F @ 2.5 V and 150 F @ 2.7 V. Regarding the Ragone plot, the larger cells are characterized by higher values of specific energy: 5.2 versus 3 Wh/kg.

4.5. TECHNOLOGY COMPARISON AND RELATIONS WITH THE MODEL PARAMETERS

Another important aspect of the introduced model is the ability to relate its parameters, which can be determined without performing the full frequency response of the device, to specific performances.

In order to accomplish this, from the analysis of Figure 4.14 and Figure 4.15, previously plotted in chapter 3 and reported again for a better exposition, a comparison between the supercapacitor cells of 140 F @ 2.5 V (BCAP0140) and 150 F @ 2.7 V (BCAP0150) is based on an analysis of their frequency response. It should be noted that the 150 F cell represents the evolution of the old 140 F version.
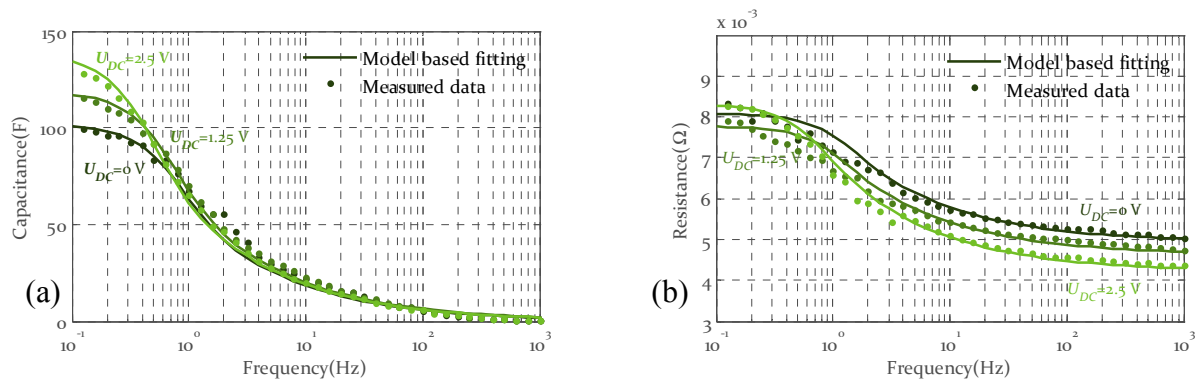
Figure 4.14 **Comparison between measured and modeled frequency responses by least square minimization of 140 F @ 2.5 V Maxwell supercapacitor (BCAP0140) cell at three different polarization voltages: 0, 1.35, 2.5 V. (a) capacitance and (b) resistance.**

Analyzing the trend of capacitance versus frequency, it is clear how the new cells are characterized, for the same frequency values, by higher capacitance values. In addition, as can be noticed, the measured equivalent capacitance in the new cell starts to decrease toward zero for higher frequencies compared to the old cell version. It is clear that there is an improvement related to this aspect, as, analyzing the trend of the measured equivalent resistance, it can be noted how the 150 F cell is characterized by higher values of internal resistance, especially at high frequency.
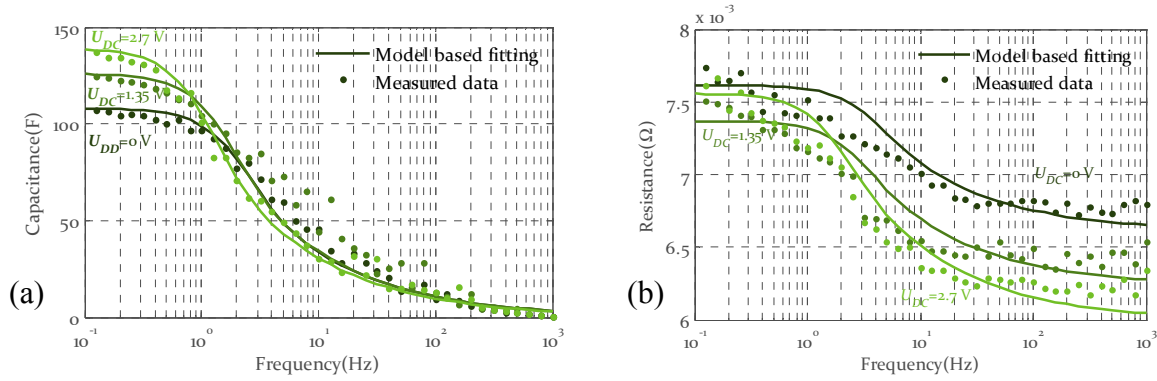
Figure 4.15 **Comparison between measured and modeled frequency responses by least square minimization of 150 F @ 2.7 V Maxwell supercapacitor (BCAP0150) cell at three different polarization voltages: 0, 1.35, 2.7 V. (a) capacitance and (b) resistance.**

Studying (4.3), which is the transfer function used to model the high dynamic of supercapacitors, i.e., for frequencies greater that 100 mHz, it is possible to relate the knee of the capacitance trend to parameter τ.

$$Z_p(jw) = \sqrt{\frac{R}{jw \cdot C}} \cdot \coth\left(\sqrt{jw \cdot R \cdot C}\right) = \frac{t \cdot \coth\left(\sqrt{jw \cdot t}\right)}{C \cdot \sqrt{jw.t}} \tag{4.3}$$

In particular, at the angular frequency equal to the inverse of τ the module of the Bode diagram of the transfer function (4. 3) has a change in slope from -20 dB/dec to -10 dB/dec, while the phase changes from -90° to -45°. Considering the capacitance, this means that, at an angular frequency equal to the inverse of τ, its value changes from 97.8% of the DC value down to the 46% a decade later.

Remembering the expression of τ in (4. 4), where C and R_1 are respectively the values of DC capacitance and resistance and R_i is the value of high frequency resistance, it is clear how the knee of the capacitance trend is strictly related to specific parameters.

$$t = 3 \cdot C \cdot (R1 - R_i) \tag{4.4}$$

It is possible to state that to increase the dynamic of the device with a rated capacitance C, it is necessary to design a cell with a low value of τ. Thus, it is necessary to reduce the difference between R_1 and R_i.

Table 4.7. **First branch parameters and influence on time constant τ(u) for two supercapacitor cells: BCAP0140 (140 F @ 2.5 V, old version) and BCAP0150 (150 F @ 2.7 V, new version).**

	U_n	Ri	R_1	C	$τ$
	[V]	[mΩ]	[mΩ]	*[F]*	[s]
BCAP0140	2.5	4.6	8.2	100.9+13.1·v	1.09+0.14·v
BCAP0 150	2.7	6.5	7.4	107.3+11.2·v	0.29+0.03·v

From Table 4.7, as from Figure 4.14 and Figure 4.15, it is clear that in the new cells, the difference between these resistances has been reduced by increasing the high frequency resistance, R_i. This explains why the supercapacitive effect extends to higher frequencies in the new cells. However, the increase of R_i implies a higher voltage drop during a fast transient, as shown in Figure 4.2(d) and Figure 4.3(d).

Surely in order to increase the dynamic response of the device at an equal capacitance, it is better to reduce the difference between R_1 and R_i by reducing the value of DC resistance, because in this way, not only are the dynamic performances of the device increased, but so is the device efficiency. Comparing the two analyzed cells in Figure 4.8 it is evident that the two cells have similar efficiencies when cycled at a low power value, which is at a low dynamic, but this gap increases in cycles at high power. This is strictly related to the fact that the new cell version has, in the entire frequency range considered, an internal resistance that is greater than the old version, and the relative difference between these resistances is greater at high frequency. It must be pointed out that typical supercapacitor applications are characterized by minimum charge/discharge cycles of several seconds. Thus, it is comprehensible for the manufacturer to try to increase the supercapacitance in a frequency range up to 1–2 Hz in order to better exploit the full capacitance, even if this affects the efficiency performances. It is also important to underline that in a high dynamic application, where it is not typically necessary to use the full capacitance and the efficiency is an important aspect, it is better to choose supercapacitor devices with a low value of internal resistance at a high frequency, R_i, such as the old version cell, BCAP0140. From a physical point of view, resistance R_i is more related to the behavior of the electrode in terms of the conductivity and geometry of the pores, while resistance R_1 is more related to the behavior of the electrolyte. To improve the dynamic of the device and its efficiency, both aspects have to be considered.

From Table 4.7, it can also be noted that the new cell is characterized by a higher value of capacitance, which is mainly due to the fact that the new cell is characterized by a higher nominal voltage (2.7V vs. 2.5V). However, as the 150F cell has a greater mass than the 140F cell (35 g vs. 29 g), this adversely affects the new version cell when the performances are compared by weight (Figure 4.5). Increasing the capacitance can be achieved by increasing the equivalent surface area and/or the operating voltage, which means acting again on the electrolyte behaviors.

4.6. BIBLIOGRAPHY

[1]   FreedomCar Ultracapacitor Test Manual September 2004

5. MANAGEMENT AND INTEGRATION OF DIFFERENT ENERGY STORAGE DEVICES

As introduced in chapter 1, the potential benefits in today's applications arising from the use of energy storage devices are more and more achievable by the use of an integrated energy storage solution. From the experimental analysis conducted in chapter 4, it is evident that the storage performances have to be fully considered in order to achieve an optimal integration. In fact, it can be said that each storage device is characterized:

- by a specific power and energy according to the Ragone plot;
- by a typical dynamic response during the charging and discharging phases;
- by redistribution and self discharge, which are particularly evident in a very low dynamic of usage;
- an efficiency that is strictly related to the dynamic of usage.

This means that, in order to fully exploit the technical performances of a storage device, and consequentially reap the greatest number of economic benefits, the specifications of the application have to very closely match the storage performances. As shown in chapter 1, there is a large number of applications in which the storage requirements cover a wide range in terms of specific energy and power, with an evident impact on the device dynamic, efficiency, and real percentage of utilization.

This is true in all applications, ranging from a grid toward industrial applications, including the transportation sector. For example, considering the electric service power quality function in a grid application [1], an energy storage system (ESS) makes it possible to avoid supply interruptions caused by short duration events. These events, which affect the level of power quality in terms of voltage sags, frequency variation from the nominal value, harmonics, and short interruptions, require energy storage in the range of several seconds up to 1 minute.

Considering electric and hybrid vehicle requirements [2], it can again be seen that a storage system has to realize an energy mission as a power mission. The power mission is required in order to realize the peak shaving function during the accelerating and braking (energy-recovering) phases, while the energy function is required in order to guarantee the vehicle autonomy. In relation to this distinction, it is clear that the required cycle life regarding the frequency of the charge/discharge cycle of the power mission is much higher than the energy mission (300.000 vs. 1000 cycles).

From all of these considerations, it appears evident that there is no unique storage technology capable of fulfilling the different requirements, which is increasingly true if the sizing of the storage system takes into account a correct optimization in terms of total system efficiency, cycle life, and maximization of the storage utilization, in terms of both the energy and power.

The benefits arising from a hybrid storage system are related to the possibility of extending the storage performances by merging the single device performances into a unique solution.

In order to accomplish this, the use of electronic power converters is required to match the different voltage levels between storage devices. Even more important is the availability of adequate control strategies that are able to guarantee the correct action of each storage device according to the objective function to be realized. The goal of the integration, in fact, can be addressed as different object functions:

- maximization of the efficiencies of the storage devices during operation;
- maximization of the recovering energy function;
- increasing the power level quality for the load and/or main source;
- peak shaving function;
- increasing the storage cycle life;
- downsizing the storage device.

The control algorithm plays an important role in this. It is evident that the different object functions are not completely unrelated, because the focus on a specific function can totally or partially influence other potential benefits arising from the integration. In the following, a theoretical approach to the two specific control strategies developed is first presented in order to:

1) increase the power quality level on the DC bus interconnection of different electrical energy storage devices;

2) minimize the total losses of the integrated electrical energy storage devices during operation.

Furthermore, these control strategies are supported by an extended experiment to investigate the multiple benefits of using a specific control algorithm for the global storage device performances.

5.1. SYSTEM LAYOUT

The general framework in which the control strategies are applied is reported in Figure 5.1. The system consist of n storage devices that are all connected to the same system's DC bus by means of appropriate DC/DC electronic power converters in order to match the storage device voltages and control the power flows independently. In addition, the active loads are connected to the same system bus, schematically grouped as a centralized equivalent load and external energy source. In principle, this source is any energy source (i.e., electrical grid, combustion engine, renewable...) that is able to deliver the mean power requested by the loads. No direct control is exerted on the external energy source by means of the control algorithm, which can directly act only on the DC/DC power converters. Thus, it can be excluded from the scheme for the control strategy implementation.
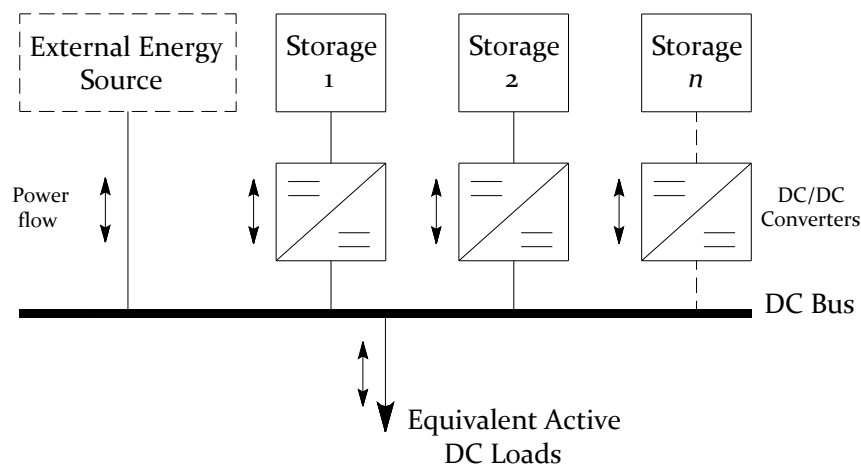
Figure 5.1   **General layout considered for analysis of energy storage control algorithms.**

In the general approach, the number of electrical storage systems is n and any technology can be considered, but the knowledge of an adequate model for the storage devices involved, in particular for the losses minimization algorithm, is a necessary condition to correctly implement the control strategies. For these reasons, the following approaches focus on the correct integration of a storage technology that has been thoroughly investigated [3-6], lead acid batteries, with the supercapacitor technology widely analyzed in the previous chapters.

In addition, the reason for the choice of the lead acid and supercapacitor technologies is strictly related to their dynamic performances. In Figure 5.2, where the Ragone plot is reported, it is evident that supercapacitors very thoroughly cover, from a

dynamic point of view, the specific power range of 10^2–10^3 kW/kg, which is a region where lead acid batteries show a consistent reduction in performance in terms of specific energy.
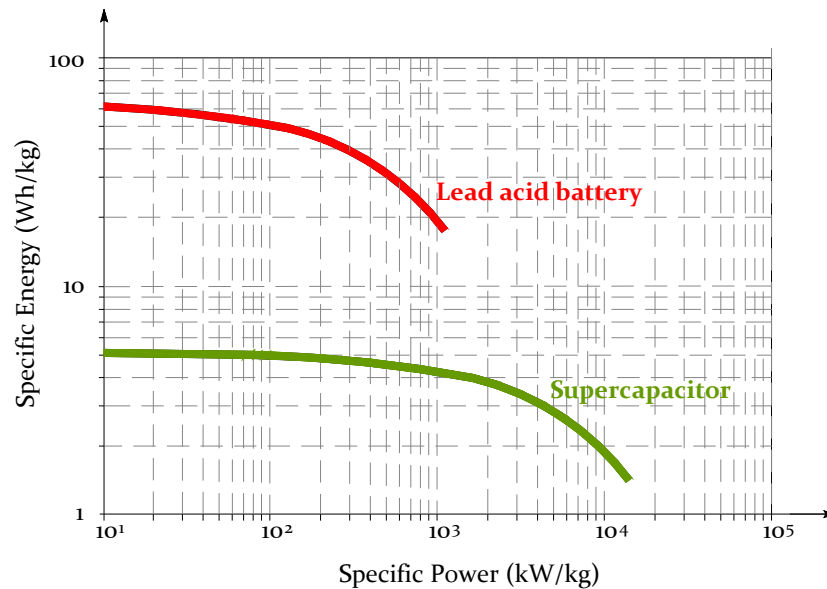
Figure 5.2　　**Ragone plot of two technologies considered in system layout: lead acid and supercapacitor.**

The experimental analysis reported in chapter 4 showed that the device efficiency is greatly reduced, by 50% or more, when the electrical storage devices are used in a dynamic condition over the knee of the Ragone plot. In all of the applications, as electrical traction or electrical service power quality functions, where the storage is used with specific power values in the range of 10^1 kW/kg up to 10^3 kW/kg and more, the benefits arising from the correct integration of the energy oriented storage device (lead acid battery) with the power oriented one (supercapacitor) can be maximized in order to reduce the overall system losses and exploit the full performances of the two devices.

5.2. POWER QUALITY INCREASING CONTROL STRATEGY

With reference to Figure 5.1, the proposed control strategy aims to improve the power quality level on the DC bus in terms of voltage variation according to the different load conditions for the requested or regenerated power.

In addition, this strategy aims:

1) to shave the power supplied by the external energy source,

2) to keep the state of charge of each storage device near a reference value,

3) to realize a fully plug and play storage system.

In order to accomplish this, the correct implementation requires, in addition to a knowledge of the typical dynamic fluctuation of the power requested by the loads, the maximum dynamic the external energy source can follow and the desired dynamic with which it has to operate. With this information, it is possible to select the correct storage units in terms of technology (i.e., strictly related to the specific energy and power) and size. In fact, limiting the dynamic of the external energy source means that the higher dynamics requested by a load have to be satisfied by the storage units, in terms of both energy and power. To do this, the storage units have to be able to supply the power quicker than the external source. Thus, it is necessary to act on the bandwidths of the controllers of the different interface converters and set these bandwidths compliant with the typical dynamic that each storage unit can follow. This means setting each controller with a lower or comparable bandwidth despite the maximum allowable or desired bandwidth with which each storage device has to charged and discharged. In this way, each storage unit works in its optimal dynamic condition; in particular, faster control will be applied to the power oriented storage, while slower control will be applied to the more energy oriented one. The remaining dynamic, the slowest one, will consequently follow the external energy source. In tuning the regulators, it is necessary to separate the dynamics of the different converters in order to avoid oscillations in the power exchanged between them.

In order to maintain the desired state of charge in the storage units, it is necessary to provide feedback to the control about the actual state of charge. In particular, each storage unit will try to place on the DC bus a voltage that is a function of its own state of charge:

$$U_{dc,ref} = U_{dc}^* - k\left(Q_{storage,ref} - Q_{storage,meas}\right)$$
(5. 1)

where ref and meas refer to the reference and measured values, respectively. Moreover, *V*$^*_{dc}$ indicates the DC reference voltage of the storage interface converter, and Q refers to the state of charge. At a steady state, if the state of charge of one storage unit is lower than the desired value, the DC voltage reference of this storage unit is reduced and, consequently, an amount of power is drawn from the DC bus to recharge the unit. In this way, the control system automatically maintains the state of charge of the storage unit around the desired value. Moreover, from (5. 1) it is clear that the reference voltage for each storage unit is obtained using only the DC bus voltage and state of charge. No external information or coordination between the units is needed. This feature makes it possible to add and substitute storage units without modifying the system. A fully plug and play structure is, therefore, obtainable. This structure can easily be updated if the network characteristic changes with the introduction of new loads or generation units.

In Figure 5.3 the scheme of the control chain of the DC/DC interface converter for each one of the storage system is reported.
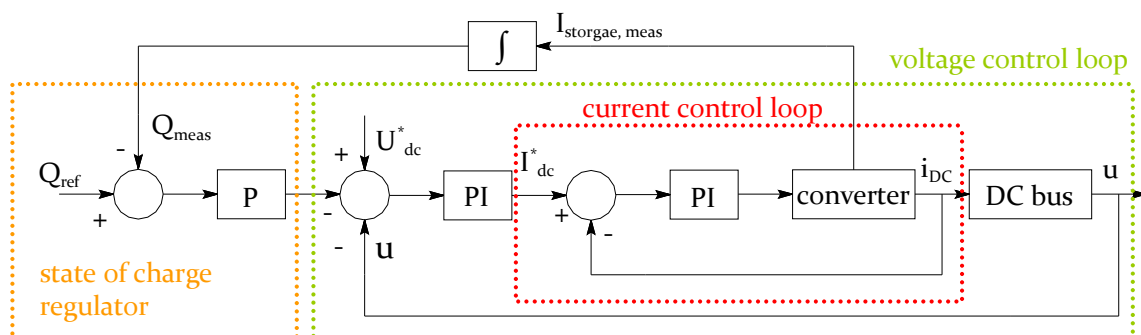
Figure 5.3　**Scheme of control chain of DC/DC interface converter for each storage device reported in Figure 5.1.**

The control chain consists of two main control loops: an internal current control loop and an external voltage control loop. The measured state of charge, Qmeas, is calculated as the difference between the initial state of charge and the charge reduction calculated as the integral of total net delivered current. Generally, this expression is not always correct, especially for electrochemical batteries. However, there are some techniques that allow the accurate estimation of the state of charge [7-8]. In contrast, supercapacitors do not suffer from this problem because of the strict relationship between the state of charge and terminal voltage.

The tuning of the regulators has to be set as follows:

1) the current PI regulator is tuned with the highest possible bandwidth compatible with the switching frequency, i.e., one decade lower than the converter switching frequency;

2) the voltage PI regulator is tuned with a bandwidth such that the device operates with the desired dynamic. Specifically, the voltage bandwidth has to be at least a decade lower than that of the current loop;

3) the voltage PI controllers of the converters are tuned with bandwidths that are at least one decade apart in order to avoid power oscillations between different storage units;

4) the state of the charge proportional regulator is tuned to the ratio between the maximum allowed state of charge variation and the maximum desired dc voltage variation.

The proposed control strategy, despite the information introduced in the next paragraph, has the peculiarity that no information regarding the equivalent electrical model of the involved storages is needed. It is necessary to have information about the real behaviors of the storage devices, particularly regarding the dynamic performances and maximum allowable bandwidth in terms of the charging and discharging rates. This is surely a strong point for realizing a plug and play solution.

It is evident that the proposed control strategy does not increase the voltage fluctuations on the DC bus. However, in addition, a peak shaving function for the main source is realized, because the dynamics higher than the desired one for the external energy source are controlled by the storage units, starting from the energy oriented units toward the power oriented ones for the higher dynamics. It is clear that, in this way, another collateral benefit is related to the possibility of using different storage units with the proper dynamic in order to increase their specific usable energy, efficiency, and lifetime. These aspects will be particularly analyzed in section 5.5, where the experimental results are reported.

5.3.   LOSSES MINIMIZATION STRATEGY

With reference to Figure 5.1, the proposed minimization algorithm focuses on the analysis of the system in Figure 5.4.
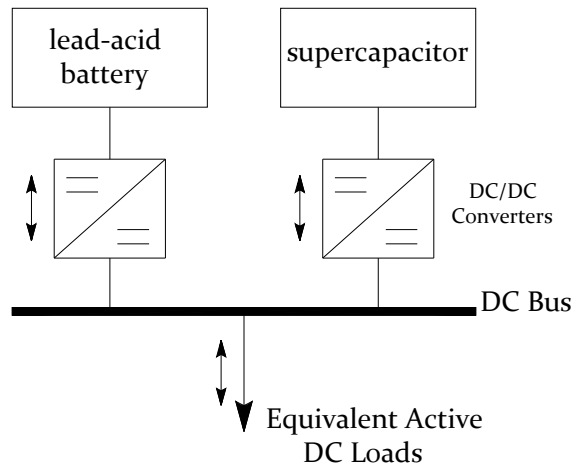
Figure 5.4   **System layout considered for loss minimization algorithm consisting of integration of two different storage technologies**

In the scheme of Figure 5.4, the two storage devices are unique energy sources that are able to supply the DC loads under all dynamic operating conditions. An algorithm for loss minimization is introduced, starting from the description of the electrical models used.

5.3.1.   ELECTRICAL STORAGE SYSTEM MODELS

- *Lead acid batteries*

The lead-acid battery has been modeled as a voltage source in series with the internal resistance, R_{ob}, and with two R-C branches that approximate the dynamic behavior of the battery Figure 5.5 [6].]. Generally, the emf values of E_m depend on the state of charge (*So*C) of the battery, according to the relationship in (5. 2) [6].
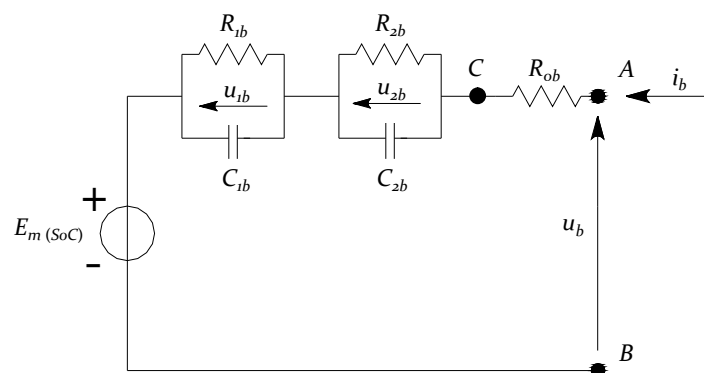
Figure 5.5   **Lead acid battery equivalent model.**

$$E_m = E_{mo} - K_E \left(273 + \lrcorner\right)\left(1 - SoC\right), \qquad (5.2)$$

where:

⌐ :   the electrolyte temperature measured in Celsius;

K_E: a constant thermal coefficient;

SoC: state of charge.

According to [6], this model is not able to take into account the parasitic effects of the water electrolysis that occurs at the end of the charging process. This approximation can be done because it is well known that lead acid batteries have a charge efficiency close to 1 when the battery voltage is lower than 2.3 V per cell. The parasitic branch at terminal C-B of Figure 5.5 can be neglected without losing generality in the proposed algorithm.

- *Supercapacitor*

The electrical equivalent model introduced in chapter 3 is used, Figure 5.6, considering three parallel branches: the first one represents the fast dynamic of the device, the second one is the redistribution phenomenon "*R*," and the last one is the self discharge, "*S*," behavior of the device. It is important to emphasize that the supercapacitor model has to take into account the redistribution and self discharge phenomena in order to correctly implement the algorithm. As seen in the previous chapter, in fact, these phenomena affect the device efficiency in a consistent way and neglecting them could result in an efficiency estimation error of up to 10%.
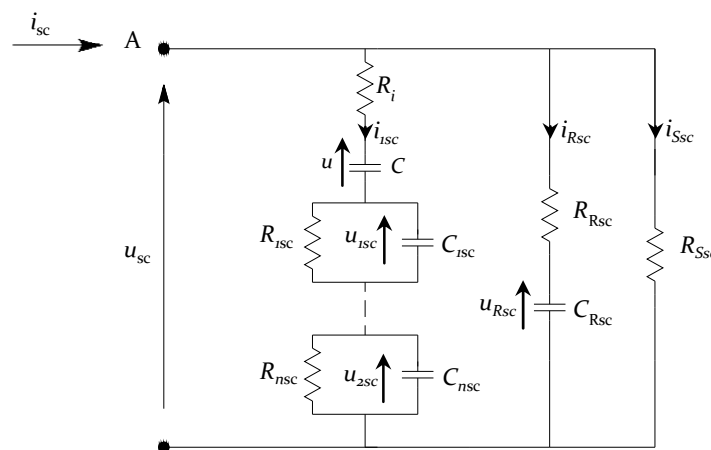
Figure 5.6   **Supercapacitor equivalent model**

5.3.2. CONTROL ALGORITHM

The object function of the proposed algorithm is to maximize the function in (5.3) representing the global system efficiency.

$$f := \mathsf{h}(I, S, T) \tag{5.3}$$

which is influenced by:

I: the vector of the storage system's currents $[i_1\ i_2\ ...\ i_n]^T$;

S: the vector of the storage system's state of charge $[S_1\ S_2\ ...\ S_n]^T$;

T: the vector of the storage system's temperature $[T_1\ T_2\ ...\ T_n]^T$.

The strategy is based on finding the optimal value, I^*, of the supplied/requested current by each storage system, so that f is maximized:

$$\mathsf{h}^* = max_I(f) \tag{5.4}$$

subjected to

$$P_{stg1} + P_{stg2} = P_{load}. \tag{5.5}$$

Equation (5. 5) represents the active power constraint between the total power requested and/or generated by the load and the power exchanged with the storage systems.

In the mathematical formulation, the influence of temperature on the global efficiency is not taken into account and, without losing generality in the approach of the methodology, the maximization of the efficiency function in (5. 3) is addressed as a minimization problem for the global devices losses.

Based on this, considering the circuit equivalent models of the lead acid battery in Figure 5.5 and supercapacitor in Figure 5.6, the global losses can be written as the sum of the energy wasted on the resistive elements:

$$f([x]) = R_{ob} \cdot i_b^2 + R_{1b} \cdot i_{1b}^2 + R_{2b} \cdot i_{2b}^2 + R_i \cdot i_{1sc}^2 + \sum_{k=1}^{n} \left(R_{nsc} \cdot i_{nsc}^2 \right) + R_{Rsc} i_{Rsc}^2 + R_{Ssc} i_{Ssc}^2 \tag{5.6}$$

with:

$$\begin{cases} i_{1b} = i_b - C_{1b}\dot{u}_{1b} \\ i_{2b} = i_b - C_{2b}\dot{u}_{2b} \\ i_{1sc} = i_{sc} - C_{Rsc}\dot{u}_{Rsc} - \dfrac{u_{sc}}{R_{Ssc}} \\ i_{nsc} = i_{1sc} - C_{nsc}\dot{u}_{nsc} \\ i_{Rsc} = C_{Rsc} \cdot \dot{u}_{Rsc} \\ i_{Ssc} = \dfrac{u_{sc}^2}{R_{Rsc}} \end{cases} \tag{5.7}$$

where the terms containing the voltage derivatives (i.e., $C\dot{u}$) represent the current flowing in the capacitance of the parallel *R-C* branches of both the battery and supercapacitor. Considering the relations in (5. 7), (5. 6) can be rewritten as:

$$f([x]) = (R_{0b} + R_{1b} + R_{2b})i_b^2 - 2(R_{1b}C_{1b}\dot{u}_{1b} + R_{2b}C_{2b}\dot{u}_{1b})i_b + \left(R_{0sc} + \sum_{k=1}^{n} R_{nsc}\right)i_{1sc}^2 +$$

$$- 2i_{1sc}\left(\sum_{k=1}^{n} R_{nsc}C_{nsc}\dot{u}_{nsc}\right) + R_{1b}C_{1b}^2\dot{u}_{1b}^2 + R_{2b}C_{2b}^2\dot{u}_{2b}^2 + \sum_{k=1}^{n} R_{nsc}C_{nsc}^2\dot{u}_{nsc}^2 + R_{Rsc}C_{Rsc}^2\dot{u}_{Rsc}^2 + \frac{u_{sc}^2}{R_{Ssc}}$$

(5. 8)

In order to minimize the total losses, the control variables with which it is possible to act by means of the DC/DC interface converters are the two storage currents i_b and i_{sc}. Consequently, the minimum of $f([x])$ can be written as:

$$\min f([x]) = \min_{[i_b, i_{sc}]} \begin{bmatrix} (R_{0b} + R_{1b} + R_{2b})i_b^2 - 2(R_{1b}C_{1b}\dot{u}_{1b} + R_{2b}C_{2b}\dot{u}_{1b})i_b + \left(R_{0sc} + \sum_{k=1}^{n} R_{nsc}\right)i_{sc}^2 + \\ - 2\left(R_{0sc} + \sum_{k=1}^{n} R_{nsc}\right)\left(C_{Rsc}\dot{u}_{Rsc} + \frac{u_{Ssc}}{R_{Rsc}}\right)i_{sc} - 2\left(\sum_{k=1}^{n} R_{nsc}C_{nsc}\dot{u}_{nsc}\right)i_{sc} \end{bmatrix}$$

(5. 9)

The losses minimization problem can, thus, be written as:

$$\min_{[x]} f([x]) = \min_{[x]}\left([x]^T[Q][x] - 2[x]^T[b]\right)$$

(5. 10)

subjected to the power constraint written in reference to the currents on the DC bus side:

$$h([x]) := [A][x] - d = 0$$

(5. 11)

where the different matrices in (5. 10) and (5. 11) are:

$$[x] = \begin{bmatrix} i_b & i_{sc} \end{bmatrix}^T$$

$$[Q] = \begin{bmatrix} R_{0_b} + R_{1_b} + R_{2_b} & 0 \\ 0 & R_{0_{sc}} + \sum_{k=1}^{n} R_{n_{sc}} \end{bmatrix}$$

$$[b] = \begin{bmatrix} R_{1b}C_{1b}\dot{u}_{1b} + R_{2b}C_{2b}\dot{u}_{2b} \\ \left(R_{0_{sc}} + \sum_{k=1}^{n} R_{n_{sc}}\right)\left(C_{R_{sc}}\dot{u}_{R_{sc}} + \frac{u_{sc}}{R_{S_{sc}}}\right) + \sum_{k=1}^{n} R_{n_{sc}}C_{n_{sc}}\dot{u}_{n_{sc}} \end{bmatrix}$$

$$[A] = \begin{bmatrix} \dfrac{u_b}{u_{DC}} & \dfrac{u_{sc}}{u_{DC}} \end{bmatrix}$$

(5.12)

and d is the load current at the DC bus. The current constraint in (5. 11), by means of the matrix [A], takes into account the difference in the voltage levels between the DC bus and the storages, due to the presence of the interface DC/DC power converters. In addition, in this analysis, their efficiency is considered equal to 1. The mathematical problem expressed in (5. 10) subjected to (5. 11) can be solved using the Lagrange multipliers method. To accomplish this, the Lagrangian function, containing the new variable "λ", which is Lagrange multiplier, is introduced in (5.13).

$$\Lambda([x],\lambda) = f[x] + \lambda\, h[x] =$$
$$= [x]^T [Q][x] - 2[x]^T [b] + \lambda\,([A][x] - d) \tag{5.13}$$

The meaning of λ is, in this case, the rate of change of the total losses as a function of the current injected or supplied by the storages devices.

By imposing the gradient of the Lagrangian function equal to zero, the current values of the storages devices that minimize the total losses subjected to the current constrain can be determined. In particular:

$$\nabla\Lambda([x],\lambda) = 0 \Rightarrow \begin{cases} 2[Q][x] - 2[b] + \lambda [A]^T = 0 \\ [A][x] - d = 0 \end{cases} \tag{5.14}$$

The solutions of (5.14) are shown in (5.15)

$$i_b = -\frac{1}{\text{tr}[\hat{Q}]}\begin{bmatrix} -\left(R_{1_b}C_{1_b}\dot{u}_{1_b} + R_{2_b}C_{2_b}\dot{u}_{2_b}\right)u_{sc} + \\ +\left(\left(R_{0_{sc}} + \sum_{k=1}^{n}R_{n_{sc}}\right)\cdot\left(C_{R_{sc}}\dot{u}_{R_{sc}} + \frac{u_{sc}}{R_{S_{sc}}}\right) + \sum_{k=1}^{n}R_{n_{sc}}C_{n_{sc}}\dot{u}_{n_{sc}}\right)u_{sc} - (d\cdot u_{DC})\left(R_{0_{sc}} + \sum_{k=1}^{n}R_{n_{sc}}\right) \end{bmatrix}$$

$$i_{sc} = -\frac{1}{\text{tr}[\hat{Q}]}\begin{bmatrix} \left(R_{1_b}C_{1_b}\dot{u}_{1_b} + R_{2_b}C_{2_b}\dot{u}_{2_b}\right)u_b + \\ -\left(\left(R_{0_{sc}} + \sum_{k=1}^{n}R_{n_{sc}}\right)\cdot\left(C_{R_{sc}}\dot{u}_{R_{sc}} + \frac{u_{sc}}{R_{S_{sc}}}\right) + \sum_{k=1}^{n}R_{n_{sc}}C_{n_{sc}}\dot{u}_{n_{sc}}\right)u_b - (d\cdot v_{DC})\left(R_{0_b} + R_{1_b} + R_{2_b}\right) \end{bmatrix} \tag{5.15}$$

$$\lambda = -\frac{2}{u_{DC}\text{tr}[\hat{Q}]}\begin{bmatrix} d\cdot\det[Q] - \left(R_{0_b} + R_{1_b} + R_{2_b}\right)\cdot\left(\left(R_{0_{sc}} + \sum_{k=1}^{n}R_{n_{sc}}\right)\cdot\left(C_{R_{sc}}\dot{u}_{R_{sc}} + \frac{u_{sc}}{R_{S_{sc}}}\right) + \sum_{k=1}^{n}R_{n_{sc}}C_{n_{sc}}\dot{u}_{n_{sc}}\right)u_{sc} + \\ -\left(R_{0_{sc}} + \sum_{k=1}^{n}R_{n_{sc}}\right)\left(R_{1_b}C_{1_b}\dot{u}_{1_b} + R_{2_b}C_{2_b}\dot{u}_{2_b}\right)u_b \end{bmatrix}$$

where:

$$[\hat{Q}] = \begin{bmatrix} u_{sc} & 0 \\ 0 & u_b \end{bmatrix}[Q] \tag{5.16}$$

The solution of (5.14) identifies the minimum value of the Lagrange function because the Hessian matrix of $\Lambda([x],\lambda)$ is positive definite and equal to:

$$\nabla^2\Lambda([x],\lambda) = 2[Q] > 0 \tag{5.17}$$

The values of currents in (5.15) those maximize the global efficiency are not able to guarantee the desired state of charge of each storage device. According to this, in order to avoid a trend of total discharge or charge of the different storage devices an additional term must be included in the expression of the optimal current values. This term is proportional to the difference between the desired S^* and the actual state of charge S^{act} of each module, so that:

$$\hat{I} = I^* + k \left(S^* - S^{act} \right)^T$$

(5.18)

where:

I^*:   the vector of storage system currents solution of (5.14);

k: the proportional constant.

The vector of the determined current, "$\hat{I}$," represents the reference currents of the interface DC/DC power converters of Figure 5.4 with which the different storage devices have to be charged or discharged.

It is worth noting that this minimization is carried out on a continuous basis, i.e., for every value of u, the algorithm sets the values of the battery and supercapacitor currents in order to minimize the losses, while satisfying the active power constraint without any prior knowledge of u. Thus, the loss minimization is not designed to be an integral energy minimization because it neither explicitly takes into account the history of each storage device (i.e., the current paths followed by each device) nor does it foresee the possible trend of u in order to perform some sort of predictive control. In fact, if the duty cycle set by the load was known a priori, an optimal share between the power supplied by (or requested from) the storage devices could be found, and this configuration could be even better than that found by the algorithm, because the latter would be obtained through the summation of the local minima, whereas the former, taking advantage of the complete knowledge of the cycle, could be found by the minimization of the overall losses. This means that the proposed control strategy is particularly suitable when the load behavior is unknown and randomly variable in time. This is typical in traction applications for electric or hybrid vehicles with an unknown driving path as the wanted performances vary with driver exigencies.

It is also important to notice that this control strategy exploits the knowledge or an estimate of the currents flowing through the resistances of the parallel R-C branches of both the batteries and supercapacitors. In the analysis that is carried out, the current flowing through the resistances are estimated knowing the initial voltages of the capacitors and the total current injected or drawn in the storage device, in other words by solving the electrical circuit models.

For the determination of the state of charge, which is needed for the implementation of a corrective current term that is able to prevent the depletion of the storage devices, the same consideration reported in the previous paragraph are valid.

5.4. EXPERIMENTAL AND SIMULATION RESULTS

In this section, an extensive analysis of the introduced control strategies is reported. In particular, thanks to a collaboration with an industrial partner, it was possible to experimentally verify a specific control strategy (the power quality increasing control strategy) in a real industrial application and experimentally verify the benefits arising from the integration of different storage technologies in a unique solution, in order to realize a hybrid storage device.

After this, further simulations results based on the real application are applied considering the loss minimization algorithm.

5.4.1. APPLICATION DESCRIPTION

The system in the analysis is an indoor full electric forklift with a nominal load capacity of 2 tons and equipped with a lead acid storage unit of 48 V and a 500 Ah rated capacity. The forklift has a weight of 951 kg. A representative picture of the system and the equivalent electrical layout considered for the study are reported in Figure 5.7.

lead-acid
battery

Equivalent Active
DC Loads:
- 3 phases induction motors
- auxiliaries

(a)   (b)
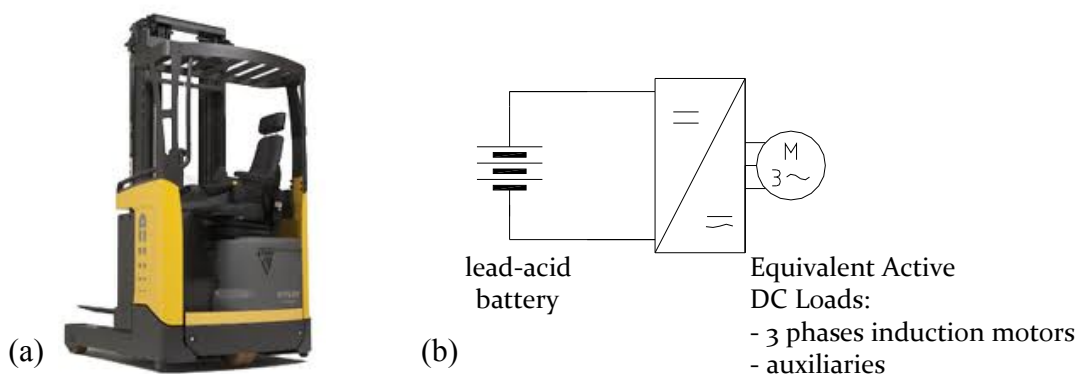
Figure 5.7   **Full electric reach truck forklift considered in experimental activity: 2 ton load capacity and equipped with lead acid battery pack of 48 V with 500 Ah rated capacity. a) Reach truck picture, b) equivalent electrical system layout considered for the experimental activity.**

In the base configuration, the vehicle is equipped only with the lead acid battery pack for the forklift mission. In this typical traction application, the storage unit has to supply the loads in order to guarantee both the power oriented mission, in particular during the accelerating and braking phases, and the energy oriented mission to supply the average

power requested to guarantee the vehicle autonomy. With reference to the Ragone plot in Figure 5.2, it is clear that lead acid battery technology fulfills the energy mission better than the power one.

To better understand this aspect, the vehicle was tested in reference to a standard cycle, and the current and voltage profiles requested of the battery storage unit by the loads are reported in Figure 5.8. The reference test cycle characteristics are reported in Table 5.1, and the cycle is consequentially repeated for the entire test duration.

Table 5.1   **Reference test cycle for reach truck forklift**

Phase	Description
1	Forks lifting without load (6m)
2	Forks lowering without load (6m)
3	Load pick up (2 tons)
4	Load lifting (6m)
5	Load lowering (6m)
6	Forklift lifting (15m)
7	Load lifting (6m)
8	Load lowering (6m)
9	Forklift lifting (15m)
10	Load lifting (6m)
11	Load lowering (6m)
12	Load pick down (2 tons)

The data reported in Figure 5.8 show the battery dynamic during the forklift operations. In particular, it is possible to indentify the traction phases. In the cycle analyzed, it is evident that the battery terminal voltage varies from the nominal value of 48 V down to 39 V in discharging and up to 54 V in the regeneration phase when the vehicle brakes.
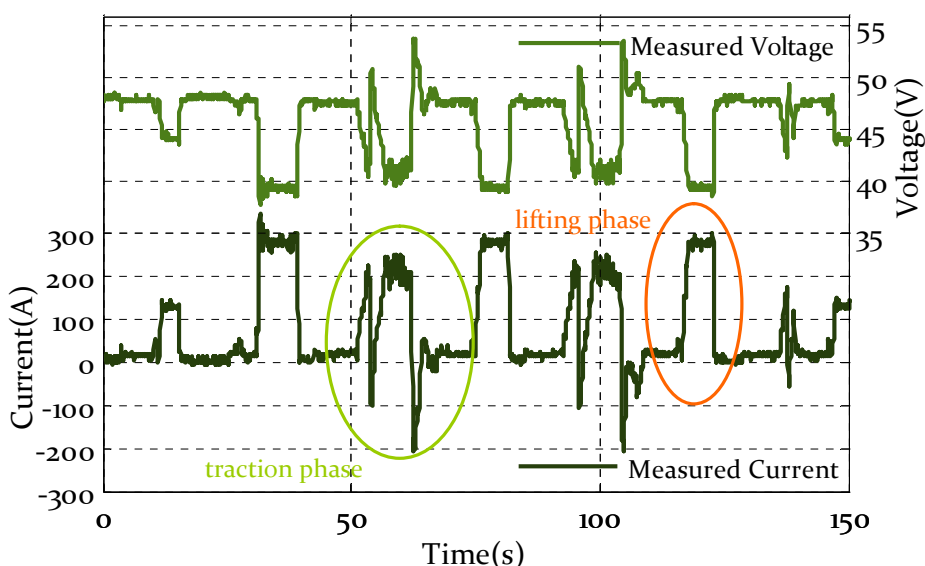

Figure 5.8   **Current and voltage profile drawn by lead acid storage of reach forklift truck during reference test cycle operation.**

A peak shaving function of the main battery, by means of a power oriented storage system, makes it possible to change the current profile toward a more constant value, which means enhancing the operative working condition of the lead acid storage unit. As shown in literature [9-12], there is a strict relationship between the battery available capacity (BAC) and discharging rates; in particular, the maximum BAC for an electrochemical battery is obtainable by discharging the device at a constant current rate, and the capacity availability increases by reducing this value. Each deviation from this condition introduces a loss in terms of the available capacitance. From this, the goal of the peak shaving function of the lead acid battery is clear in relation to the available capacity.

5.4.2. SYSTEM INTEGRATION BY MEANS OF THE POWER QUALITY INCREASING STRATEGY

Taking into account the load requirements with reference to Figure 5.8, the power quality increasing strategy is used to realize a peak shaving function for the main battery. In this application, with reference to Figure 5.9, the objective function of this control strategy, which consists of reducing the voltage fluctuations of the DC bus when the lead acid battery is connected, is not primarily to improve the power quality on the DC bus, but rather to realize a peak shaving function for the main battery. The power quality increase in term of reduced voltage fluctuations is a secondary effect. In fact, the peak shaving function is realized by reducing the battery terminal voltage variation by means of an appropriate power oriented storage device that is able to inject (or absorb) current into (or from) the loads during the high dynamic current request (or regeneration). With reference to the general scheme reported in Figure 5.1, the lead acid battery is the external energy source and the power oriented storage device, which is a supercapacitor module in this case, is interfaced to the DC bus by means of appropriate DC/DC power converters.
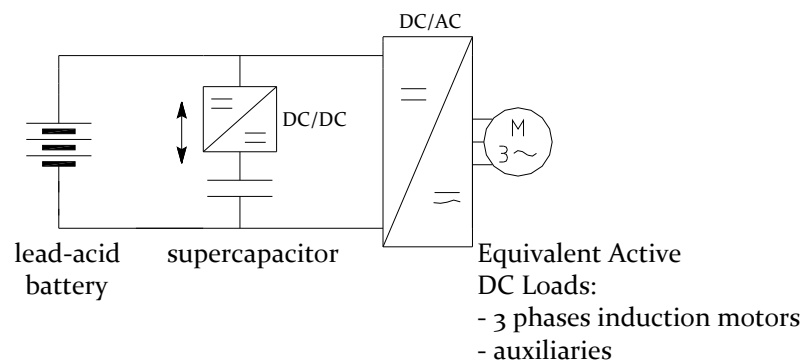
Figure 5.9   **Forklift system layout with integration of supercapacitor storage unit.**

Considering the control strategy and system layout, the DC/DC power converter has to be bidirectional and designed to exchange the maximum cycle peak power minus the cycle average power supplied by the battery: about 7.2 kW in this case. The bidirectional converter structure can be chosen as a:

1) step up converter toward the DC-Bus,

2) step down converter toward the DC-Bus,

3) step up/down converter toward the DCc-Bus.

This choice is related to the electrical characteristics of the supercapacitor module. Based on the converter structure, the supercapacitor module voltage over all of the system's operating conditions has to be:

1) always lower than the DC-bus voltage,

2) always greater than the DC-bus voltage,

3) independent of the DC-bus voltage.

The above conditions guarantee the correct power management for the supercapacitor module, independently of the control strategy adopted. The technical limits of the first two solutions are reflected in a simpler converter structure because only one converter leg is required to realize the DC/DC converter. In contrast, the last structure requires two converter legs to realize the step up/down function for the same direction of power flow. In addition, the third solution requires a more complicated modulation technique.

For the system layout, the choice is a step up converter toward the DC-Bus (Figure 5. 10), in order to avoid uncontrolled power flows from the DC-Bus toward the supercapacitor module in a case of failing or absence of switching modulation.
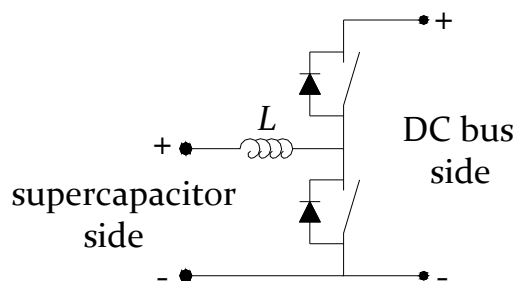
Figure 5. 10   **Structure of DC/DC converter interface with supercapacitor module.**

In particular, the converter hardware has been realized by using one leg of a commercially available inverter (Zapi Dual AC2 + HP Power Inverters High Frequency Mosfet Inverter for Asynchronous Motors), with a nominal current of 700 A_{rms} and a

switching frequency of 8 kHz, complete with a driver board. Control strategies capable of controlling the switches, according to paragraph 5.2, have been implemented by means of a microchip microcontroller: dsPIC30F4013.

The criterion adopted for the choice of the supercapacitor bank consists of evaluating the maximum delta-energy (W_{max}) requested by the equivalent load at currents greater than a threshold (set at 150 A for our purpose). This energy will be delivered by supercapacitors considering the admissible voltage variation between the initial and final voltages (respectively V_i and V_f are considered to be 45 V and 24 V). The minimum storage size is:

$$C_{min} = \frac{2 \cdot W_{max}}{\left(U_i^2 - U_f^2\right)} = 99.1F \tag{5.19}$$

Considering the commercial availability, the storage consists of 24 cells, manufactured by Maxwell Technologies, with a 3000 F rated capacitance (Appendix 7.1) connected in series, for a total rated value of 125 F at a nominal voltage of 64.8 V. At this stage, thanks to the DC/DC converter, it would be possible to use a system with a lower nominal voltage, e.g., 50V. In any case, we selected 64.8 V to ensure a fail safe for the supercapacitor module in the case of a DC/DC converter failure, in particular during the recharging of the lead acid battery.

5.4.3. EXPERIMENTAL RESULTS WITH THE POWER QUALITY INCREASING STRATEGY

In the following, comparisons between the battery and supercapacitor currents and voltages are first reported in Figure 5.11.
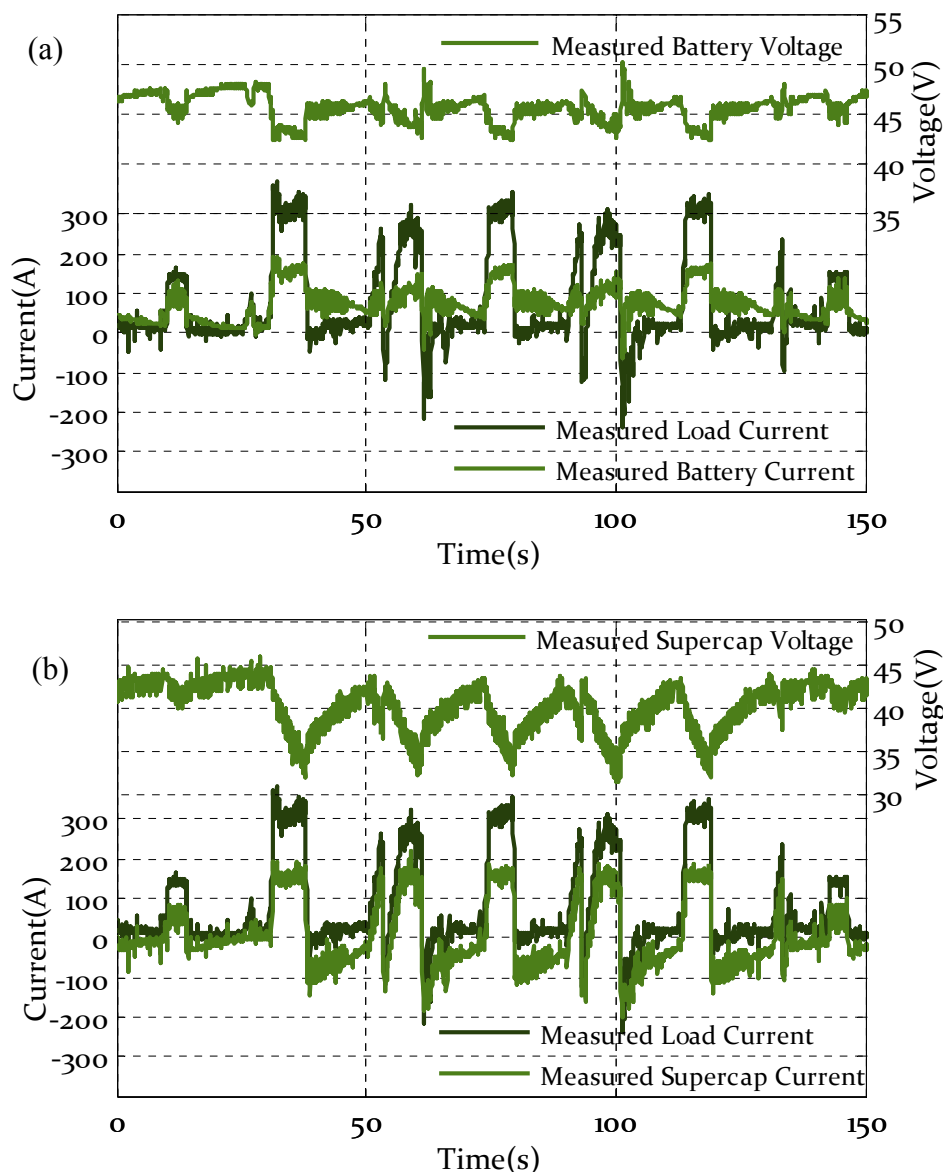
Figure 5.11   **Storage working conditions to supply loads when integrated with increasing power quality strategy: a) measured battery voltage and current, b) measured supercapacitor voltage and current.**

These figures, which represent the storage working conditions for the entire test duration of more than 4 h, show how the presence of the supercapacitor storage unit makes it possible to greatly reduce the maximum current delivered by the lead acid battery under all operating conditions to a maximum value of 150 A. The difference, in terms of energy, is supplied by the supercapacitor storage system, which delivers a maximum

current of 180 A. In contrast, during the recharging phases, the supercapacitor absorbs a maximum of 200 A. However, it is important to note that the maximum current delivered by the lead acid battery to recharge the supercapacitor is 100 A; the difference arises from the regenerated energy during the braking phases. The effective energy used by the supercapacitor is in the voltage range of 45 V to 30 V, in compliance with the project specifications and, in particular, a little lower because of the oversizing of the storage system.

These functionalities have been obtained by the power quality increasing strategy, which is used to reduce the voltage variation on the battery storage system. In Table 5.2 the main data are reported for the operating conditions of supercapacitor and lead acid battery in presence of and without the power storage system.

Table 5.2   **Comparison between systems with and without storage devices**

	Battery parameters					Supercapacitor parameters				
	$I_{average}$	$V_{average}$	$P_{average}$	$\Delta U_{dc}/U_{dc}$	I_{rms}	$I_{average}$	$V_{average}$	$P_{average}$	$\Delta U_{dc}/U_{dc}$	I_{rms}
	[A]	[V]	[W]	[%]	[A]	[A]	[V]	[W]	[%]	[A]
without supercapacitor	76.2	45.5	3467	35.4	132.1			-		
with supercapacitor	75.8	45.5	3449	19.8	86.2	3.1	45.4	140.7	31.3	90.1
relative variation [%]	~0	0	~0	-44.1	-34.7			-		

From , it is evident that the power storage system contributes to stabilizing the battery voltage fluctuations that pass from a range of 54 V–37 V (without supercapacitor storage) down to 51 V–41.5 V (with supercapacitor storage), which represents a relative reduction of 44.1%. In addition, the battery's root mean square current decreases by about 34.7%. From these considerations, it is clear that the control strategy is also implicitly a peak shaving strategy. No particular deviations are measured for the average quantities, which is correct due to the fact that the same energy is requested by the loads.

In order to verify the improving effect related to the battery's available capacity, the above reported test cycle in Figure 5.1 was repeated two times considering the presence or absence of the supercapacitor storage system. In these two identical cycles, starting with the same condition for the state of charge (SoC) of the lead acid battery, the test was repeated for 4 h, and the battery SoC profile in each case was measured. In particular, the SoC was measured as the specific gravity of the battery electrolyte and, in Figure 5.12 the specific gravity trends with and without the supercapacitor storage system are reported.

.
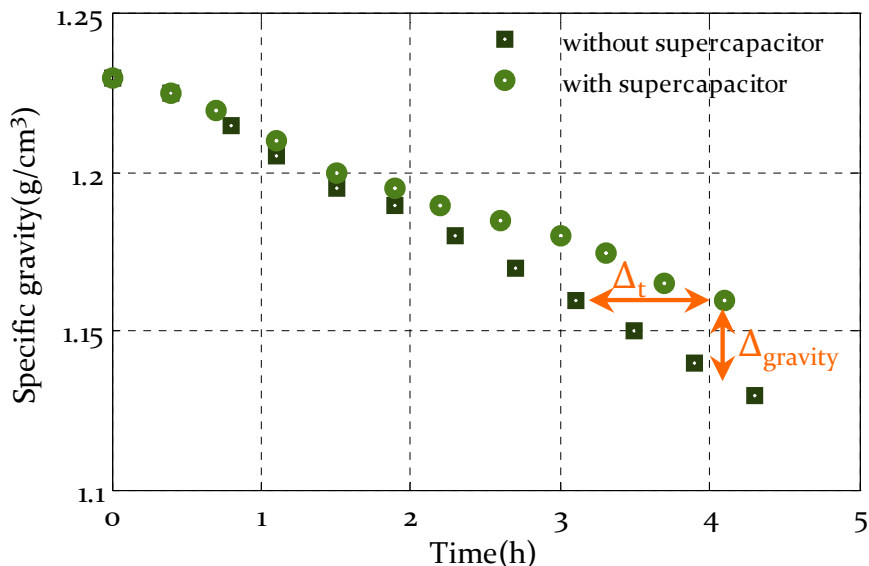
Figure 5.12   **gravity trend of lead acid battery electrolyte tested in presence and absence of supercapacitor storage device in order to realize peak shaving function.**

From Figure 5.12, the benefits of using the lead acid battery are experimentally evident in terms of the available capacity when discharged in an operating condition more closely related to the constant current profile. From a quantitative point of view, the main data are collected in Table 5.3.

Table 5.3   **Comparison between systems with and without storage devices.**

	Initial gravity [g/cm^3]	Final gravity [g/cm^3]	Initial time [h]	Final time [h]
without supercapacitor	1.23	1.16	0	3.1
with supercapacitor	1.23	1.16	0	4.1
relative variation [%]	-	-	-	+32%
only lead acid battery	1.23	1.1275	0	4.1
with supercapacitor storage	1.23	1.16	0	4.1
relative variation [%]	-	-18.6%	-	-

The above reported results are greatly encouraging in considering the multiple benefits arising from the storage system integration. In particular, with this control strategy, the following functionalities have been implemented:

- voltage stabilization (the battery voltage fluctuations go down to 19.8% from 35.4%);
- peak shaving (the battery route mean square current go down to 86.2 A from 132.1 A);
- energy saving (the battery electrolyte specific gravity variation is reduced by 18.6%);
- autonomy increase (the battery is operated for +32% of the time).

It is clear that only a global system vision makes it possible to exploit the multiple benefits arising not only from a technical point of view, but also from an economic point of view. Without performing an economic analysis, it is clear that a single obtainable benefit would not justify, from an economic point of view, the investment related to the storage integration. Yet, it is surely justifiable, also in a short time horizon, when the sum of the economic benefits is considered.

5.4.4. SIMULATIONS RESULTS WITH LOSS MINIMIZATION STRATEGY

The above reported experimental analysis did not specifically focus on the total loss reduction related to the two storage systems. It is clear that, by reducing the root mean square current, an additional benefit is also obtainable from the aspect of losses.

Based on this, in the following, considering the same working conditions experimentally analyzed previously, the benefits arising from system integration based on the loss minimization strategy are considered, and a comparison with the power quality increasing strategy is done. The analysis is carried out based only on simulation results.

First, in Table 5.4, the two storage equivalent model parameters, referring to the models of Figure 5.5 and Figure 5.6, are reported.

Table 5.4　　　**Supercapacitor and lead acid battery equivalent model parameters.**

	U_n	R_i	R_1	C		R_{Rsc}	C_{Rsc}	R_{Ssc}
	[V]	[mΩ]	[mΩ]	[F]		[Ω]	[F]	[kΩ]
supercapacitor	64.8	6.9	8.35	84.5+0.625·v		8.3	3.45	28
	E_m	R_{0b}	R_{1b}	C_{1b}	R_{2b}	C_{2b}		
	[V]	[mΩ]	[mΩ]	[F]	[mΩ]	[F]		
lead acid battery	48.3	24	5	37	4	100		

In order to verify the accuracy of the lead acid equivalent model, Figure 5.13, reports a comparison between the simulated and measured battery voltage profiles, when the storage is subjected to the real measured current profile of Figure 5.8.

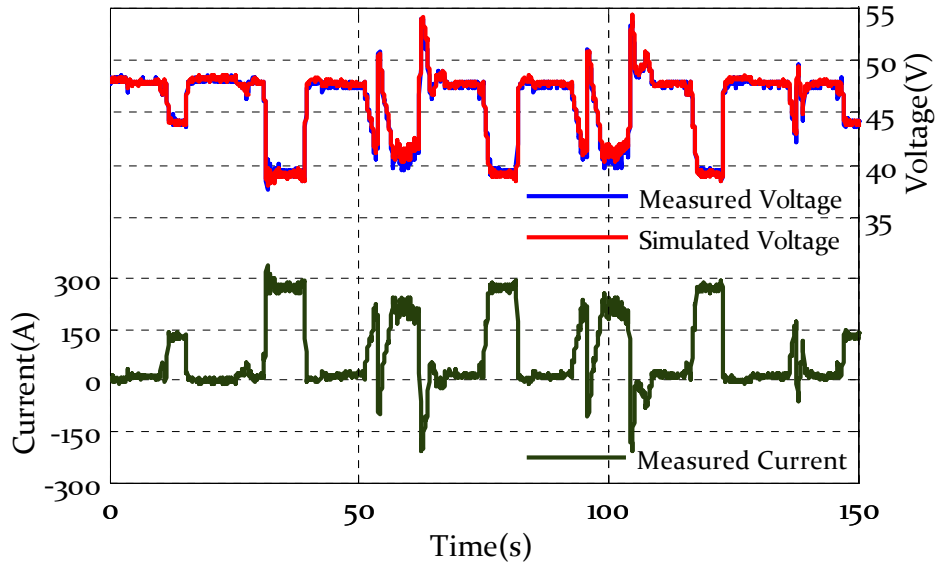**Figure 5.13**   **Comparison between measured and simulated lead acid battery voltage profiles when subjected to measured current profile.**

The loss minimization strategy is applied to the case study to verify its validity. In particular, Figure 5.14 reports a comparison between the battery and supercapacitor currents and voltages when the storages are controlled with the loss minimization algorithm.
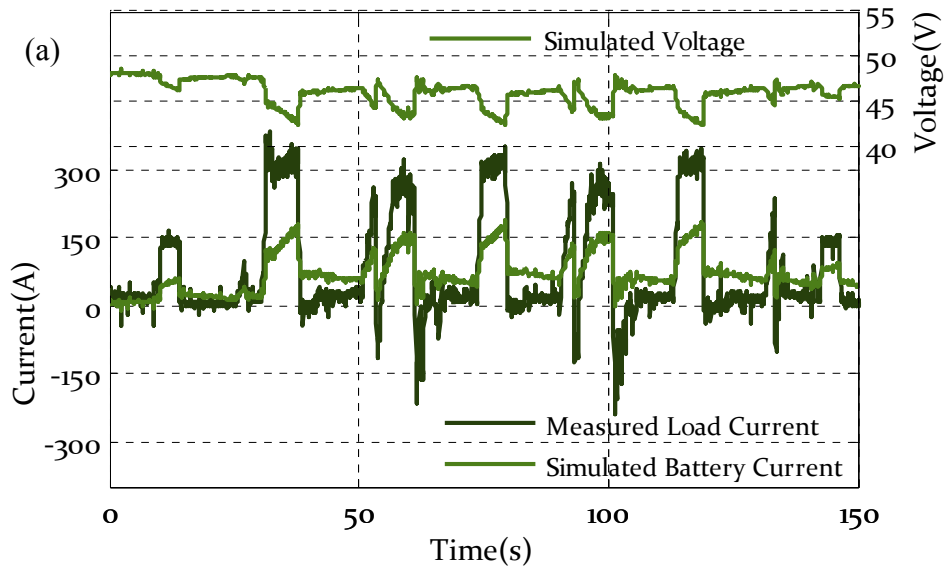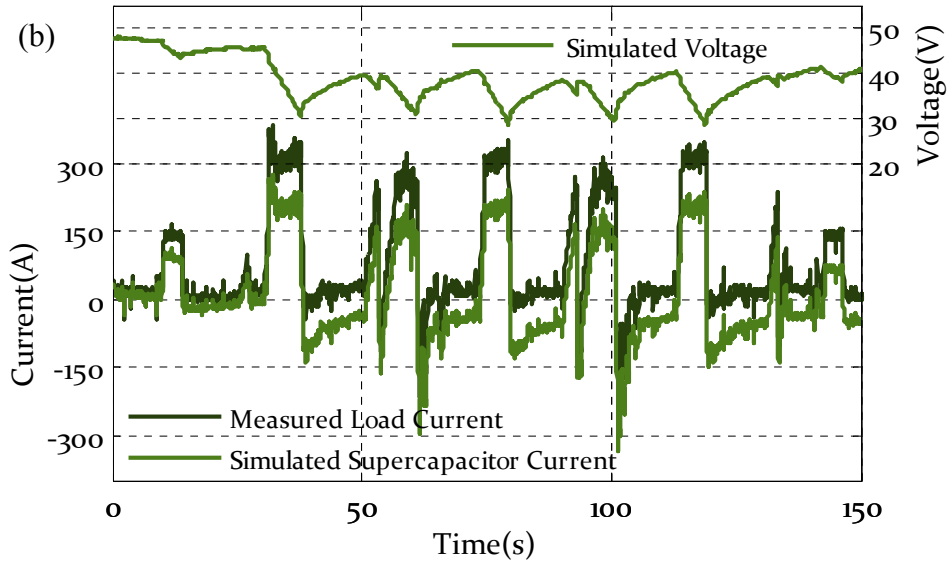
Figure 5.14 **Working conditions for simulated storages when devices are controlled by loss minimization strategy: a) battery voltage and current, b) supercapacitor voltage and current.**

As shown in Figure 5.14, the loss minimization strategy has, for the storage currents, an effect very similar to the power quality increasing strategy. Moreover, in this case, an evident peak shaving action can be noted for the supplied battery currents. Similar to the previous case in Table 5.5 , the main data are reported for the operating conditions of the supercapacitor and lead acid battery, with the values of mean power wasted on the modeled internal resistances, in the presence of and without the power storage system.

Table 5.5 **Comparison between systems with and without storage devices.**

	Battery parameters					Supercapacitor parameters				
	$I_{average}$	$U_{average}$	$\Delta U_{dc}/U_{dc}$	I_{rms}	P_{wasted}	$I_{average}$	$U_{average}$	$\Delta U_{dc}/U_{dc}$	I_{rms}	P_{wasted}
	[A]	[V]	[%]	[A]	[W]	[A]	[V]	[%]	[A]	[W]
without supercapacitor	76.2	45.5	35.4	132.1	568			-		
with supercapacitor	79.3	45.5	18.7	95.5	254	8.5	39.2	31.3	120.3	96
relative variation [%]	~0	0	-47.0	-27.7	-55.2			-		

As shown in Table 5.5, , the effectiveness of the loss minimization algorithm is proved by the simulation results; in fact, the total storage losses go down to 350 W from 568 W in the presence of only the lead acid battery storage. This is shown to underline that, in these simulations, the DC/DC converter, interfaced with the supercapacitor module, is considered to have an efficiency equal to 1. In addition, considering a converter efficiency of 85%, for example, the total energy wasted is lower than considering the presence of only the electrochemical batteries.

It is worth noting that, by minimizing the total losses on the modeled resistive elements of the storages devices, benefits similar to those obtained with the power quality increasing strategy are obtained. In fact, the simulations demonstrate a function of:

- voltage stabilization (the battery voltage fluctuations go down to 18.7% from 35.4%);

- peak shaving (the battery root mean square current goes down to 95.5 A from 132.1 A).

It is correct to expect similar benefits from this strategy, compared to the previous ones, in terms of increased efficiency and autonomy of the electrochemical battery due to the similar improvements in terms of the voltage stabilization and peak shaving function.

At this point, it is necessary to focus on the meaning of the increased efficiency. With the experimental results obtained with the power quality increasing strategy, the increase in the time window operations is 1 h, considering the same variation in the specific gravity of the electrolyte of the lead acid battery in the presence of or without the power storage system. In other words, with the same state of charge for the lead acid battery, it is possible to use a greater quantity of energy (about 3.45 kWh) or, considering the same time window operation, it is possible to save about 3.45 kWh. This saved energy does not totally arise from the lower energy wasted on the resistive elements of the electrochemical battery. In fact, with the loss minimization algorithm, considering a time window of 4 h and a DC/DC converter efficiency of 85%, the total amount of energy saved on the resistive elements is about 0.776 kWh, which is significantly lower than 3.45 kWh. In other terms, this means that there is an efficiency term related to the energy wasted on the resistive elements of the electrochemical device and an efficiency term related to the electrochemical reactions that take place with a greater efficiency when the battery is operated with lower values of root mean square current. The loss minimization algorithm, by optimizing the energy wasted on the resistive elements, also optimizes the global efficiency of the lead acid battery.

Finally, comparing this strategy with the previous one, it is possible to say that the benefits arising from the two algorithms are very similar; certainly, from an integration point of view, the power quality increasing strategy is simpler than the second one, because it does not require any on-line calculation to estimate the currents flowing in the various branches of the modeled storages and then calculate the current references to

inject into the different storages. In addition, the power quality increasing strategy does not require any modeling of the storage system, with the exception of the dynamic behaviors, in order to correctly set the bandwidth of the different control loops.

In contrast, the loss minimization algorithm presents a plus when many storage devices have to be connected on the same DC bus. The power quality strategy, in fact, requires that the voltage control loop bandwidth of each interfaced DC/DC converter is at least 1 decade different from the others in order to avoid power oscillations between storages. This represents a limitation in the maximum number of interface converters connected to a DC bus with this strategy. This limitation does not exist with the loss minimization algorithm, because there are no specifications on the bandwidths of the interfaced converters. In addition, this strategy does not use any voltage control loop and directly impose the current reference to charge or discharge the different devices.

5.5. BIBLIOGRAPHY

[1]   "Electric Energy Storage Technology Options: A White Paper Primer on Applications, Costs, and Benefits", EPRI, Paolo Alto, CA, 2010. 10206.

[2]   "2006 Progress Report for Energy Storage Research and Development", U.S. Department of Energy Office of FreedomCAR and Vehicle Technologies.

[3]   P. Mauracher and E. Karden, "Dynamic modelling of lead/acid batteries using impedance spectroscopy for parameter identification,"Journal of Power Sources, vol. 67, no. 1-2, pp. 69–84, 1997, proceedings of the Fifth European Lead Battery Conference.

[4]   H. Andersson, I. Petersson, and E. Ahlberg, "Modelling electrochemical impedance data for semi-bipolar lead acid batteries," Journal of Applied Electrochemistry, vol. 31, pp. 1–11, Jan. 2001.

[5]   N. Moubayed, J. Kouta, A. El-Ali, H. Dernayka, and R. Outbib, "Parameter identification of the lead-acid battery model," in Photovoltaic Specialists Conference, 2008. PVSC '08. 33rd IEEE, May 2008, pp. 1–6.

[6]   M. Ceraolo, "New dynamical models of lead-acid batteries," IEEE Trans. Power Syst., vol. 15, no. 4, pp. 1184–1190, Nov. 2000.

[7]   F. Codecà, S. M. Savaresi, and G. Rizzoni, "On battery state of charge estimation: A new mixed algorithm," in Control Applications, 2008. CCA 2008. IEEE International Conference on, Sep. 2008, pp. 102–107.

[8]   C. R. Gould, C. M. Bingham, D. A. Stone, and P. Bentley, "New battery model and state-of-health determination through subspace parameter estimation and state-observer techniques," IEEE Trans. Veh. Technol., vol. 58, no. 8, pp. 3905–3916, Oct. 2009.

[9]   R. Mino, S.Hara, "A Pulsed Discharge Control of Battery," TENCON 2006. 2006 IEEE Region 10 Conference , vol., no., pp.1-4, 14-17 Nov. 2006.

[10]   W.X. Shen, "State of available capacity estimation for lead-acid batteries in electric vehicles using neural network", Energy Conversion and Management, Volume 48, Issue 2, Pages 433-442, Feb. 2007.

[11]   W.X Shen, C.C Chan, E.W.C Lo, K.T Chau, "A new battery available capacity indicator for electric vehicles using neural network", Energy Conversion and Management, Volume 43, Issue 6, Pages 817-826, April 2002.

[12]   D. Doerffel, S. A. Sharkh, "A critical review of using the Peukert equation for determining the remaining capacity of lead-acid and lithium-ion batteries", Journal of Power Sources, Volume 155, Issue 2, Pages 395-400, 21 April 2006.

6.   *SUPERCAPACITOR STORAGE SIZING CRITERIA*

As analyzed in chapter 5, there are many benefits that arise from the system integration of a supercapacitor storage system in different applications. In addition to technical benefits, the economic return on investment has to be evaluated in order to sustain, from an industrial-economic point of view, the addition of the storage system in the specific application.

Today's storage system cost represents an important, if not the largest, component cost of the total system, which is much higher than the power electronic converters cost. It is very important, according to the application, to correctly size the storage system in order to globally optimize the technical and economic benefits obtainable.

In this chapter, in particular, considering applications characterized by a power profile comprehensive of the absorption and regeneration phases, two sizing criteria for a supercapacitor storage system are analyzed in order to realize the energy recovery and peak shaving functions. The system sizing trade off takes into account the amount of money saved by the implementation of these two functionalities.

First, the technical and economic sizing of the storage is approached for a specific application characterized by a known working power profile. In this case, the supercapacitor storage sizing follows deterministic criteria based on the amount of storable energy needed for the application, and an economic analysis based on the actual costs is reported. Second, the same case study is further investigated considering a case in which more than one load is electrically connected to the same distribution bus. In this case, taking into account the technical and economic constraints, it is a winning solution to design a centralized storage system for the recovery of the power regenerated. In particular, it is assumed that the loads follow deterministic power cycles, but are shifted by an uncertain amount in relation to each other. Therefore, the recoverable energy and, consequently, the storage size, requires the optimization of a random cost function that arises from a probabilistic approach, as addressed in [1-5].

6.1. DETERMINISTIC APPROACH TO SUPERCAPACITOR STORAGE SIZING

6.1.1. SYSTEM LAYOUT AND MAIN COMPONENT SIZING

Starting from the system layout reported in Figure 6.1, the analysis, based on the actual costs of the different integrated components in the system, aims to identify the total cost for the integration of the supercapacitor storage and to quantify the return of the investment, taking into account the money savings related to the energy savings.
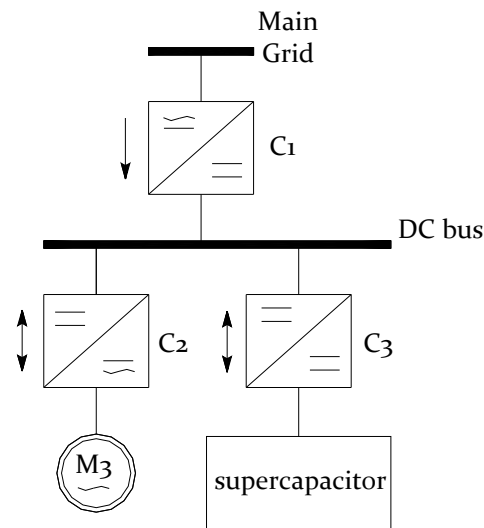
Figure 6.1   System layout.

The system reported in Figure 6.1 consists of a rectifier converter, C_1, to supply the DC bus system, where the loads and supercapacitor storage system are connected by means of inverter C_2 and DC/DC converter C_3, respectively. Considering the great difficulty in regenerating energy toward the main grid, due to the high limitations imposed by the distributor or more general technical constraints, in the reported topology converter C_1 is assumed to be unidirectional. In addition, without losing generality in the methodology approached, the power profile absorbed by the load, as reported in Figure 6.2(a), consists of an absorption phase at constant power P_1 followed, after a rest period with no power, by a regenerating phase at constant power P_2 lower than P_1. The absorption phase lasts for interval T_r, while the regenerating phase lasts for time interval T_d. In the following analysis, only for convenience in formulating the different mathematical expressions, the two time intervals have the same duration equal to T_o.

The two functions addressed by the presence of the supercapacitor storage system are:

- total recovering of the energy regenerated by the load;
- peak shaving function of the power drawn by the interface converter with the main grid, C_1, Figure 6.2(b).
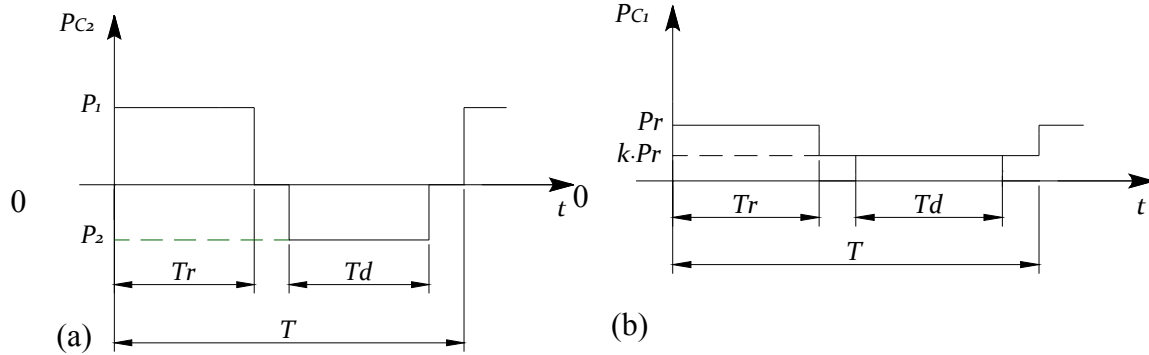
Figure 6.2 **(a) Power profile drawn by load. (b) Power profile drawn by C1 interface converter when peak shaving strategy is implemented. The absorption phase lasts for time interval Tr, while the regenerating phase lasts for time interval Td.**

In particular, by realizing the peak shaving function, the maximum power, Pr, absorbed by the grid is lower than the maximum power, P_1, absorbed by the load. In general, the total net energy absorbed by the load in each cycle is:

$$W_{net\,cycle} = P_1 T_o - |P_2 T_o| = P_r T_o + k P_r (T - T_o) = P_r [kT + (1-k)T_o] \qquad (6.1)$$

where k represents the level of peak shaving realized on the converter interfaced with the main grid, which is defined as:

$$k = \frac{(P_1 - |P_2| - P_r) \cdot T_o}{P_r (T - T_o)}. \qquad (6.2)$$

Thus, the size of power converter C_1 can be determined as:

$$P_{C_1} = P_r = \frac{(P_1 - |P_2|)T_o}{[kT + (1-k)T_o]}, \qquad (6.3)$$

and the size of power converter C_3 as:

$$P_{C_3} = P_{C_2} - P_{C_1}, \qquad (6.4)$$

while the size of converter C_2 is equal to the maximum power drawn by the load and equal to P_1. Finally, the size of the supercapacitor storage system, which is a function of the peak shaving level of the power profile of interface converter C_1, is the sum of the total energy regenerated by the load and the energy absorbed by interface converter C_1 in time interval $T-T_r$. The minimum energy size of the supercapacitor storage is:

$$W_{SC} = |P_2|T_d + kP_r(T - T_r) = \frac{kP_1 T_o (T - T_o) + |P_2| T_o^2}{k(T - T_o) + T_o}. \qquad (6.5)$$

From (6. 5), it is evident that the energy size of the supercapacitor storage system is strictly related to the peak shaving level of the power absorbed from converter C_1 (parameter k). In particular, the two limits are with $k = 0$ and $k = 1$, which mean, respectively, no peak shaving function and a total peak shaving function, in order to absorb from the grid a constant power equal to the average power of the cycle. In the two limits considered, the minimum energy size for the supercapacitor storage system is:

$$\begin{cases} k = 0 & W_{SC} = |P_2|T_o \\ \\ k = 1 & W_{SC} = \dfrac{P_1 T_o (T - T_o) + |P_2|T_o^2}{T} \end{cases} \tag{6.6}$$

6.1.2. COMPONENTS COST

In this section, the actual costs of the different components are reported in order to correctly quantify the total system integration cost as the savings arising from the energy regenerated. The costs reported in the following are industrial costs and based on a market analysis.

- **Supercapacitor Storage Cost (COST$_{SC}$)**

Starting from the supercapacitor cell cost, the specific energy cost for the supercapacitor storage system is identified considering that the exploitable energy in a supercapacitor is normally in the range of the nominal voltage, U_n, and its half. In this way, in fact, it is possible to use about 75% of the stored energy (this is completely true considering an ideal capacitance of constant value operated between U_n and $U_n/2$).

The analysis, based on a direct market cost analysis conducted on the Maxwell Technologies supercapacitor cells and modules, considered different supercapacitor cells and modules in order to identify the specific energy cost. In addition, it also considered the influence of the system module voltage on the specific cost. Considering a storage system consisting of a single branch of cells connected in series, the total system voltage, which represents an electrical specification of the storage, because the nominal elementary cell voltage is fixed in the range of 2.5–2.7 V, determines the number of cells in series. Consequently, the cell size is determined by the total amount of energy that has to be stored divided by the number of cells in series. Due to the fact that the specific energy cost is influenced by the cell size, it is clear that the specific energy cost is influenced by the nominal voltage of the system module. This is particularly clear in Figure 6.3 Considering

the need to store 150 Wh of energy, technically the module's nominal voltage can be designed to be 400 V or 800 V. The former solution requires the realization of a module with 296 elementary cells of 650 F @ 2.7 V, while the second one can be realized with one string of 148 cells of 1500 F @ 2.7 V. Due to the lower specific cost for the greater size of supercapacitor cells, the former solution makes it possible to realize a supercapacitor storage module with a specific energy cost of about 95 €/Wh, while the second one has a consistently lower cost of about 58 €/Wh.
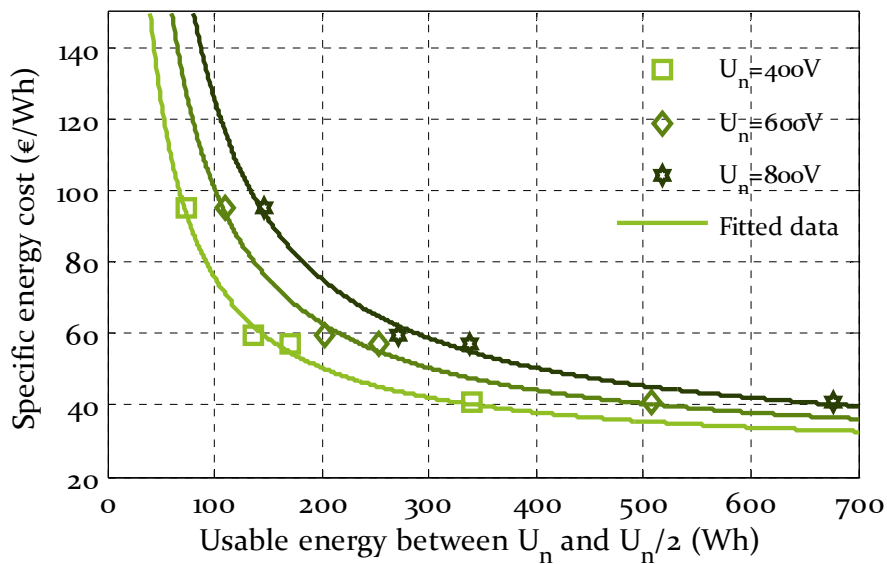
Figure 6.3   **Specific supercapacitor storage cost vs. usable stored energy between nominal system voltage and its half. These costs were evaluated considering different voltages for the total storage system (400, 600, 800 V). The total system energy is stored by using different sizes of supercapacitor cells: 650 F, 1200 F, 1500 F, 3000 F. By selecting the same elementary cell to realize the module and, consequently the same specific energy cost, it is possible to store different amounts of energy by varying the total system voltage, which is the number of cells connected in series.**

By fitting the collected data, it is possible to identify the cost expressed in Euros of the supercapacitor storage as a function of the usable energy needed and the nominal system voltage, in particular:

$$COST_{SC} = a \cdot U_{SC} + b \cdot W_{SC} + c = 12.44 U_{SC} + 27.49 W_{SC} + 34.09 \tag{6.7}$$

where:

a,b,c: are coefficients determined on the basis of a direct market cost analysis conducted on the Maxwell Technologies supercapacitor cells and modules;

U_{SC}:   is the nominal system voltage in [V];

W_{SC}:   is the amount of usable energy in the storage in [Wh].

As expected, the specific storage cost is lowed by using the largest available supercapacitor cell. From a technical point of view, this is not always possible due to the voltage constraints with which the storage system has to be realized. Storing a certain amount of energy using larger supercapacitor cells lowers the system voltage. Taking into account the supercapacitor interface converter, this means, at an equal value of power exchanged, a greater value of current, with consequential issues related to the converter specifications and performances.

The above reported specific cost function takes into account, not only the supercapacitor cell cost, but also the global module cost consisting of the sum of different components. The cost shares of different components are reported in Table 6.1.

Table 6.1   **Relative weight factors on total cost of supercapacitor storage system.**

Component	Relative weight on the total cost
Cells	55 % $COST_{SC}$
Case	30 % $COST_{SC}$
Cooling system	5 % $COST_{SC}$
Integration labour	10 % $COST_{SC}$

- *Electronic Power Converter Cost (COST$_{UPS}$)*

In order to identify the actual industrial cost of the rectifier converter, C_1, and the DC/DC supercapacitor interfaced converter, C_3, a market analysis was conducted on the uninterruptible power systems (UPSs) commercially available in the power range of 10–80 kVA. This choice is strictly related to the fact that a UPS consists of the integration of all the electronic converters shown in the system layout of Figure 6.1 UPS devices typically consist of an input inverter, output inverter, bidirectional DC/DC converter for the storage device, and static switch.

Collecting the costs of the UPS power converters made it possible to introduce the following cost function, expressed in Euros:

$$COST_{UPS} = d + e \cdot P_{UPS} = 3380 + 62 \cdot P_{UPS} \tag{6. 8}$$

where:

d,e: are coefficients determined on the basis of ;

P_{UPS}:   is the nominal power of the UPS [kW].

Figure 6.4 reports a comparison between real UPS costs and fitted data by means of (6. 8). In order to identify the function cost of the rectifier power converter and DC/DC bidirectional power converter, Table 6.2 reports the relative weight of the main parts constituting a UPS device.
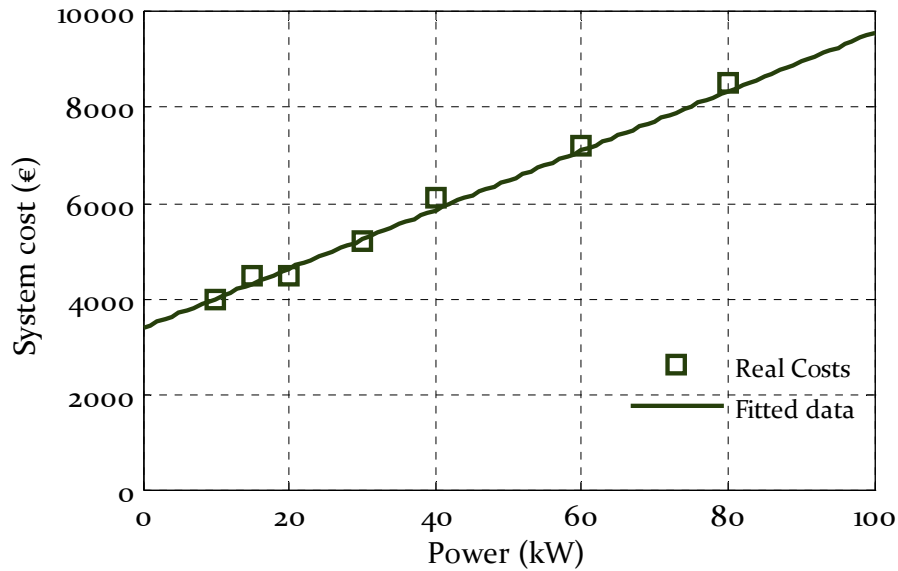
Figure 6.4   **Comparison between real UPS cost based on market analysis and fitted curve by means of function cost in (6. 8).**

From the data collected in , the cost of bidirectional DC/DC converter C3 and rectifier converter C1 can be determined considering the impact that each factor has on the complete UPS device.

Table 6.2   **Relative weight on total cost of main parts constituting UPS device.**

Component	Relative weight on the total cost
Case	15 % $COST_{UPS}$
Input inverter	20 % $COST_{UPS}$
Output inverter	20 % $COST_{UPS}$
Battery DC/DC converter	10 % $COST_{UPS}$
Static switch	5 % $COST_{UPS}$
Integration labor	10% $COST_{UPS}$
Other	20% $COST_{UPS}$

- *DC/DC Converter Cost (COST$_{DC/DC}$)*

For a DC/DC power converter interfaced with a supercapacitor storage system, the cost of the mains parts, in reference to the cost of the mains parts constituting a UPS device, are as follows:

- the case cost is about 60% of that for a UPS device. Even if it is simpler, certain safety and mechanical requirements have to be satisfied;

- the DC/DC bidirectional converter is 50% higher, taking into account that a converter interfaced with a supercapacitor has to manage similar currents during the charging and discharging phases, in contrast to the DC/DC converter interfaced with batteries in a UPS;

- the integration and testing labor is simpler and estimated as 30% of that for the UPS device;

- no inverter and static thyristor bridge are present.

From these considerations, Table 6.3 reports the relative weight of the main parts constituting the bidirectional DC/DC converter, in relation to the UPS main component costs.

Table 6.3   **Relative weight on total cost of main parts constituting bidirectional DC/DC converter.**

Component	Relative weight on the total cost
Case	9 % $COST_{UPS}$
DC/DC bidirectional converter	15 % $COST_{UPS}$
Integration labor	3% $COST_{UPS}$
Other	15% $COST_{UPS}$

From Table 6.3, the total cost of the bidirectional DC/DC converter is 42% of a complete UPS characterized by the same nominal power. The cost in Euros of the DC/DC converter is as follows:

$$COST_{DC/DC} = 0.42(d + e \cdot P_{DC/DC}) = 1420 + 26 \cdot P_{DC/DC} \tag{6.9}$$

where $P_{DC/DC}$ is the nominal power of the DC/DC converter expressed in kW.

- ***Rectifier Converter Cost (COST_{RECT})***

Finally, the cost of rectifier inverter C_1 is evaluated similarly to the previous analysis and, in particular, considering that in reference to the cost of the mains parts constituting a UPS device, the main components of rectifier C_1 are:

- the case cost is about the 60% of that for a UPS device;

- the cost of the thyristor bridge is considered to be totally equal to the static switch of the UPS device, in fact the power electronic and driver boards used are the same;

- the integration and testing labor is simpler and does not exceed 20% of that for a UPS device;

- no inverter and bidirectional DC/DC converter are present.

The relative weights of the main parts constituting the controlled rectifier converter thyristor are collected in Table 6.3.

Table 6.4 **Relative weight on total cost of main parts constituting controlled rectifier converter thyristor.**

Component	Relative weight on the total cost
Case	9 % $COST_{UPS}$
Thyristor bridge	5 % $COST_{UPS}$
Integration labor	2% $COST_{UPS}$
Other	10% $COST_{UPS}$

The total cost of the rectifier converter is 26% of that for a complete UPS characterized by the same nominal power. The cost in Euros is:

$$COST_{RECT} = 0.26(d + e \cdot P_{RECT}) = 879 + 16.1 \cdot P_{RECT} \tag{6.10}$$

where P_{RECT} is the nominal power of the rectifier converter expressed in kW.

Considering the presence of a three-phase input power transformer at 50 Hz, an additional cost has to be considered. In particular, based on the market analysis, it is possible to relate the transformer cost to its size according to (6.11).

$$COST_{TRANSF} = (f + g \cdot P_{TRANSF}) = 48.5 + 42.7 \cdot P_{TRANSF} \tag{6.11}$$

where:

    f,g: are coefficients;

    P_{TRANSF}: is the nominal power of the transformer in kW.

The total cost of the rectifier converter considering the presence of the input transformer is equal to:

$$COST_{RECT+TRANSF} = COST_{RECT} + COST_{TRANSF} = 927.5 + 58.8 \cdot P_{RECT+TRANSF}. \tag{6.12}$$

The last component cost that has to be evaluated in order to fulfill the economic analysis is the cost of the electrical energy. In our analysis, this cost is based on a low voltage, not that distributed to domestic Italian customers (based on the data supplied by the Italian authority "Acquirente Unico AU" for the last trimester 2011). In particular, it is possible to express the annual electrical energy cost in Euros as a function of the contractual power and energy consumed as:

$$COST_{ENERGY} = h \cdot P_{CONT} + i \cdot W_{CONS} + l = 27.2 \cdot P_{CONT} + 0.1537 \cdot W_{CONS} + 137.1 \tag{6.13}$$

where:

    h,i,l: are coefficients;

    P_{CONT}:   is the contractual power expressed in kW;

    W_{CONS}: is the total amount of energy in kWh consumed in 1 year.

It is important to note that the energy cost is a function of the contractual power level with the distributor and not just a function of the consumed energy. This aspect is very important when considering system sizing optimization.

6.1.3. *OPTIMAL SIZING BASED ON THE RETURN OF INVESTMENT*

Considering the above reported function costs, it is possible to evaluate the saved money as:

$$S = COST_{rif} - COST_{system} \qquad (6.14)$$

where:

$COST_{rif}$:   is the total system cost in the absence of the energy saver system based on the supercapacitor technology;

$COST_{system}$:   is the total system cost in the presence of the energy saver system.

The addition of the energy recovery system is related to:

- the cost of the supercapacitor storage (additional cost);
- the cost of the DC/DC bidirectional converter interfaced with the storage (additional cost);
- the cost of the grid interface rectifier (reduced cost in the case of peak shaving);
- the cost of the electrical energy (reduced cost).

In particular, by actualizing the total costs at the initial time taking into account the discount rate, "*i*", and the increasing energy cost rate, "*j*" [6], the money saved at time zero is:

$$S_{act} = COST^{0}_{C_1\,Without\,ES} - COST^{0}_{C_1\,ES} + COST^{0}_{DC/DC} + COST^{0}_{SC} - \sum_{k=1}^{n}\left[COST_{energy}\left(\frac{1+j}{1+i}\right)^{n}\right] \qquad (6.15)$$

where:

$COST^{0}_{C_1\,Without\,ES}$:   is the cost at time zero of converter C_1 in the absence of the energy recovery system. The converter is thus designed for the total power, P_1, absorbed by the load;

$COST^{0}_{C_1\,ES}$:   is the cost at time zero of the C_1 converter in the presence of the energy recovery system. The converter is thus designed for the maximum power, P_r, function of the peak shaving level;

$COST_{DC/DC}^{o}$: is the cost of the C3 converter at time zero;

$COST_{SC}^{o}$: is the cost the supercapacitor storage at time zero;

$\sum_{k=1}^{n}\left[COST_{energy}\left(\dfrac{1+j}{1+i}\right)^{n}\right]$: is the actualized income arising from the energy saved by the presence of the energy recovering system.

With the above approach, and considering the power profile in Figure 6.2(a), the total investment has been calculated considering the two cases reported in Table 6.5.

Table 6.5 **Power profile parameters in reference to Figure 6.2(a).**

Case	P1	P2	T	Tr	Td	i	j	N
	[kW]	[kW]	[s]	[s]	[s]	[%]	[%]	Cycles per day
Case 1	20	13	160	60	60	3	5	50, 150, 200
Case 2	20	1.3						

The parameters of the considered cycles are typical for a heavy bridge crane or an industrial elevator application. In particular, the analysis focuses on the economic benefits obtainable in the case of a large amount of recoverable energy, case 1 of Table 6.5, or in the case of a small recoverable energy, case 2 of Table 6.5.

The simulation results, considering different values of cycles per day, are respectively reported in Figure 6.5 and Figure 6.6. In the (a)-figures, where the costs of the different components needed to realize the energy recovery system are reported, it is evident that the main relative weight on the total cost is represented by the cost of the supercapacitors. In addition, it can be seen that increasing the peak shaving function level (parameter k, maximum for $k = 1$) increases the supercapacitor cost, while the cost of the rectifier converter C_1 decreases. This is because it has to be designed for lower values of nominal power.

Figure 6.5 **Referring to system layout of Figure 6.1 and power profile parameters of Table 6.5, case 1, this figure reports: (a) cost of energy recovery system components, (b) Pay Back Time and Net Present Value versus peak shaving level k, for different values of cycles per day, N**

The (b)-figures report the pay back time (PBT) expressed in years and the net present value (NPV) of the investment expressed in Euros. The analysis considers a total system lifetime of 20 years. In particular, $N \cdot 5 \cdot 45$ per year cycles are considered (corresponding to 45 working weeks per year and 5 working days per week).
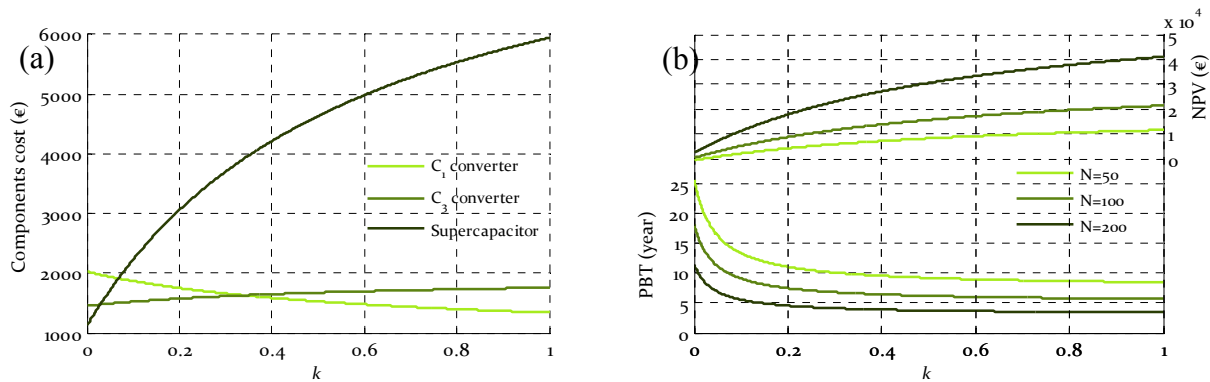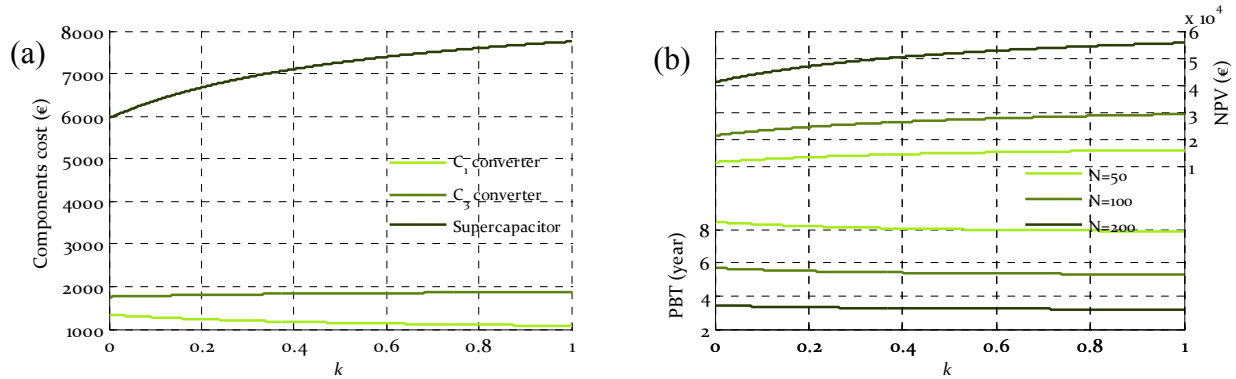

Figure 6.6   **Referring to system layout of Figure 6.1 and power profile parameters of Table 6.5, case 2, this figure reports: (a) cost of energy recovery system components, (b) Pay Back Time and Net Present Value versus peak shaving level k, for different values of cycles per day, N..**

The simulation analyses show, independently of the specific numerical results, that the cost related to the addition of the recovery energy system is quickly paid back if the storage system is used primarily to realize a peak shaving function and not the energy recovery function. By analyzing the energy cost in (6. 13), it is clear that the motivation is the relatively higher weight of the cost of power compared to the cost of energy (the coefficients *h* and *i*). In the two simulations, in fact, independently of the NPV value, the PBT values are similar when the *k* value is greater than 0.4, and the minimum value of PBT or the maximum NPV is obtained when the maximum peak shaving function is realized. This means that, quite independently from the recovered energy, the total investment is mainly paid from the lower cost of the contractual power needed to fulfill the load requirements. The last consideration is particular true when the cycle is characterized by a low value of recoverable energy.

In general, and not only when the application is directly connected to the electrical grid, as for example, when the main source is a internal combustion engine characterized by an inability to regenerate power and a low efficiency during dynamic transients, the specific power cost is relatively higher that the specific energy cost, because the main source is designed from a technical and economic point of view to deliver energy and not power with a high dynamic. Thus, it is clear that the economic benefit in realizing the peak shaving function is again related to a technical motivation, because, in this way, the total

system efficiency is increased, not only because the regenerated energy from the load is recovered, but also because the main source works at a higher efficiency over its range of usage.

From these considerations, if the storage system is mainly used to recover the regenerated power from the loads, it could be that the number of years required to recover the investment is inacceptable from an economic point of view; see Figure 6.5(b) with $k = 0$.

6.2. STATISTICAL APPROACH TO SUPERCAPACITOR STORAGE SIZING

Due to the importance of correctly sizing the supercapacitor storage system, both from a technical and economic point of view, the statistical approach is an effective method when a centralized storage system has to be designed in order to supply the power and energy requests from different electric drives that are all connected to the same distribution bus.

6.2.1. SYSTEM LAYOUT AND GENERAL MATHEMATICAL APPROACH FOR DETERMINATION OF TOTAL RECOVERABLE ENERGY

The system layout for the analysis is reported in Figure 6.7. It is assumed that the drives follow deterministic and fixed power cycles, with reference to the power profile of Figure 6.2(a), but are shifted by an uncertain amount in relation to each other. The hypothesis of a fixed power profile is introduced in order to give some analytical results in a closed form; from an application point of view it is not as restrictive because there are many applications such as underground trains, where a single requested train power profile can be assumed to be fixed and a priori known.
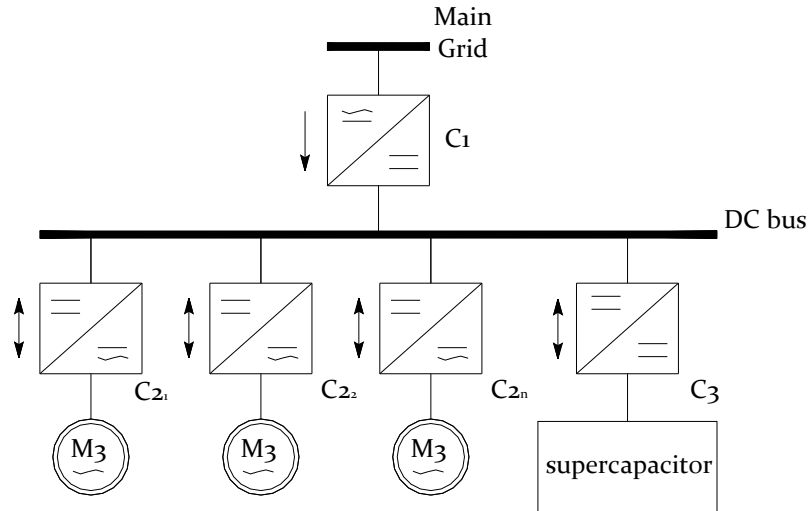
Figure 6.7   System layout considered for statistical approach to supercapacitor storage sizing

By combining the different power profiles, the total power requested by the aggregated load is not known a priori and, in this situation, in order to maximize the saving, it makes no sense to design the storage system to recover all of the energy from the electric drives in a case where they are all regenerating at the same time, because this event has low probability. Instead, a statistical approach makes it possible to determine the probability distribution of the amount of recoverable energy and, consequently, the storage size arises from the optimization of a random cost function, embedding both the plant total cost and savings due to the reduced energy consumption during the useful life of the storage.

In order to introduce a general framework, the time axis is subdivided into equal intervals in the following, with length L, starting at time zero, so that the interval indexed by t is:

$$[tL, (t+1)L) \qquad \text{as } t = 0, 1, 2, \dots \tag{6.16}$$

To each interval, t, the pair (E_t, S_t) denotes, respectively, the total amount of energy recovered and stored in the interval t (E_t) and the level of storage at the end of the interval (S_t). It should be noted that, in general, E_t may be lower than the total braking energy produced in interval t. This is possible in a case of storage with limited capability despite the total recoverable energy. This means the exciting energy has to be shaved in those cases. The storage level, S_t, in each interval is obtained from the previous level, S_{t-1}, and adding the total net energy exchanged by the storage in interval t.

At this point, with the hypothesis of L chosen in such a way that the work is done independently and homogeneously in the various intervals, that is with a random

mechanism that is independent from t, and with a finite storage size $E_t{}^*$, then the recovered energy, E_t, in time interval t depends stochastically only on storage level S_{t-1} in interval $(t-1)$, and storage level St depends only on S_{t-1}. In other words, the process (E_t, S_t) is Markovian. Thus, the probability of the recoverable energy and storage level in interval t depends only on the level of energy, S_{t-1}, reached by the storage in the interval $(t-1)$. Mathematically this can be expressed as follows:

$$\Pr(E_t, S_t \mid E_{t-1}, S_{t-1}, E_{t-2}, S_{t-2}, \ldots) = \Pr(E_t, S_t \mid S_{t-1}).$$

(6. 17)

By removing the hypothesis of a finite storage size, E_t is an independent sequence, but process S_t is still a homogeneous Markovian. Considering a general process until the time interval $(t-1)$ characterized by the sequence $(S_1, \ldots, S_{t-1})$, that is:

$$S_*^{t-1} = (S_1, \ldots, S_{t-1}),$$

(6. 18)

the marginal density of S_t given by S_*^{t-1} can be expressed as:

$$\Pr(S_t \mid S_*^{t-1}) = \int \Pr(E_t, S_t \mid S_*^{t-1}) dE_t = \int \Pr(E_t, S_t \mid S_{t-1}) dE_t = \Pr(S_t \mid S_{t-1}).$$

(6. 19)

The expression in (6. 19) means that the probability of S_t does not depend on the history of the storage levels, and consequently on time t, but only on the storage level in the previous interval, S_{t-1}. It is possible to make an expression of the stationary distribution, $\pi(S_t)$, of the Markov chain by solving the following expression with respect to $\pi(S_t)$:

$$p(S_t) = \int p(S_{t-1}) \Pr(S_t \mid S_{t-1}) dS_{t-1}.$$

(6. 20)

From this expression, it is possible to define the stationary distribution of the recoverable energy, Et, as:

$$p(E_t) = \int p(S_t) \Pr(E_t \mid S_t) dS_t.$$

(6. 21)

Equation (6. 21) derives from the conditional independence relationship shown in (6. 17) and consequently the marginal distribution of E_t, conditioned by the past history, can be expressed by integrating the marginal distribution, $\Pr(E_t, S_t)$, and the stationary distribution, $\pi(S_t)$, with respect to S_t. By knowing the stationary distribution of E_t, the expected recoverable energy in each epoch, t, can be determined as:

$$m = \int E_t p(E_t) dE_t,$$

(6. 22)

while the covariance between the recovered energies in two distinct epochs at distance h can be expressed as:

$$g(h) = \operatorname{Cov}(E_t, E_{t+h}).$$

(6. 23)

Using the central limit theorem for Markov chains, [7], it follows that the total recoverable energy can be approximately expressed as:

$$E_{tot} \approx N\left(\alpha\mu, \alpha\left\{g(0) + 2\sum_{h=1}^{\infty} g(h)\right\}\right) = N(\alpha\mu, \alpha\sigma^2).$$

(6.24)

The total energy is thus approximated with a Gaussian distribution with mean value $\alpha\mu$ and variance $\alpha\sigma^2$, which depend on the Markov chain transition kernel (6. 17). The mean is known as soon as the stationary distribution, $\pi(E_t)$, is available, whereas the variance parameter depends on an infinite sum, (6.24). In particular it is possible giving a closed form expression if (E_t, S_t) takes a value in a finite state space and the transition probability (6. 17) between any two pairs is known, [8]. In any case, it will become clear that it is not straightforward to obtain both the elements of the state space and the transition kernel, and consequently $\pi(S_t)$ and $\pi(E_t)$ to determine the requested values of mean and variance requested in (6.24). Based on this, in the following, the mean and variance values are determined by means of Monte Carlo simulations, in which a large number of epochs are simulated and the requested values are determined by means of sample statistics.

6.2.2. STATISTICAL APPROACH APPLIED TO OPTIMAL ECONOMIC SOLUTION

In order to verify the feasibility and convenience of a centralized storage system, different simulations were conducted considering, with respect to Figure 6.7, different numbers of loads (N = 4 and N = 10, Table 6.6), which are characterized by the same power profile shown in Figure 6.2(a) with the main parameters of Table 6.5.

Table 6.6   Power profile parameters in reference to Figure 6.2(a).

Case	N	P1 [kW]	P2 [kW]	T [s]	Tr [s]	Td [s]	i [%]	j [%]	N Cycles per day
Case 1	4	20	13						
Case 2	4	20	1.3	160	60	60	3	5	50, 150, 200
Case 3	10	20	13						
Case 4	10	20	1.3						

In particular, the analysis aims to show the effectiveness of the statistical approach to size the storage system. In addition, a comparison is made to the deterministic case.

The sizing of the different components takes into account the distribution of the numerical results obtained by the Monte Carlo simulations. In particular, because the total recoverable energy follows a Gaussian distribution, in order to correctly size the storage

system, it is necessary to define the percentage of cases in which the storage system has to fulfill the required function of energy recovery. In the following simulation results, this percentage value is considered to be equal to 95.5%, which means, for a Gaussian distribution, sizing the supercapacitor system to store an energy equal to $\alpha\mu+2\cdot\alpha^{0.5}\cdot\sigma$, (6.24).

The sizing of the different interface converters has to take into account the fact the maximum power they convert has a certain probability of occurring. In particular, the C_1 and C_{2n} converters are sized, similar to the consideration made for supercapacitor storage size, in order to cover 95.5% of the occurrences. By changing the probability value of the occurrences that it is necessary to satisfy, the sizes of the converters change. In other words, there are some cases, 4.5% of the total cases, in which the total power requested by the load is greater than the maximum power that the converters can supply.

The sum of the total load power profile in two distinct epochs is reported in Figure 6.8 in a case with 10 drives, each of which has a power profile shifted randomly in relation to each other. From this figure, it is evident that certain shift conditions determine the possibility of regenerating power, while others, in which the total power requested by the aggregated load is always greater than zero, do not allow this condition. In this last case, the presence of the power oriented storage system is useful only to realize a peak shaving function.
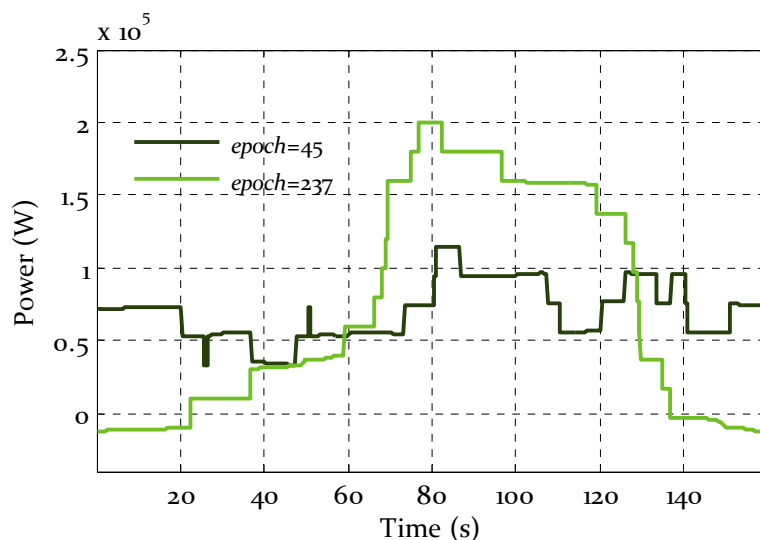
Figure 6.8   **In reference to system layout of Figure 6.7, total load power profile in presence of 10 drives shifted randomly in two distinct epochs.**

In order to have adequate confidence about the simulation results, in each simulation, 45,000 epochs are considered and, for each group of simulations, different

values of cycles per day (N) and different values of maximum power drawn by means of the C1 converter (C1 size) are considered to realize different levels of peak shaving. In particular, the storage is sized in order to recover all of the regenerated power and to guarantee the peak shaving functions according to the desired maximum power requested from the grid. Table 6.7 reports the main data for the sizes of the different components.

Table 6.7   **Referring to power profiles defined in Table 6.6, equivalent load parameters used to size components in system layout of Figure 6.7 are reported.**

Case	$P_{C3\,avg}$	$P_{C3\,max}$	P_{C1}	$W_{rec\,max}$	W_{rec}		W_{SC}		P_{C3}
					μ	σ	μ	σ	
	[kW]	[kW]	[kW]	[Wh]	[Wh]	[Wh]	[Wh]	[Wh]	[kW]
1	10.5	80	20	867	331	211.1	907.1	548.7	68.2
			40				508.2	525.5	48.2
			60				208.1	291.5	28.2
			80				159.6	195.8	8.1
2	28.2	80	30	86.7	22.6	23	807	244	55.6
			40				234	314	45.6
			60				32.8	126	25.6
			80				6.02	15.2	12.2
3	26.6	160	40	2160	381.8	320.1	1497	867.6	120
			100				385	646.8	59.1
			150				207.3	304.9	9.1
			200				201.6	279.3	9.1
4	69.8	160	70	216	3.6	13.5	1700	437	96
			100				230	446	66
			150				8.1	81	47
			200				3.6	7.5	47

In particular:

$P_{C3\,avg}$:   represents the average power requested by the total load.

$P_{C3\,max}$:   represents the maximum power that can be requested by the total load, in a case where all of the single drive power profiles are used with no shift in relation to each other.

P_{C1}:   is the size of the C1 converter. This value represents the maximum power requested from the grid. This value has to be greater than the average power of the cycle.

W_{rec_max}: is the maximum recoverable energy (which is the integral of the power regenerated by the total load), in a case where all of the drives regenerate at the same time. This value represents the minimum size of the supercapacitor storage in the case of deterministic sizing criteria.

W_{rec}:   is the recoverable energy determined using the statistical approach.

W_{SC}:   is the size of a supercapacitor storage system determined using the statistical approach in order to recover all of the regenerated power and realize the peak shaving function in 95,5% of the cases. It should be noted that the size of the supercapacitor module can be lower than the total amount of recoverable energy, especially when no peak shaving is done. This is because the storage size is calculated taking into account the real energy level of the storage, which can charge and discharge more than once in each period. In other words, it is very low probable that all of the drives will regenerate at the same time. By increasing the maximum power size of the C_1 converter, the requested size of the supercapacitor needed to realize the peak shaving function decreases.

P_{C_3}:   is the size of the C_3 converter. This is calculated in order to satisfy the power request of the load in 95,5% of the cases, as the difference between the maximum power requested by the load in 95,5% of the cases and the power supplied by the C_1 converter: ($\mathbb{E}(\max(P_{C_3})+2 \cdot \sigma(\max(P_{C_3})-P_{C_1})$. The sum of the C_3 and C_1 converter sizes can exceed the maximum power requested by the load.

In all of the cases reported in , it should be noted that the recoverable energy in 95,5% of the cases and equal to $\mu_{Wrec}+2\sigma_{Wrec}$ is always lower than the maximum recoverable energy determined using the deterministic criteria. In fact, especially with a high number of electric drives, case 4, the reduction goes down to a maximum of -86%. This means a consistent difference in the minimum size of the supercapacitor storage with the two criteria.

For the 4 cases considered, the economic results in terms of components cost, PBT and NPV, are reported in Figure 6.9 to Figure 6.12 In these figures, parameter *k*, which is related to the peak shaving level, is defined as:

$$k = \frac{P_{C3\max} - P_{C3}}{P_{C3\max} - P_{C3\,avg}}$$

(6.25)

First, it should be noted that the different plotted quantities, especially when the number of electrical drives considered is low, are characterized by consistent discontinuities. Taking into account the fact that the aggregated power profile changes with discontinuity (see Figure 6.8) and the size of the supercapacitor storage is

determined, according to the peak shaving level desired, as a function of the size of the C_1 converter, there are certain zones where varying the maximum power of C_1, and consequently of *k*, produces no variation, from a statistical point of view, in the size of supercapacitor because the same energy is requested to realize the peak shaving function in 95,5% of the cases. This means, consequently, that with the same storage, that is with the same cost, e.g., Figure 6.9(a), different values of peak shaving can be realized, which means different cost savings related to the power components of the energy cost (6. 13). In particular, by increasing the value of *k*, with the same storage size, the NPV value continues to increases until the value of *k* determines a step variation in the supercapacitor size. At this point, consistent additional system costs are registered without a relative similar increase in the money saved related to the recovered energy, and consequently the NPV decreases for a certain step. The more the aggregated power profile resembles a continuous line without discontinuity, the more the trend of the analyzed economic quantities, in the following report, are also without discontinuity.
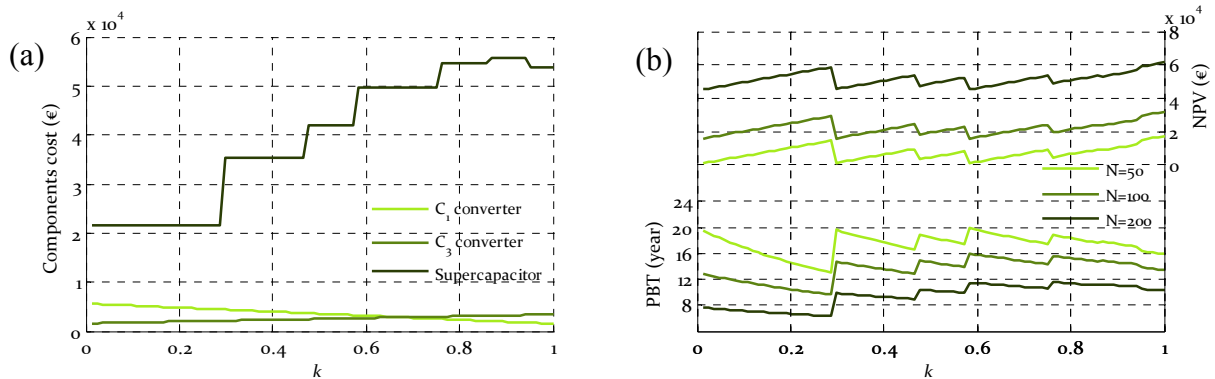
Figure 6.9   **In reference to system layout of Figure 6.7 and power profile parameters of Table 6.7, case 1, this figure reports: (a) cost of energy recovery system components, (b) Pay Back Time and Net Present Value versus peak shaving entity k, for different values of cycles per day, N.**
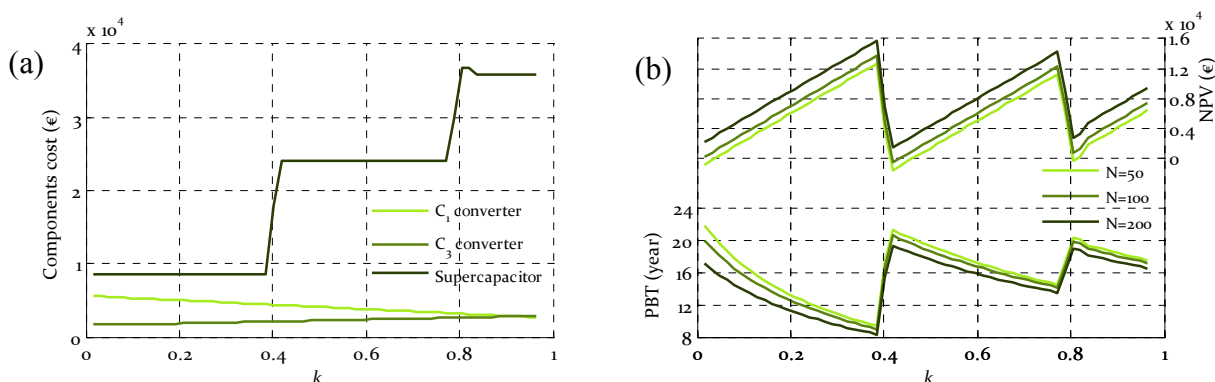
Figure 6.10   **In reference to system layout of Figure 6.7 and power profile parameters of Table 6.7, case 2, this figure reports: (a) cost of energy recovery system components, (b) Pay Back Time and Net Present Value versus peak shaving entity k, for different values of cycles per day, N.**

Figure 6.11   In reference to system layout of Figure 6.7 and power profile parameters of Table 6.7, case 3, this figure reports: (a) cost of energy recovery system components, (b) Pay Back Time and Net Present Value versus peak shaving entity k, for different values of cycles per day, N
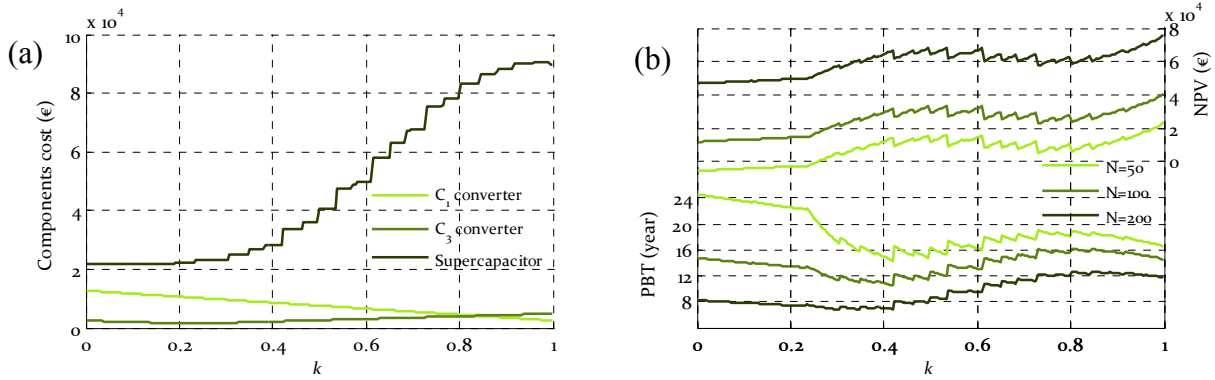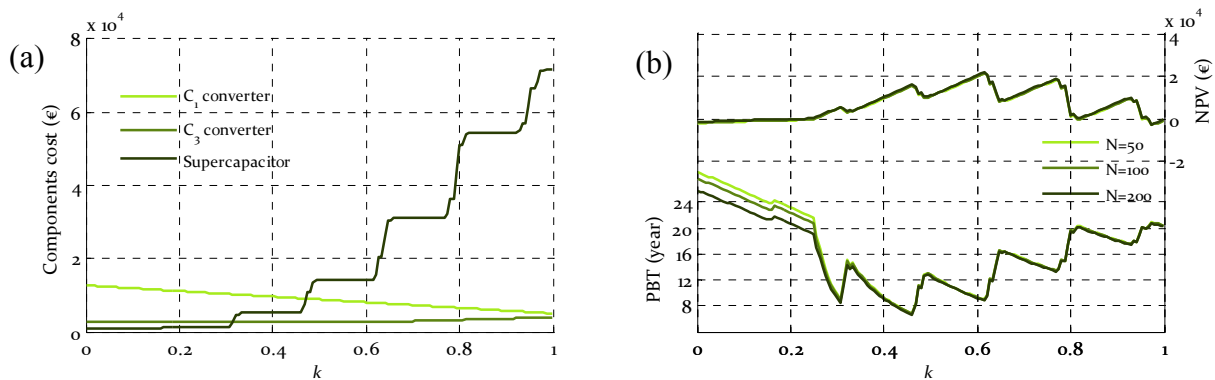

Figure 6.12   In reference to system layout of Figure 6.7 and power profile parameters of Table 6.7, case 4, this figure reports: (a) cost of energy recovery system components, (b) Pay Back Time and Net Present Value versus peak shaving entity k, for different values of cycles per day, N.

Analyzing the simulated data in the above figures and comparing them with Figure 6.5 and Figure 6.6, where the deterministic single cycle was analyzed, again shows that the best economic sizing of the energy recovery system is obtainable when the storage is designed to not only recover the regenerated energy, but also implement a peak shaving function for the main source. A substantial difference compared to the deterministic case is that, in the case of multiple drives connected to the same distribution bus, the optimal sizing to reduce the PBT is for $k < 1$ and not for $k = 1$ (deterministic case), which is the limit point corresponding to a storage size big enough to guarantee the sizing of the grid connected interface at a value equal to the average power requested by the aggregated load. In the above considered cases, the optimal sizing for k is in the range of 0.35–0.45.

Regardless of the number of electric drives considered, the minimum PBT achievable is, for the economic analysis considered, on the order of 8 years. This time is not very short from an industrial-economic point of view, but is certainly acceptable because, first, it does not require any incentive mechanism and, secondly, the expected lifetime of an energy

recovery system based on supercapacitor technology is 1 million complete charge/discharge cycles, which in our analysis correspond to more than 20 years in the case of 200 cycles per day. If, independently from the considered case, the best PBT values are similar, the actualized net present values, considering a time horizon for the investment of 20 years, is significantly different if the reference cycle is characterized by a low or high value of regenerated power P2 (Figure 6.2(a)). Comparing, for example, Figure 6.9(b) with Figure 6.10(b), where case 1 and case 2 of Table 6.6 are analyzed, the maximum NPV for case 1 is about 60 k€, while it is 16 k€ for case 2, which is characterized by a low value for the regenerated power of the single power profile. Similar considerations can be made by comparing case 3 with 4. In addition, when the single load cycle is characterized by low values of regenerated power, case 2 and case 4, the PBT, and consequently the NPV trend as a function of the cycles per day, are very close; see Figure 6.10(b) and Figure 6.12(b). In these cases, in fact, the regenerated energy from an electric drive is, with high probability, directly used by another drive that is in the absorption phase. This means that in these situations, the recoverable energy is negligible, and the storage system investment is economically paid back mainly by the savings related to the peak shaving function, which is unrelated to the number of cycles per day. When, in contrast, there is a significant recoverable energy, the PBT and NPV vary significantly with the number of cycles per day, N; see Figure 6.9(b) and Figure 6.11(b) The difference in the recovered energy between case 1 (or 3) and case 2 (or 4) is reflected in the maximum value of NPV, which is higher when, in addition to the peak shaving function, there is also an economic benefit related to the recovered regenerated energy.

In conclusion, the probabilistic approach again shows that the function of energy recovery, with all its benefits related to the environmental and energy factors, is also economically sustainable when it is accompanied by a peak shaving function for the power requested by the main source. Moreover, in this case, it was confirmed that it is possible to realize a system that is also sustainable from an economic point of view only with a system vision and the integration of multiple functions and their related benefits (the energy recovery and peak shaving functions in this case).

6.3. BIBLIOGRAPHY

[1]   L. Grigans, L. Latkovskis, "Estimation of the power and energy requirements for track-side energy storage systems," in EPE '09. 13th European Conference on Power Electronics and Applications, 2009., pp.1-7, 8-10 Sept. 2009

[2]   L. Latkovskis, L. Grigans, "Estimation of the untapped regenerative braking energy in urban electric transportation network," in EPE-PEMC 2008. 13th International Power Electronics and Motion Control Conference, pp.2066-2070, 1-3 Sept. 2008.

[3]   B. Klockl, P. Stricker, G. Koeppel,"On the properties of stochastic power sources in combination with local energy storage", Cigre, Symposium on power Systems with dispersed generation, 13-16 April, 2005, Athens.

[4]   J. P.Barton, D. G. In_eld,"A probabilistic method for calculating the usefulness of a store with finite energy capacity for smoothing electricity generation from wind and solar power", Journal of Power Sources 162 (2006), pp. 943-948, Elsevier.

[5]   P. Pinson, G. Papaefthymiou, B. Klockl, J. Verboomen, "Dynamic sizing of energy storage for hedging wind power forecast uncertainty," in PES '09. IEEE Power & Energy Society General Meeting, pp.1-8, 26-30 July 2009.

[6]   European Commission, Directorate-General for Energy (2009) EU energy trends to 2030-Update 2009.

[7]   Meyn S.P., Tweedie R.L. (1993) Markov Chains and Stochastic Stability. Springer Verlag: New York.

[8]   Iosifescu M. (1980) Finite Markov Processes and Their Applications. John Wiley & Sons

CONCLUSION

The work that was carried out has analyzed the supercapacitor storage system as an innovative technology, considering all aspects of its characterization, modeling, management, integration, and sizing in real industrial applications. In addition to examining the technical and economic aspects of this technology, more generally, all of the work was performed considering the fact that storage systems are an important element for future applications. Therefore, all aspects of the technology have to be evaluated, taking into account the technical and economic impact on the global system in which the storage operates.

According to this, a new supercapacitor model was developed considering its importance for the correct understanding of the technology behaviors and performances. Starting from models available in the literature and apparently unrelated, a first important step was represented by the introduction of a new supercapacitor model able to represent the full dynamic of a supercapacitor device in its typical dynamic of use during charge/discharge cycles ranging from continuous up to several hundred Hertz. This model is characterized by parallel branches, each of which represents a precise dynamic of the device. Thus, by neglecting a certain number of branches, it is known a priori what kind of dynamic is neglected, and consequently the error done in simulating the device behaviors. In addition, this new model represents a reference model. In fact, it can be reduced to almost all of the available models in the literature by introducing a certain number of simplifications. Another important aspect relates to the parameter identification procedure. In fact, this new model is characterized by a very simplified procedure for the parameter identification. Despite the fact that the model is able to represent the full dynamic of the device, the different parameters with clear physical meanings can be determined with specific simple tests, without using the full frequency response of the device. This is another important key aspect, because with a clear and simple parameter identification procedure anyone can model supercapacitor devices without being an expert in modeling or storage technologies, which could be very useful if it was necessary to start from the device model in order to integrate the supercapacitor technology in a more complex structure. Moreover, by knowing the physical meaning of different model parameters, it is possible to know which are typical dynamic behaviors and expected performances according to the dynamic of use.

The first part of this work represents an important key aspect, not only for the technology investigation, but also for the subsequent presented work in which the system integration, from both technical and economic points of view, has been investigated.

In order to realize, in today's systems, the innovative functions arising from the presence of storage technologies, the key is system integration. More and more, in order to correctly manage energy and power, a system vision is required for all of the applications. In fact, this is impossible if the reciprocal influences that load requirements and energy source availability have on the global system efficiency and performances are not taken into account. In a system, the correct integration, coordination, and management of different devices represent the solution to fully exploit the functionalities of single elements. This aspect is fundamental when the final goal is correct energy management and the elements are represented by different storage technologies. In fact, in all industrial, transportation, and grid applications, the presence of an opportunely integrated storage system makes it possible to realize, not only new functions such as the electric mission in a pure electric vehicle, but also the optimization of the system design. This aspect is very important because what is changing is the approach with which new designs are realized and, in this process, storage technologies are not an option but a system need. Supercapacitors, in particular, as power oriented storage devices, can manage energy with considerable efficiency, in a time horizon of up to one hundred seconds. This possibility is very useful when they are opportunely coupled with energy oriented sources such as electrochemical batteries, internal combustion engines, fuel cells, and, in general, sources that from a dynamic and efficiency point of view are able to deliver energy and not power. In all of these situations, it is clear that great advantages arise from the integration of a system of power oriented storage technology. Yet, it is also evident that for correct integration, new technical issues arise. First, it is necessary to thoroughly know the performances of different sources and storages according to their typical dynamic of use. Moreover, it is very important to define the control strategy with which different storages and energy sources are managed and controlled. To accomplish this, the second part of the work focused on two possible control algorithms with which supercapacitors can be integrated in order to optimize the system operations. In particular, the first control strategy was designed to increase the voltage quality level on a DC bus where different storages and loads are connected. In contrast, the second control strategy was designed to

maximize the global efficiency of multiple storages technologies connected to the same DC bus in order to satisfy the load requirements. Technically, these two strategies were approached in different ways. In fact, the former controls the different storages by means of interfaced power converters, which present different control loop bandwidths set according to the typical dynamics of the storage devices, while the second control strategy makes it possible to maximize the efficiency by controlling the different power converters in such a way that the current drawn by each converter minimizes the overall storage losses. The second control strategy, in particular, can be implemented only if an adequate modeling, from both a dynamic and efficiency point of view, of the storage technologies is available.

What has emerged from the experimental activity is that the system integration makes it possible to realize a series of multiple benefits, independently from the control strategy implemented, which are in the direction of the system optimization. In fact, peak shaving, voltage stabilization, and a loss minimization function are obtained. By just considering the sum of the multiple benefits, it is possible to understand the advantage arising from system integration, which has to be considered, not as a plus in designing a new system, but as a base need to correctly approach the design of new optimized solutions.

This is true not only from a technical point of view, but also from an economic point of view. With this consideration, the third part of the thesis aimed at the economic opportunity arising from the integration of supercapacitor technology in real applications in order to realize the peak shaving and energy recovery functions. Taking into account the total system cost and, in particular, that of the supercapacitors, which is the predominant cost of the system, two sizing criteria for the storage system were analyzed. The first is based on the deterministic approach, which is valid when the power profile required by the load is well known and a priori defined. In contrast, the second approach is very useful when the power profile required by the load cannot be evaluated in a deterministic way because arises from the sum of the identical power profiles of multiple loads casually shifted in time. In this case, the use of a centralized storage system is very useful if the size of the storage takes into account the very low probability that all of the multiple loads work simultaneously. The probabilistic approach makes it possible to size the storage system according to the probability with which the events occur. In both cases,

what arises from the economic evaluation is a confirmation of the previous technical evaluation and, in particular, that the integration of the supercapacitor storage technology is a winning solution when the multiple benefits are evaluated. If only a specific function is considered, as for example the energy recovery function, the optimization is not obtained from either a technical or economic point of view. In this case, no investments can be sustained from an industrial point of view, despite the high importance of the energy recovery function in our society. When the system is designed in order to be completely optimized by using the power oriented storage solution, multiple benefits are obtained, including the possibility of sizing the plant for the mean power rather than the maximum required by the load, along with increasing the total system efficiency, expected lifetime, and efficiency of the primary energy sources. The energy recovery function could also be listed among these benefits. In this case, all these functionalities are obtained by means of the same storage system, and consequently the storage is also a convenient investment from an economic point of view.

In conclusion, this work has analyzed supercapacitor storage technology considering all of the aspects needed for its correct use and integration in real applications, starting from the modeling and concluding with an economic evaluation of the system integration. The model represents an effective tool with which the control strategy and system integration have been evaluated and validated. This could be a valid approach to investigate other storage technologies such as the world of electrochemical batteries, in order to increase our understanding of the storage technology options, not only from an electrical/electrochemical point of view, but also in relation to the complete exploitation of the opportunities arising from their use in real applications.

7. *APPENDIX*

7.1. *DATA SHEETS OF THE INVESTIGATED SUPERCAPACITOR STORAGE DEVICES*

Part Number	PC 10 old version
Capacitance, C (F)	10 ±20%
Nominal Voltage (V)	2.5
Surge Voltage (V)	2.7
Internal Resistance, RDC [Ω]	0.18
Internal Resistance, 1 kHz [Ω]	0.13
Leakage current [mA]	0.04
Short circuit current [A]	19
Max continuous current [A]	2.5
Specific power [W/kg]	660
Geometry	Prismatic
Length [mm]	29.6
Width [mm]	23.6
Thickness[mm]	4.8
Life time	ΔC <20% decrease, ΔRDC < 100% increase from initial value after 10 year @25°C
Cycle life	ΔC <20% decrease, ΔRDC < 100% from initial value after 500k cycles @ 25°C (I=0.5A). Cycle defined as nominal charge to half charge states cycle

Part Number	PC 10 new version
Capacitance, C (F)	10 ±20%
Nominal Voltage (V)	2.5
Surge Voltage (V)	2.7
Internal Resistance, RDC [Ω]	0.18
Internal Resistance, 1 kHz [Ω]	0.13
Leakage current [mA]	0.04
Short circuit current [A]	19
Max continuous current [A]	2.5
Specific power [W/kg]	660
Geometry	Prismatic
Length [mm]	29.6
Width [mm]	23.6
Thickness[mm]	4.8
Life time	ΔC <20% decrease, ΔRDC < 100% increase from initial value after 10 year @25°C
Cycle life	ΔC <20% decrease, ΔRDC < 100% from initial value after 500k cycles @ 25°C (I=0.5A). Cycle defined as nominal charge to half charge states cycle

Part Number	BCAP0140 E250
Capacitance, C (F)	140 +20%
Nominal Voltage (V)	2.5
Surge Voltage (V)	2.7
Internal Resistance, RDC [mΩ]	7.2
Internal Resistance, 1 kHz [mΩ]	3.6
Leakage current [mA]	0.10
Short circuit current [A]	530
Max continuous current [A]	13
Specific power [W/kg]	3500
Geometry	Cylindrical
Length [mm]	51
Diameter [mm]	26
Life time	ΔC <20% decrease, ΔRDC < 100% increase from initial value after 10 year @25°C
Cycle life	ΔC <20% decrease, ΔRDC < 100% from initial value after 500k cycles @ 25°C. Cycle defined as nominal charge to half charge states cycle

Part Number	BCAP0150 P270
Capacitance, C (F)	150 +20%
Nominal Voltage (V)	2.7
Surge Voltage (V)	2.85
Internal Resistance, RDC [mΩ]	14
Internal Resistance, 1 kHz [mΩ]	8
Leakage current [mA]	0.5
Short circuit current [A]	193
Max continuous current [A]	9,1
Specific power [W/kg]	1700
Geometry	Cylindrical
Length [mm]	50
Diameter [mm]	25
Life time	ΔC <30% decrease, ΔRDC < 100% increase from initial value after 10 year @25°C
Cycle life	ΔC <30% decrease, ΔRDC < 100% from initial value after 500k cycles @ 25°C. Cycle defined as nominal charge to half charge states cycle

Part Number	BCAP3000 P270
Capacitance, C (F)	3000 +20% -5%
Nominal Voltage (V)	2.7
Surge Voltage (V)	2.85
Internal Resistance, RDC [mΩ]	0.29
Internal Resistance, 1 kHz [mΩ]	0.24
Leakage current [mA]	5.2
Short circuit current [A]	4800
Max continuous current [A]	121
Specific power [W/kg]	5400
Geometry	Cylindrical
Length [mm]	138.0
Diameter [mm]	60.4
Life time	ΔC <30% decrease, ΔRDC < 150% increase from initial value after 10 year @25°C
Cycle life	ΔC <30% decrease, ΔRDC < 150% from initial value after 1000k cycles @ 25°C. Cycle defined as nominal charge to half charge states cycle

Part Number	BCAP3000 P270
Capacitance, C (F)	63 +20%
Nominal Voltage (V)	125
Surge Voltage (V)	135
Internal Resistance, RDC [mΩ]	18
Internal Resistance, 1 kHz [mΩ]	-
Self discharge	50% of initial voltage, 30 days, 12 charge and hold
Max peak current, 1s [A]	750
Max continuous current [A]	150
Specific power [W/kg]	1750
Geometry	
Length [mm]	619.0
Width [mm]	349.8
High [mm]	306.0
Life time	ΔC <30% decrease, ΔRDC < 150% increase from initial value after 10 year @25°C
Cycle life	ΔC <20% decrease, ΔRDC < 150% from initial value after 1000k cycles @ 25°C. Cycle defined as nominal charge to half charge states cycle

7.2. CURRICULUM VITAE

Personal information

First name(s) / Surname(s)	VINCENZO MUSOLINO
Address(es)	Via Montello, 27 Lissone (MB), 20851, Italy
Telephone(s)	Mobile: +39 349 3719582
Nationality	Italian
Date of birth	22/12/1982

Work experience

Dates	From January 2008
Occupation or position held	Collaboration as Field Application Engineer
Main activities and responsibilities	- Extended support in writing the technical and economical budget proposals of two regional, two national and one European funded project. Actually all five admitted projects, regarding the integration of supercapacitor storage devices at subsystem level for transportation and industrial applications, involve me for the electrical technical aspects. - Designing and simulating electrical storage system based on supercapacitor technology. The activities often include the commercial approach with the final customer.
Name and address of employer	DIMAC RED S.r.l. Via Giovanni XXIII, 25 Biassono (MB), 20853, Italy
Type of business or sector	Design, development, consulting and trading of electronic components and subsystem under manufacturer's brand name.
Dates	From September 2007 to December 2007
Occupation or position held	Stage as Field Application Engineer
Main activities and responsibilities	Technical Support in designing and simulating electrical storage system based on supercapacitor technology
Name and address of employer	DIMAC RED S.r.l. Via Giovanni XXIII, 25 Biassono (MB), 20853, Italy
Type of business or sector	Trading of electronic components and subsystem under manufacturer's brand name.

Education and training

Dates	2012
Title of qualification awarded	PHd Student in Electrical Engineering
Principal subjects/occupational skills covered	- Modelling of electrostatic and electrochemical storage system devices. - Studying and implementation of algorithms and control strategies in Power Electronic Interface Converter for DC smart grid and electric drives applications. - Participation, with other Italian Universities and Industrial partners, including Fincantieri, in a regional research project regarding the analysis and exploitation of benefits arising from a medium-low voltage DC distribution for large ships with electric propulsion.
Name and type of organisation providing education and training	Politecnico di Milano
Level in national or international classification	ISCED 6

Dates	2007
Title of qualification awarded	Master degree in Electrical Engineering (110L/110)
Principal subjects/occupational skills covered	- Electric Power Plant, electric power distribution, modelling - Electric machines, electric drives, modelling and controls.
Name and type of organisation providing education and training	Politecnico di Milano
Level in national or international classification	ISCED 5

Pubblications

- ""New full frequency range supercapacitor model with easy identification procedure," Industrial Electronics, IEEE Transactions on, 10 Feb. 2012.

- "A statistical approach to electrical storage sizing with application to the recovery of braking energy", Energy, Volume 36, Issue 11, November 2011, Pages 6697-6704.

- "A control strategy for optimizing the power flows supplied by two different storage units," PowerTech, 2011 IEEE Trondheim , pp.1-6, 19-23 June 2011.

- "Management of different energy storage devices using a losses minimization algorithm," Clean Electrical Power (ICCEP), 2011 International Conference on , pp.420-425, 14-16 June 2011

- "A comparison of supercapacitor and high-power lithium batteries," Electrical Systems for Aircraft, Railway and Ship Propulsion (ESARS), 2010 , pp.1-6, 19-21 Oct. 2010.

"Simulations and field test results for potential applications of LV DC distribution network to reduce flicker effect," Harmonics and Quality of Power (ICHQP), 2010 14th International Conference on , pp.1-6, 26-29 Sept. 2010.

- "Supercapacitor characterization in power electronics applications: proposal of a new model", Clean Electrical Power, 2009 International Conference on, pp. 376-383, 9-11 June 2009.

- "Electrical modeling of Double Layer Capacitor", chapter of the Ebook titled "Energy Storage", Nova   publisher. 2011 ISBN: 978-1-61324-814-0.